Thermodynamics and kinetics of phase transformations in the Fe-N-C system

Thomas Wöhrle

Dissertation
an der
Universität Stuttgart

Thermodynamics and kinetics of phase transformations in the Fe-N-C system

Von der Fakultät Chemie der Universität Stuttgart zur Erlangung der
Würde eines Doktors der Naturwissenschaften (Dr. rer. nat.)
genehmigte Abhandlung

vorgelegt von

Thomas Wöhrle

aus Heilbronn

Hauptberichter:	Prof. Dr. Ir. E. J. Mittemeijer
Mitberichter:	Prof. Dr. J. Bill
Prüfungsvorsitzender:	Prof. Dr. T. Schleid
Tag der Einreichung:	18.01.2012
Tag der mündlichen Prüfung:	16.03.2012

Contents

Contents

Chapter 1

General Introduction

Thermochemical surface treatment procedures such as nitriding and nitrocarburizing are of great technological and scientific importance, in particular concerning the development of high-performance materials. The advantage of these processes is that the properties of the material can be improved by the formation of a compound layer and/or a surface adjacent diffusion zone without affecting the properties of the bulk material. The compound layer can lead to a significant improvement of the wear and corrosion resistance [1, 2], whereas the diffusion zone can lead to a significant improvement of the fatigue strength [3, 4].

Upon nitriding and nitrocarburizing, nitrogen or nitrogen and carbon are dissolved into the surface of iron or iron-based steels, usually at temperatures between 550 °C and 580 °C [5-10]. The nitriding and nitrocarburizing processes are, thereby, directly connected with the phase equilibria of the metastable[1] Fe-N and Fe-N-C systems. If the chemical potential of nitrogen and/or carbon are sufficient high, a compound layer develops, which is typically composed of γ'-Fe$_4$N$_{1-z}$ iron nitride (fcc type arrangement of iron atoms), ε-Fe$_3$(N,C)$_{1+x}$ iron(carbo)nitride (hcp type arrangement of iron atoms) and under certain nitrocarburizing conditions also cementite θ-Fe$_3$C (complicated orthorhombic arrangement of iron atoms). Underneath the compound layer a so-called diffusion zone develops, where nitrogen and/or carbon are dissolved interstitially in the solid matrix. The diffusion zone in pure iron can also contain precipitates of α''-Fe$_{16}$N$_2$ and γ'-Fe$_4$N$_{1-z}$. The compound layer and the diffusion zone are schematically illustrated in Fig. 1.1. The compound layers developing upon nitriding/nitrocarburizing can be divided into separate (sub)layers (with a lateral homogeneous phase composition) perpendicular to the surface normal. According to the phase rule a sublayer in the binary Fe-N system can only be composed a single phase, whereas a sublayer in the ternary Fe-N-C system can be composed either of a single phase or of two different phases [11-13].

The sequence of phases which can be formed upon nitriding and nitrocarburizing is based on the corresponding Fe-N and Fe-N-C phase diagram, respectively. The

---

[1] The phases occurring in the Fe-N and Fe-N-C system are metastable with respect to the decomposition into iron solid solution, molecular nitrogen and/or graphite.

sequence of phases developing in the compound layer is governed by both thermodynamics (e.g. phase equilibria) and kinetics (e.g. diffusion coefficients of each component) in the system considered.
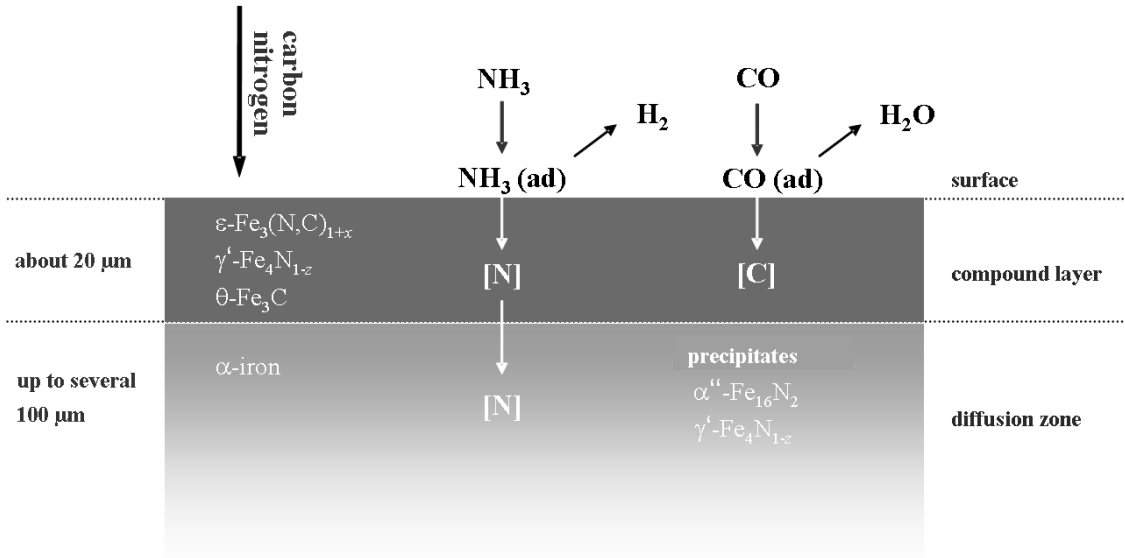
Fig. 1.1: Schematic illustration of the nitrocarburized region showing a compound layer at the surface and a diffusion zone underneath, as typically obtained upon nitrocarburizing of pure α-iron in an $NH_3/H_2/CO$ containing gas mixture. The nitrogen and carbon transfer from the gas phase to the solid phase occurs via NH_3 as nitriding medium and CO as carburizing medium. The phases developing in the compound layer depend on the process parameters, i.e. temperature, pressure and the composition of the gas mixture.

The control of the nitriding/nitrocarburizing process involves both the knowledge of the thermodynamics prescribing the gas-solid and solid-solid phase equilibria of the Fe-N and Fe-N-C systems and kinetics governing the (multicomponent) diffusion of each component in the solid phases formed during the heat treatment.

Although nitriding and nitrocarburizing have been widely investigated a fundamental knowledge about the thermodynamics and kinetics, in particular in the Fe-N-C system is still lacking. For that reason the present work is focused on (i) the thermodynamics and kinetics of phase transformations in the Fe-N-C system and (ii) the thermodynamics of the γ' phase in the Fe-N system.

In the present work, gas nitriding/nitrocarburizing experiments were performed in a vertical, three-zone, quartz-tube furnace with a diameter of 28 mm. The temperature

was controlled within ± 1 K in the middle of the furnace, where the specimen was placed by a quartz fibre. The flow of each gas component was adjusted by a separate mass-flow controller. After the heat treatment the quartz fibre was mechanically destroyed and the specimen was quenched to room temperature in nitrogen-flushed water. The furnace is schematically shown in Fig. 1.2.
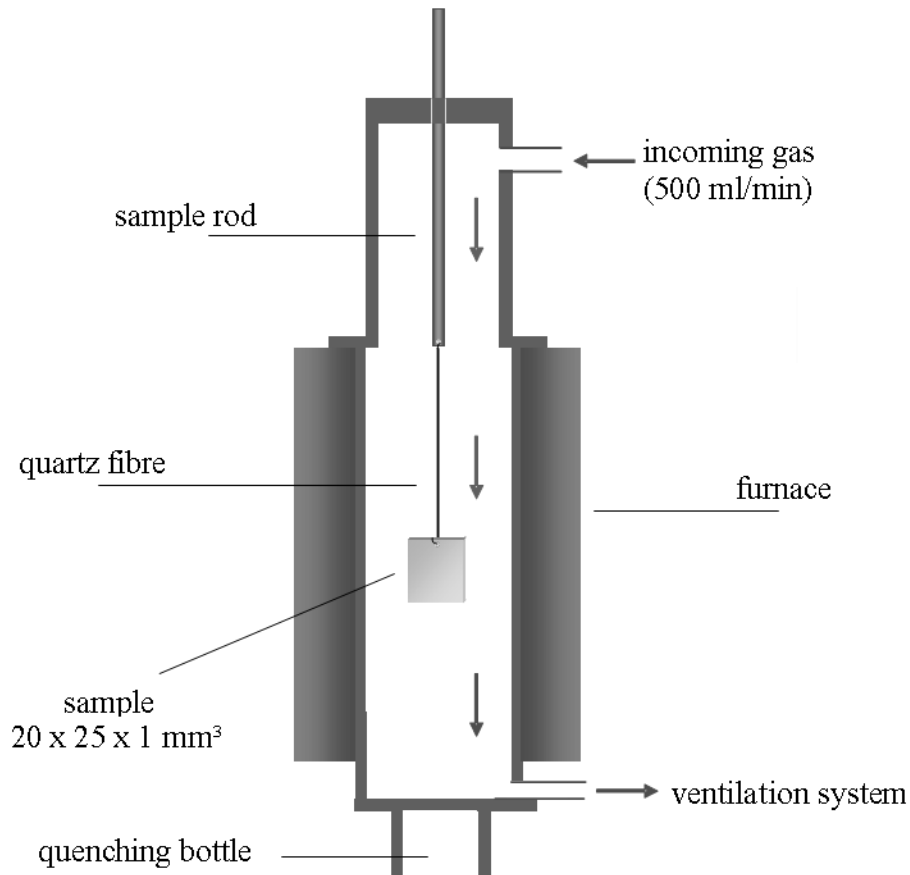
Fig. 1.2: Schematic illustration of the vertical quartz-tube furnace used for gaseous nitriding and nitrocarburizing. The composition of the incoming gas is controlled by separate mass-flow controllers for each gas component.

1.1   Gas Nitriding

Nitriding of iron and iron-based alloys is usually performed in ammonia containing gas atmospheres. The uptake of nitrogen from the gas atmosphere is thereby governed by (i) the rate of ammonia transport from the gas phase to the surface of the workpiece; (ii) the rate of dissociation of adsorbed ammonia (possibly catalyzed) at the surface to the

workpiece, leading to adsorbed nitrogen atoms; (iii) the rate of recombination and desorption of adsorbed nitrogen atoms; (iv) the rate of diffusion of absorbed nitrogen into the workpiece. Upon nitriding, the diffusion of absorbed nitrogen into the solid matrix is usually the rate-demining step.

In the case of an NH_3/H_2 gas mixture (all gases considered are assumed to be ideal) typically used for nitriding, dissolution of nitrogen in a solid phase ϕ is induced by the dissociation of ammonia at the surface of the workpiece [6-8, 14]. The reaction of ammonia is given by

$$NH_3 \rightleftharpoons \frac{1}{2} N_{ads} + \frac{3}{2} H_2 , \qquad (1.1)$$

where N_{ads} denoted nitrogen atoms adsorbed at the surface of the workpiece.

The nitrogen atoms adsorbed at the surface can either recombine and desorb

$$N_{ads} \rightleftharpoons \frac{1}{2} N_2 , \qquad (1.2)$$

or the adsorbed nitrogen atoms can be dissolved into the solid phase ϕ

$$N_{ads} \rightleftharpoons [N], \qquad (1.3)$$

where $[N]$ denotes nitrogen dissolved in the solid.

If reaction (1.2) can be neglected as compared to reaction (1.3), local equilibrium can be assumed to prevail[2] between the gas phase and the solid phase and the following equation holds at the surface of the solid matrix

---

[2] If the rate of recombination and desorbtion of adsorbed nitrogen atoms from the specimen surface (reaction (1.2)) cannot be neglected as compared to the rate of adsorbed nitrogen atoms dissolved in the solid phase (reaction (1.3)), a stationary state instead of a local equilibrium occurs, i.e. the chemical potential of nitrogen in the solid at the surface of the specimen is lower than that pertaining to the nitrocarburizing atmosphere. The desorption of N_2 can not fully be neglected for temperatures above 725 K [7].

$$NH_3 \rightleftharpoons [N] + \frac{3}{2}H_2 . \tag{1.4}$$

The relation between the chemical potentials (partial Gibbs energy) of each component can then be derived as

$$\bar{G}_{NH_3} = \bar{G}_N^\phi + \frac{3}{2}\bar{G}_{H_2} , \tag{1.5}$$

where $\bar{G}$ is the partial Gibbs energy and ϕ indicates the solid solution in equilibrium with the gas atmosphere.

According to Eq. (1.5) it holds that

$$\bar{G}_N^\phi = \left({}^0G_{NH_3} - \frac{3}{2}{}^0G_{H_2} \right) + RT \ln {}^0p^{1/2} + RT \ln \frac{p_{NH_3}}{p_{H_2}^{3/2}} , \tag{1.6}$$

where R is the gas constant, T is the absolute temperature, p is the partial pressure ${}^0G$ is the partial Gibbs energy in the reference state and ${}^0p$ is the standard pressure in the reference state.

The thermodynamic equilibrium constant $K_{th}^{(1.4)}$ of reaction (1.4) is related to the Gibbs energy change in the reference state $\Delta_R^0 G$ as

$$RT \ln K_{th}^{(1.4)} = -\Delta_R^0 G = -\left({}^0G_{NH_3} - \frac{3}{2}{}^0G_{H_2} - {}^0G_N^\phi \right). \tag{1.7}$$

From Eqs. (1.6), (1.7) and $\bar{G}_N^\phi = {}^0G_N^\phi + RT \ln a_N$, it follows for the activity of nitrogen a_N

$$a_N = {}^0p^{1/2} \cdot K_{th}^{(1.4)} \cdot r_N \tag{1.8}$$

with $r_N = \dfrac{p_{NH_3}}{p_{H_2}^{3/2}} ,$ (1.9)

where r_N (with the dimension of pressure$^{-1/2}$) is the so-called nitriding potential, which can be directly related to the chemical potential of nitrogen as pertaining to the nitriding atmosphere [6]. From equation (1.9) it follows that (very) high nitriding potentials can be achieved by changing the ratio of the partial pressures of p_{NH_3} and p_{H_2}.

The activity of nitrogen, as pertaining to the nitriding atmosphere can now be obtained from Eq. (1.8) and by selecting $^0G_N^\phi \equiv \frac{1}{2}\,^0G_{N_2}$, i.e. the equilibrium constant $K_{th}^{(1.4)}$ of reaction (1.4) is equal to the equilibrium constant $K_{th}^{(1.10)}$ of the following reaction[3], i.e. the dissociation of ammonia in the gas phase

$$NH_3 \rightleftharpoons \frac{1}{2}N_2 + \frac{3}{2}H_2 . \tag{1.10}$$

The thermodynamic equilibrium constant $K_{th}^{(1.10)}$ of reaction (1.10) is then related with the corresponding "pressure equilibrium constant" by $K_p^{(1.10)} = \,^0p^{1/2} \cdot K_{th}^{(1.10)}$, where $K_p^{(1.10)}$ has the dimension of pressure$^{1/2}$. The reference state of $^0G_{NH_3}, {}^0G_{H_2}$ and $^0G_{N_2}$ is (usually) selected as $^0p = 1$ atm at the temperature considered.

The use of N_2 gas as a nitriding medium yields the nitrogen activity as $a_N = p_{N_2}^{1/2} / \,^0p_{N_2}^{1/2}$, i.e. a very high partial pressure of N_2 is needed to obtain the same nitrogen activity as pertaining to a NH_3/H_2 gas mixture at atmospheric pressure. Thus, for practical application the use of N_2 is not suitable for the typical nitriding temperatures. However, when using NH_3/H_2 gas mixture for nitriding it should be recognized that (for thermodynamic equilibrium) the dissociation of NH_3 in the gas phase is almost complete at temperatures higher than 600 °C [7]. Significant dissociation of NH_3 can be prevented by sufficient high gas flow rates due to the comparable slow kinetics of reaction (1.10), enabling nitriding in NH_3 gas mixtures even at elevated temperatures.

---

[3] It is in principle also possible to calculate the activity of nitrogen directly from Eq. (1.8), if the equilibrium constant $K_{th}^{(1.4)}$ (cf. Eq. (1.7)) is known e.g. by the thermodynamic evaluation of experimental results [15].

The so-called Lehrer diagram [16] shows which Fe-N phases are in (local) equilibrium with the gas atmosphere as a function of temperature and nitriding potential. Note that the Lehrer diagram is directly related with the Fe-N phase diagram (cf. Fig. 1.3). A modified version of the Lehrer diagram [17] showing also lines of constant nitrogen concentration is given in Fig. 1.4.
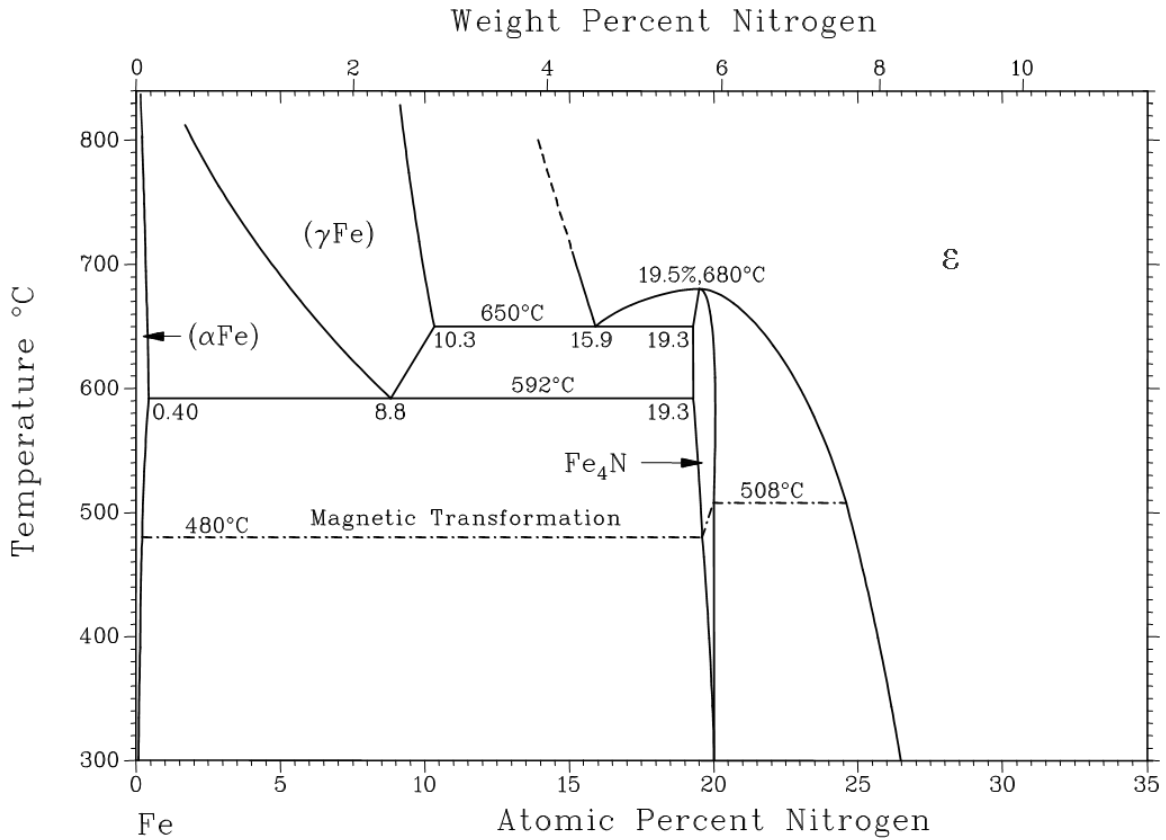
Fig. 1.3: Part of the (metastable) binary Fe-N phase diagram redrawn according to Ref. [18].
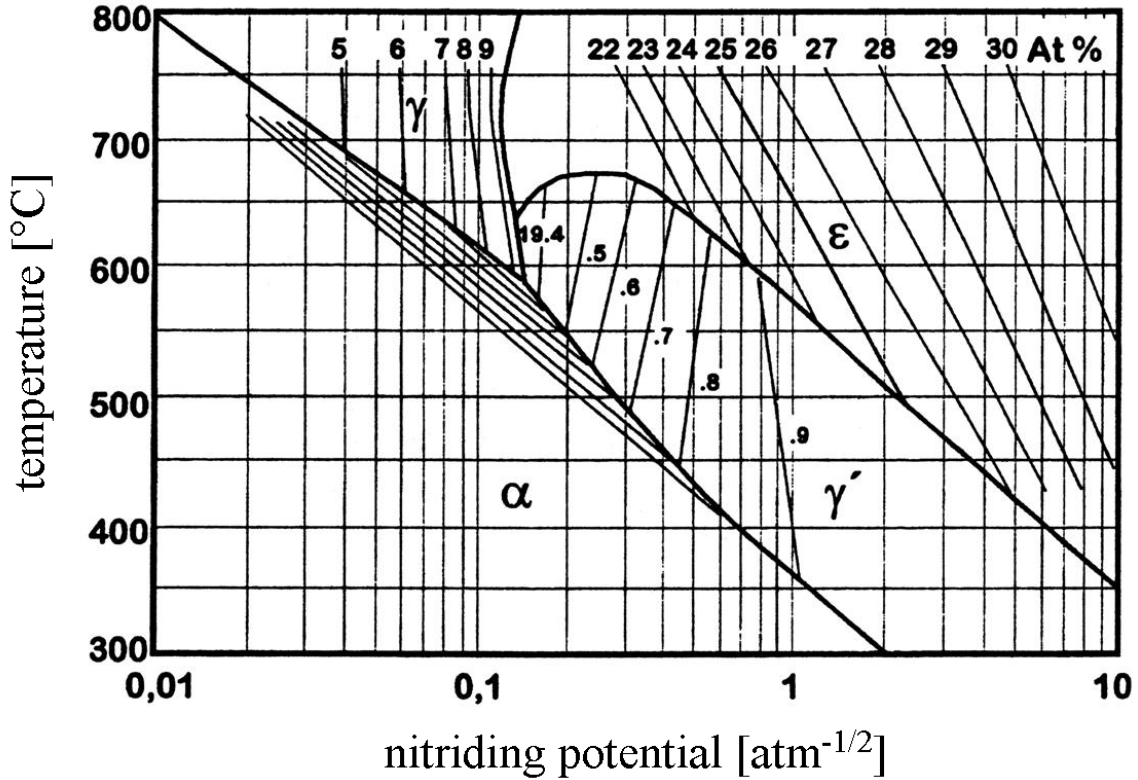
Fig. 1.4: Extended Lehrer diagram [17] showing the phase in equilibrium with the gas atmosphere upon nitriding of pure iron as a function of temperature and nitriding potential. In addition to the phase boundaries, the corresponding isoconcentration lines within a phase are indicated.

1.2 Gas Nitrocarburizing

For a nitrocarburizing atmosphere typically containing of a $NH_3/H_2/CO$ gas mixture, the dissolution of carbon in the solid phase ϕ at the surface of the workpiece can occur by the following reactions (local equilibrium is assumed to prevail between the gas phase and the solid phase) [8, 14, 19]

$$2CO \rightleftharpoons CO_2 + [C] \tag{1.11}$$

$$CO + H_2 \rightleftharpoons H_2O + [C], \tag{1.12}$$

where reaction (1.11) is the so-called Boudouard reaction and reaction (1.12) is the heterogeneous water-gas reaction. The corresponding partial Gibbs energies of carbon dissolved in the solid phase are

$$\bar{G}_C^\phi = 2\,^0G_{CO} - {}^0G_{CO_2} - RT \ln {}^0p + RT \ln \frac{p_{CO}^2}{p_{CO_2}} \tag{1.13}$$

$$\bar{G}_C^\phi = {}^0G_{CO} + {}^0G_{H_2} - {}^0G_{H_2O} - RT \ln {}^0p + RT \ln \frac{p_{CO}\,p_{H_2}}{p_{H_2O}}. \tag{1.14}$$

Using the relation $RT \ln K_{th} = -\Delta_R\,{}^0G$ and $\bar{G}_C^\phi = {}^0G_C^\phi + RT \ln a_C$ yields

$$a_C^{(1.11)} = \left({}^0p\right)^{-1} \cdot K_{th}^{(1.11)} \cdot \frac{p_{CO}^2}{p_{CO_2}} = \left({}^0p\right)^{-1} \cdot K_{th}^{(1.11)} \cdot r_C^{(1.11)} \tag{1.15}$$

$$a_C^{(1.12)} = \left({}^0p\right)^{-1} \cdot K_{th}^{(1.12)} \cdot \frac{p_{CO}\,p_{H_2}}{p_{H_2O}} = \left({}^0p\right)^{-1} \cdot K_{th}^{(1.12)} \cdot r_C^{(1.12)}, \tag{1.16}$$

where r_C (with the dimension of pressure) is defined as the carburizing potential. If thermodynamic equilibrium has been established in the gas atmosphere, the activity of nitrogen as pertaining to reaction (1.11) and reaction (1.12) are equal, i.e. $a_C^{(1.11)} = a_C^{(1.12)}$ [8, 14]. As indicated in Ref. [20], under non-equilibrium conditions the carbon transfer into the solid can be fully described by reaction (1.12) due to the comparably slow carbon transfer via reaction (1.11). At the temperature considered the reference states ${}^0G_{CO_2}$, ${}^0G_{CO}$, ${}^0G_{H_2}$ and ${}^0G_{H_2O}$, are (usually) selected as ${}^0p = 1$ atm and the reference state ${}^0G_C^\phi$ is (usually) selected as the chemical potential of graphite in the reference state at ${}^0p = 1$ atm, i.e. ${}^0G_C^\phi = {}^0G_C^{gr}$ (note that the equilibrium constants of reaction (1.12) and (1.13) change correspondingly; see section 1.1).

1.3 Sublattice model to describe the ternary Fe-N-C solid solutions

For an accurate description of a specific phase, the choice of the corresponding thermodynamic model must take into account the physical and chemical properties of that phase. Besides, it is not practical to use a very detailed model, if a phase can be also described with a simple model. In this context, it should be mentioned that experimental data can as well be fitted to incorrect or even wrong models.

The thermodynamics of Fe-N-C phases ϕ can be described by subdividing the crystal structure into a basic "substitutional" sublattice with a number of a sites per formula unit occupied by iron and a separate interstitial sublattice (also more sublattices may be considered) with a number of c sites per formula unit occupied by nitrogen (N), carbon (C) and vacant sites (Va) [15, 21-23]. For thermodynamic calculations the solid solution is considered as a "substitutional" mixture of Fe_aN_c, Fe_aC_c and Fe_aVa_c compound components. The number of sites a and c per formula unit depends on the crystal structure of the phase considered (note that a and c can also be multiplied by a common factor of N for a given phase). For further information about the sublattice model (compound-energy formalism) for the Gibbs energy of a phase see Refs. [24-26].

The Gibbs energy of that "substitutional" mixture (per mole formula units $(Fe)_a(N,C,Va)_c$) can be expressed in the same way as it would be the case for the Gibbs energy of the elemental components

$$G_m^\phi = y_N \bar{G}_{Fe:N}^\phi + y_C \bar{G}_{Fe:C}^\phi + y_{Va} \bar{G}_{Fe:Va}^\phi , \qquad (1.17)$$

where y_i is the site fraction of component i on the sublattice considered (with $y_{Va} = 1 - y_N - y_C$), and where $\bar{G}_{Fe:N}^\phi$ is the partial Gibbs energy of the compound component Fe_aN_c and so on .

Alternatively to Eq. (1.17) the molar Gibbs energy of such a "substitutional" mixture can be written as (by employing an ideal configurational entropy and an enthalpy of mixing)

$$G_m^\phi = y_C\, {}^0G_{Fe:C}^\phi + y_N\, {}^0G_{Fe:N}^\phi + y_{Va}\, {}^0G_{Fe:Va}^\phi + cRT(y_C \ln y_C + y_N \ln y_N + y_{Va} \ln y_{Va})$$

$$+ y_N y_{Va} L_{Fe:N:Va}^\phi(y_N, y_C, y_{Va}) + y_C y_{Va} L_{Fe:C:Va}^\phi(y_N, y_C, y_{Va}) \qquad (1.18)$$

$$+ y_C y_N L_{Fe:C:N}^\phi(y_N, y_C, y_{Va})$$

where ${}^0G^\phi$ is the reference state of a component and the interaction parameters $L_{Fe:N:Va}^\phi(y_N, y_C, y_{Va})$, $L_{Fe:C:Va}^\phi(y_N, y_C, y_{Va})$ and $L_{Fe:C:N}^\phi(y_N, y_C, y_{Va})$ describe excess-enthalpy contributions to the otherwise ideal mixture of the components, y_i is site fraction of

component i on the sublattice considered (the number of vacant sites are consequently included), a is the number of basic sites and c is the number of octahedral sites per formula unit.

The partial Gibbs energy for a certain compound component d (e.g. Fe_aN_c) is [24, 25]

$$\bar{G}_d^\phi = G_m^\phi + \sum_s \left(\frac{\partial G_m^\phi}{\partial y_{j_s}} - \sum_i y_{i_s} \frac{\partial G_m^\phi}{\partial y_{i_s}} \right),$$ (1.19)

where j is the elemental component in sublattice s.

The partial Gibbs energies of the compound components according to Eq. (1.17) can thus be calculated from Eq. (1.19) as follows

$$\bar{G}_{Fe:N}^\phi = G_m^\phi + (1 - y_N) \frac{\partial G_m^\phi}{\partial y_N} - y_C \frac{\partial G_m^\phi}{\partial y_C}$$ (1.20)

$$\bar{G}_{Fe:Va}^\phi = G_m^\phi - y_N \frac{\partial G_m^\phi}{\partial y_N} - y_C \frac{\partial G_m^\phi}{\partial y_C}$$ (1.21)

$$\bar{G}_{Fe:C}^\phi = G_m^\phi - y_N \frac{\partial G_m^\phi}{\partial y_N} + (1 - y_C) \frac{\partial G_m^\phi}{\partial y_C},$$ (1.22)

which can be written out in full by using Eq. (1.18) for G_m^ϕ.

Furthermore, the partial Gibbs energies (chemical potentials) of the elemental components can be obtained from the partial Gibbs energies of the several compound components. The total number N_i of i atoms of an element is given by the summation over all compound components

$$N_i = \sum_d a_d^i N_d,$$ (1.23)

Chapter 1

where a_d^i represents the number of i atoms in a formula unit of compound components d and N_d is the total number of formula units of the compound component d in the specimen.

Moreover, the partial Gibbs energy of a phase ∂G^ϕ (absolute, not molar) of a phase is in general given by

$$\partial G^\phi = \sum \bar{G}_i^\phi \partial N_i ,$$

(1.24)

where $\bar{G}_i^\phi$ is the partial Gibbs energy of the elemental component.

Equation (1.24) results in the expression (see Eq. (1.23) and Eq. (1.24))

$$\partial G^\phi = \sum \bar{G}_i^\phi \partial N_i = \sum_i \bar{G}_i^\phi \left(\sum_d a_d^i \partial N_d \right) = \sum_i \left(\sum_d a_d^i \bar{G}_i^\phi \right) \partial N_d .$$

(1.25)

Thus, the chemical potential of a compound component d (e.g. Fe_aN_c) can be related to the chemical potential of an elemental component by the expression [24]

$$\bar{G}_d^\phi = \left(\frac{\partial G^\phi}{\partial N_d} \right)_{T,P,N_e} = \frac{\sum_i \left(\sum_d a_d^i \bar{G}_i^\phi \right) \partial N_d}{\partial N_d} = \sum_i a_d^i \bar{G}_i^\phi ,$$

(1.26)

where N_e indicates that all component compounds are kept constant expect for N_d.

From Eq. (1.26) it is possible to calculate the chemical potential $\bar{G}_d^\phi$ of any compound, species or combination of atoms what will be demonstrated in the following.

The chemical potential of pure iron (obtained from component Fe_aVa_c) is

$$\bar{G}_{Fe:Va}^\phi = a\bar{G}_{Fe}^\phi$$

(1.27)

and therefore

$$\bar{G}_{Fe}^\phi = \frac{1}{a} \bar{G}_{Fe:Va}^\phi .$$

(1.28)

18

Note that vacancies in the sublattice must be also treated as an element imposing a chemical potential $\bar{G}_{\text{Va}}^{\phi}$. At equilibrium the chemical potential of a vacancy can be defined as zero, i.e. $\bar{G}_{\text{Va}}^{\phi} = 0$.

Moreover, the chemical potential of a component Fe_aN_c is

$$\bar{G}_{\text{Fe:N}}^{\phi} = a\bar{G}_{\text{Fe}}^{\phi} + c\bar{G}_{\text{N}}^{\phi}. \tag{1.29}$$

Then, it follows for the chemical potentials of pure N (see Eq. (1.27) and (1.29)) and C

$$\bar{G}_{\text{N}}^{\phi} = \frac{1}{c}\left[\bar{G}_{\text{Fe:N}}^{\phi} - \bar{G}_{\text{Fe:Va}}^{\phi}\right] \tag{1.30}$$

$$\bar{G}_{\text{C}}^{\phi} = \frac{1}{c}\left[\bar{G}_{\text{Fe:C}}^{\phi} - \bar{G}_{\text{Fe:Va}}^{\phi}\right]. \tag{1.31}$$

Accordingly, for an interstitial solid solution phase ϕ-(Fe)$_a$(N,C,Va)$_c$, where regular solution parameters are assumed, $L_{\text{Fe:N:Va}}^{\phi}(y_{\text{N}}, y_{\text{C}}, y_{\text{Va}}) = {}^{0}L_{\text{Fe:N:Va}}^{\phi}$, $L_{\text{Fe:C:Va}}^{\phi}(y_{\text{N}}, y_{\text{C}}, y_{\text{Va}})$ $= {}^{0}L_{\text{Fe:C:Va}}^{\phi}$ and $L_{\text{Fe:N:C}}^{\phi}(y_{\text{N}}, y_{\text{C}}, y_{\text{Va}}) = {}^{0}L_{\text{Fe:N:C}}^{\phi}$ (see. Eq. (18)), the chemical potentials of the pure elements iron, nitrogen and carbon can be calculated from the chemical potentials of the compound components (see Eq. (1.19) to (1.22) and Eq. (1.18) and using Eqs. (1.28), (1.30) and (1.31)), as follows

$$\bar{G}_{\text{Fe}}^{\phi} = \frac{1}{a}\bar{G}_{\text{Fe:Va}}^{\phi} \tag{1.32}$$
$$= {}^{0}G_{\text{Fe}}^{\phi} + \frac{c}{a}RT\ln(1 - y_{\text{N}}^{\phi} - y_{\text{C}}^{\phi}) + \frac{1}{a}\left[(y_{\text{N}}^{\phi})^2 \cdot {}^{0}L_{\text{Fe:N:Va}}^{\phi} + (y_{\text{C}}^{\phi})^2 \cdot {}^{0}L_{\text{Fe:C:Va}}^{\phi} + y_{\text{N}}^{\phi}y_{\text{C}}^{\phi}\Delta L^{\phi}\right]$$

$$\bar{G}_{\text{N}}^{\phi} = \frac{1}{c}\left(\bar{G}_{\text{Fe:N}}^{\phi} - \bar{G}_{\text{Fe:Va}}^{\phi}\right) = \frac{1}{c}\left(\frac{\partial G_{\text{m}}^{\phi}}{\partial y_{\text{N}}^{\phi}}\right) \tag{1.33}$$
$$= {}^{\text{H}}G_{\text{N}}^{\phi} + RT\ln\frac{y_{\text{N}}^{\phi}}{1 - y_{\text{N}}^{\phi} - y_{\text{C}}^{\phi}} - \frac{1}{c}\left[2y_{\text{N}}^{\phi} \cdot {}^{0}L_{\text{Fe:N:Va}}^{\phi} + y_{\text{C}}^{\phi}\Delta L^{\phi}\right]$$

$$\bar{G}_{\mathrm{C}}^{\phi} = \frac{1}{c}\left(\bar{G}_{\mathrm{Fe:C}}^{\phi} - \bar{G}_{\mathrm{Fe:Va}}^{\phi}\right) = \frac{1}{c}\left(\frac{\partial G_{\mathrm{m}}^{\phi}}{\partial y_{\mathrm{C}}^{\phi}}\right)$$

$$= {}^{\mathrm{H}}G_{\mathrm{C}}^{\phi} + RT \ln \frac{y_{\mathrm{C}}^{\phi}}{1 - y_{\mathrm{N}}^{\phi} - y_{\mathrm{C}}^{\phi}} - \frac{1}{c}\left[2y_{\mathrm{C}}^{\phi} \cdot {}^{0}L_{\mathrm{Fe:C:Va}}^{\phi} + y_{\mathrm{N}}^{\phi}\Delta L^{\phi}\right] \tag{1.34}$$

where ${}^{0}G_{\mathrm{Fe}}^{\phi} = \frac{1}{a}{}^{0}G_{\mathrm{Fe:Va}}^{\phi}$, ${}^{\mathrm{H}}G_{\mathrm{N}}^{\phi} = \frac{1}{c}\left[{}^{0}G_{\mathrm{Fe:N}}^{\phi} - {}^{0}G_{\mathrm{Fe:Va}}^{\phi} + {}^{0}L_{\mathrm{Fe:N:Va}}^{\phi}\right]$,

${}^{\mathrm{H}}G_{\mathrm{C}}^{\phi} = \frac{1}{c}\left[{}^{0}G_{\mathrm{Fe:C}}^{\phi} - {}^{0}G_{\mathrm{Fe:Va}}^{\phi} + {}^{0}L_{\mathrm{Fe:C:Va}}^{\phi}\right]$ and $\Delta L^{\phi} = {}^{0}L_{\mathrm{Fe:N:Va}}^{\phi} + {}^{0}L_{\mathrm{Fe:C:Va}}^{\phi} - {}^{0}L_{\mathrm{Fe:N:C}}^{\phi}$.

Equation (1.18) may have to be modified according to the interactions of interstitials within a phase. As an example, the ternary ε iron-(carbo)nitride phase (e.g. $a = c = 1$; see Ref. [15]) can be described by a subregular solution model (the parameter $L_{\mathrm{Fe:N:Va}}^{\varepsilon}(y_{\mathrm{N}}, y_{\mathrm{C}}, y_{\mathrm{Va}})$ is now depending on ${}^{0}L_{\mathrm{Fe:N:Va}}^{\varepsilon}$ and ${}^{1}L_{\mathrm{Fe:N:Va}}^{\varepsilon}$) using a Redlich-Kister type polynomial

$$L_{\mathrm{Fe:N:Va}}^{\varepsilon} = \left[{}^{0}L_{\mathrm{Fe:N:Va}}^{\varepsilon} + \left(y_{\mathrm{N}} - y_{\mathrm{Va}}\right){}^{1}L_{\mathrm{Fe:N:Va}}^{\varepsilon}\right], \tag{1.35}$$

where ${}^{0}L_{\mathrm{Fe:N:Va}}^{\varepsilon}$ and ${}^{1}L_{\mathrm{Fe:N:Va}}^{\varepsilon}$ are the interaction parameters describing the subregular solution.

In contrast to the subregular description for nitrogen dissolved in ε-iron, the parameters $L_{\mathrm{Fe:C:Va}}^{\varepsilon}(y_{\mathrm{N}}, y_{\mathrm{C}}, y_{\mathrm{Va}})$ and $L_{\mathrm{Fe:N:C}}^{\varepsilon}(y_{\mathrm{N}}, y_{\mathrm{C}}, y_{\mathrm{Va}})$ can be estimated as regular solution parameters [15]

$$L_{\mathrm{Fe:C:Va}}^{\varepsilon}(y_{\mathrm{N}}, y_{\mathrm{C}}, y_{\mathrm{Va}}) = {}^{0}L_{\mathrm{Fe:C:Va}}^{\varepsilon} \tag{1.36}$$

$$L_{\mathrm{Fe:N:C}}^{\varepsilon}(y_{\mathrm{N}}, y_{\mathrm{C}}, y_{\mathrm{Va}}) = {}^{0}L_{\mathrm{Fe:N:C}}^{\varepsilon}, \tag{1.37}$$

where ${}^{1}L_{\mathrm{Fe:C:Va}}^{\varepsilon}$ and ${}^{1}L_{\mathrm{Fe:N:C}}^{\varepsilon}$ are assumed to be zero.

The partial Gibbs energies of the pure elemental components in ε thus are

$$
\begin{aligned}
\bar{G}_{\text{Fe}}^{\varepsilon} &= \bar{G}_{\text{Fe:Va}}^{\varepsilon} \\
&= {}^{0}G_{\text{Fe}}^{\varepsilon} + RT\ln(1 - y_{\text{N}}^{\varepsilon} - y_{\text{C}}^{\varepsilon}) \\
&\quad + \left\{ (y_{\text{N}}^{\varepsilon})^{2} \left[{}^{0}L_{\text{Fe:N:Va}}^{\varepsilon} + \left(4y_{\text{N}}^{\varepsilon} - 3 \right){}^{1}L_{\text{Fe:N:Va}}^{\varepsilon} \right] + (y_{\text{C}}^{\varepsilon})^{2} \cdot {}^{0}L_{\text{Fe:C:Va}}^{\varepsilon} + y_{\text{N}}^{\varepsilon} y_{\text{C}}^{\varepsilon} \Delta L_{\text{Fe}}^{\varepsilon} \right\}
\end{aligned}
\tag{1.38}
$$

$$
\begin{aligned}
\bar{G}_{\text{N}}^{\varepsilon} &= \bar{G}_{\text{Fe:N}}^{\varepsilon} - \bar{G}_{\text{Fe:Va}}^{\varepsilon} = \frac{\partial G_{\text{m}}^{\varepsilon}}{\partial y_{\text{N}}^{\varepsilon}} \\
&= {}^{\text{H}}G_{\text{N}}^{\varepsilon} + RT\ln\frac{y_{\text{N}}^{\varepsilon}}{1 - y_{\text{N}}^{\varepsilon} - y_{\text{C}}^{\varepsilon}} - \left\{ 2y_{\text{N}}^{\varepsilon} \left[{}^{0}L_{\text{Fe:N:Va}}^{\varepsilon} + 3\left(y_{\text{N}}^{\varepsilon} - 1 \right){}^{1}L_{\text{Fe:N:Va}}^{\varepsilon} \right] + y_{\text{C}}^{\varepsilon} \Delta L_{\text{N}}^{\varepsilon} \right\}
\end{aligned}
\tag{1.39}
$$

$$
\begin{aligned}
\bar{G}_{\text{C}}^{\varepsilon} &= \bar{G}_{\text{Fe:C}}^{\varepsilon} - \bar{G}_{\text{Fe:Va}}^{\varepsilon} = \frac{\partial G_{\text{m}}^{\varepsilon}}{\partial y_{\text{C}}^{\varepsilon}} \\
&= {}^{\text{H}}G_{\text{C}}^{\varepsilon} + RT\ln\frac{y_{\text{C}}^{\varepsilon}}{1 - y_{\text{N}}^{\varepsilon} - y_{\text{C}}^{\varepsilon}} - \left[2y_{\text{C}}^{\varepsilon} \cdot {}^{0}L_{\text{Fe:C:Va}}^{\varepsilon} + y_{\text{N}}^{\varepsilon} \Delta L_{\text{C}}^{\varepsilon} \right]
\end{aligned}
\tag{1.40}
$$

where the following expressions are used

$$
{}^{0}G_{\text{Fe}}^{\varepsilon} = {}^{0}G_{\text{Fe:Va}}^{\varepsilon}
\tag{1.41}
$$

$$
{}^{\text{H}}G_{\text{N}}^{\varepsilon} = \left[{}^{0}G_{\text{Fe:N}}^{\varepsilon} - {}^{0}G_{\text{Fe:Va}}^{\varepsilon} + {}^{0}L_{\text{Fe:N:Va}}^{\varepsilon} - {}^{1}L_{\text{Fe:N:Va}}^{\varepsilon} \right],
\tag{1.42}
$$

$$
{}^{\text{H}}G_{\text{C}}^{\varepsilon} = \left[{}^{0}G_{\text{Fe:C}}^{\varepsilon} - {}^{0}G_{\text{Fe:Va}}^{\varepsilon} + {}^{0}L_{\text{Fe:C:Va}}^{\varepsilon} \right]
\tag{1.43}
$$

$$
\Delta L_{\text{Fe}}^{\varepsilon} = \left[{}^{0}L_{\text{Fe:N:Va}}^{\varepsilon} + \left(6y_{\text{N}}^{\varepsilon} + 2y_{\text{C}}^{\varepsilon} - 2 \right){}^{1}L_{\text{Fe:N:Va}}^{\varepsilon} \right] + {}^{0}L_{\text{Fe:C:Va}}^{\varepsilon} - {}^{0}L_{\text{Fe:N:C}}^{\varepsilon}
\tag{1.44a}
$$

$$
\Delta L_{\text{N}}^{\varepsilon} = \left[{}^{0}L_{\text{Fe:N:Va}}^{\varepsilon} + \left(6y_{\text{N}}^{\varepsilon} + y_{\text{C}}^{\varepsilon} - 2 \right){}^{1}L_{\text{Fe:N:Va}}^{\varepsilon} \right] + {}^{0}L_{\text{Fe:C:Va}}^{\varepsilon} - {}^{0}L_{\text{Fe:N:C}}^{\varepsilon}
\tag{1.44b}
$$

$$
\Delta L_{\text{C}}^{\varepsilon} = \left[{}^{0}L_{\text{Fe:N:Va}}^{\varepsilon} + \left(3y_{\text{N}}^{\varepsilon} + 2y_{\text{C}}^{\varepsilon} - 2 \right){}^{1}L_{\text{Fe:N:Va}}^{\varepsilon} \right] + {}^{0}L_{\text{Fe:C:Va}}^{\varepsilon} - {}^{0}L_{\text{Fe:N:C}}^{\varepsilon}
\tag{1.44c}
$$

or approximately ($y_N \approx 0.25$ and $y_C \approx 0.05$ for the typical nitrogen and carbon content in the ε phase)

$$\Delta L^\varepsilon = \Delta L_{Fe}^\varepsilon = \Delta L_N^\varepsilon = \Delta L_C^\varepsilon \cong \left({}^0L_{Fe:N:Va}^\varepsilon - 0.5 \cdot {}^1L_{Fe:N:Va}^\varepsilon \right) + {}^0L_{Fe:C:Va}^\varepsilon - {}^0L_{Fe:N:C}^\varepsilon . \tag{1.45}$$

1.4 Solid-gas phase equilibria

In order to calculate the conditions for equilibrium of the gas atmosphere and a Fe-N-C solid solution at the surface, the partial Gibbs energies of the elemental components in both phases have to be equal

$$\bar{G}_N^{gas} = \bar{G}_N^\phi \tag{1.46}$$

$$\bar{G}_C^{gas} = \bar{G}_C^\phi . \tag{1.47}$$

The solubility of iron in the gas phase (and thus the partial pressure of iron) is that low at nitrocarburising temperatures that equilibrium between gaseous and solid iron can establish by bare evaporation of Fe from the solid ($\bar{G}_{Fe}^{gas} = \bar{G}_{Fe}^\phi$) without applying an external iron-delivering gas. Due to the very low partial pressure of iron in the gas atmosphere the partial pressure of other gas components (and thus the chemical potential of these components) are barely influenced. Thus the equilibrium condition of iron $\bar{G}_{Fe}^{gas} = \bar{G}_{Fe}^\phi$ needs, therefore, not be considered for solid-gas phase equilibrium calculations.

Now, from equation (1.6) and (1.39) as well as from equation (1.14) and (1.40) the nitrogen and carbon concentrations in ε can be calculated if nitriding and carburizing potentials are known. The nitriding and carburizing potentials can be calculated reversely by the knowledge of y_N and y_C [15, 21, 27].

1.5   Solid-solid phase equilibria

Calculation of solid state equilibria between two phases ϕ_1 and ϕ_2 requires that the chemical potential of an elemental component (e.g. Fe, N and C) in the solid phase ϕ_1 is equal to the chemical potential of the same elemental component in the solid phase ϕ_2, i.e.

$$\bar{G}_{\text{Fe}}^{\phi_1} = \bar{G}_{\text{Fe}}^{\phi_2} \tag{1.48}$$

$$\bar{G}_{\text{N}}^{\phi_1} = \bar{G}_{\text{N}}^{\phi_2} \tag{1.49}$$

$$\bar{G}_{\text{C}}^{\phi_1} = \bar{G}_{\text{C}}^{\phi_2} \ . \tag{1.50}$$

From Eq. (1.48) to (1.50) and the thermodynamic model of the corresponding phases (for the ε phase see Eqs. (1.38) to (1.40)) it is now possible to calculate the ternary phase diagram Fe-N-C at any temperature.

1.6   Multicomponent Diffusion

In a one-dimensional system the flux $J_k^{(\phi)}$ of a species k in a phase ϕ is given by the following expression for a n-component solution [12, 28]

$$J_k^{(\phi)} = v_k^{(\phi)} c_k^{(\phi)} = -\sum_{i=1}^{n} L_{ki} \frac{\partial \mu_i}{\partial x} = -\sum_{j=1}^{n} D_{kj} \frac{\partial c_j}{\partial x} \ , \tag{1.51}$$

where $v_k^{(\phi)}$ is the velocity of a species and L_{ki} is the concentration-dependent "Onsager phenomenological coefficient" with $L_{kk} = M_k c_k$ and, here, $L_{ki} = 0$ for $k \neq i$ (i.e. for interstitial diffusion the kinetic correlations between sublattices are negligible [12]), M_k is the mobility of species k, $\partial \mu_i / \partial x$ is the gradient of the chemical potential, D_{kj} is the (possibly concentration-dependent) intrinsic diffusion coefficient (expressed as a quantity per unit volume) and $\partial c_j / \partial x$ is the gradient of the concentration. Note that the relation

between L_{ki} and D_{kj} is not trivial e.g. for real solutions the diffusional cross-terms $D_{kj}\left(k \neq j\right)$ are *non-zero*, whereas the kinetic cross-terms $L_{ki}\left(k \neq i\right)$ can be *zero* [12].

The intrinsic diffusion coefficient is given by [29]

$$D_{kj} = D_k^* \frac{c_k}{RT}\frac{\partial \mu_k}{\partial c_j} = D_k^* c_k \frac{\partial \ln a_k}{\partial c_j} = D_k^* \varphi_{kj}, \tag{1.52}$$

where D_k^* is the self-diffusion coefficient and φ_{kj} is the thermodynamic factor.

For non-steady state diffusion in one-dimensional systems, the concentration profile of species k in phase ϕ can be obtained from Fick's second law

$$\frac{\partial c_k}{\partial t} = \frac{\partial}{\partial x}\left(\sum_{j=1}^{n} D_{kj}\frac{\partial c_j}{\partial x}\right), \tag{1.53}$$

where t is the time and x is the location coordinate.

1.7 Outlook of the theses

Although the formation and growth of compound layers formed upon nitrocarburizing of pure iron has been investigated by a large number of experimental and theoretical works [14, 19, 21-23, 30-43], little is known about the thermodynamics and the growth kinetics of the phases in the Fe-N-C system.

In chapter 2, the time-dependent and the atmosphere-dependent microstructural evolution of compound layers developing upon nitrocarburizing of pure α-iron and nitrogen pre-saturated α-iron substrates at 580 °C were studied. The phases formed in the compound layer were investigated by optical microscopy, X-ray diffraction analysis (XRD), electron-probe microanalysis (EPMA) and electron back-scatter diffraction (EBSD). The time-dependent microstructural evolution of the compound layer starts with the formation of carbon-rich cementite (Fe_3C) and develops into the direction of the nitrogen-richer phases ε and γ'. This evolution is a consequence of the kinetics of the

nitrogen and carbon uptake from the gas phase into the solid phase and the establishment of local equilibria at the solid-solid interphase boundaries as caused by significantly different solubilities of nitrogen and carbon in ferrite. The microstructural evolution of the compound layer as observed upon increasing treatment time at constant gas composition and as observed upon increasing nitriding potential at constant treatment time are identical. At the surface of the compound layer local equilibrium conditions so not necessarily prevail, whereas the phases formed within the compound layer are compatible with the establishment of local equilibrium conditions at the solid-solid phase boundaries.

In chapter 3 it is shown that at a given temperature and treatment time the activities of nitrogen and carbon as imposed by the gas atmosphere have a strong influence on the microstructure and composition of the compound layers formed upon nitrocarburizing of α-iron. At 550 °C the compound layers were composed of either γ' single-phase or ε / γ' double layers, whereas at 580 °C and very high carbon activities also the formation of $\varepsilon / \varepsilon + \gamma'$ double layers is possible. With increasing carbon activity in the gas phase the amount of nitrogen in ε at the surface of the compound layer decreases, whereas the amount of carbon increases, i.e. nitrogen is substituted by carbon. As for experiments presented in chapter 1, a local equilibrium may only occur at the interphase boundaries within the compound layer, but not at the surface of the compound layer.

Chapter 4 focuses on multicomponent diffusion in the ε-$Fe_3(N,C)_{1+x}$ phase. The growth rate and composition of ε / γ' double layers grown at 550 °C on α-iron upon nitrocarburizing (cf. compound layers presented in chapter 2) were used together with models for the growth of bilayers to determine (for the first time) the intrinsic diffusion coefficients of N and C in ε-$Fe_3(N,C)_{1+x}$, i.e. D_{NN}^{ε}, D_{CC}^{ε}, D_{NC}^{ε} and D_{CN}^{ε}. It is found that all of the intrinsic diffusion coefficients are positive. The off-diagonal diffusivities D_{NC}^{ε} and D_{CN}^{ε} indicate significant thermodynamic interactions of both interstitial elements and can thus *not* be neglected for modeling the growth of ε / γ' double layers upon nitrocarburizing of pure α-iron.

Chapter 5 deals with the nitrogen concentration-depth profiles in γ'-Fe$_4$N$_{1-z}$ layers obtained upon nitriding of α-iron. The profiles were simulated adopting thermodynamic descriptions of the γ' phase and then compared to experimental results given in the literature [30, 44]. The strikingly concave shape of nitrogen concentration-depth profiles in massive γ' layers, as reported in the literature [30, 44], can be explained by a concentration independent *self*-diffusion coefficient of nitrogen in γ' and a concentration dependent thermodynamic description of the γ' phase taking into account the ordered arrangement of nitrogen atoms on the octahedral, interstitial lattice sites of the host lattice of iron atoms. The shape of concentration-depth profiles of such phases can thus provide crucial information on the thermodynamics and/or the diffusion mechanism.

Chapter 2

Microstructural and phase evolution of compound layers growing on α-iron upon gaseous nitrocarburizing

T. Woehrle[1], A. Leineweber[1], E.J. Mittemeijer[1,2]

[1]*Max Planck Institute for Intelligent Systems (formerly Max Planck Institute for Metals Research), Heisenbergstraße 3, D-70569 Stuttgart, Germany*

[2]*Institute for Materials Science, University of Stuttgart, Stuttgart, Germany*

Abstract

The microstructural evolution of compound layers grown on 1mm thick α-iron substrates upon nitrocarburizing at 853 K in $NH_3/H_2/N_2/CO$ gas mixtures was investigated by light optical microscopy and X-ray diffraction. The evolution of the microstructure can be divided into several stages. Starting with the formation of the carbon-rich phase cementite, that practically does not contain nitrogen, the phase constitution of the compound layer develops through successive stages of microstructural change into the direction of the nitrogen-richer and carbon-poorer phases ε and γ'. These results are the consequences of (i) the kinetics of nitrogen and carbon uptake at the gas-solid interface and the considerably different solubilities of nitrogen and carbon in the α-iron substrate and (ii) the occurrence of local equilibrium conditions prevailing at the solid-solid interphase boundaries in the compound layer. The change of the microstructure as function of depth in the compound layer is shown to be compatible with so-called "diffusion paths" in the ternary Fe-N-C phase diagram.

2.1   Introduction

Diffusion-controlled phase transformations in multicomponent solid-state systems are of great technological importance in a wide range of applications including diffusion bonding, solder joints, welded alloys, microelectronic devices and the thermochemical surface treatments. All these technologies are based on the modification and (meta)stability of microstructures induced by directional long-range diffusion and chemical reactions at the surface and/or the interfaces of intimately connected phases; thereby the properties of multicomponent materials can be greatly varied [5, 45]. The driving forces for diffusion in such heterogeneous systems are the gradients of the chemical potentials of the components in the reaction zone. If the rate of diffusion is very slow as compared to the rate of reaction, i.e. the rate of reaction is controlled by the rate of diffusion, so-called local thermodynamic equilibria can be assumed to prevail at the solid-solid phase interfaces in the reaction zone [11, 46, 47]. The establishment of local equilibria implies a continuous variation of the chemical potentials of the components through the reaction zone, associated with the possible formation of (one or more) phases within the reaction zone. The sequence and composition of these phases then is described by a so-called diffusion path in (the isothermal section of) the corresponding phase diagram [11, 12, 46, 48]. At a given temperature and pressure, the diffusion path is defined by the course of the average composition in a direction perpendicular to the original interface of the diffusion couple [46, 49]. The course of a diffusion path is governed by both the thermodynamics and the kinetics of the interacting components of the system considered.

In the field of thermochemical surface treatments an important case of (usually) diffusion-controlled phase transformations is met in nitrocarburizing, where nitrogen and carbon are supplied simultaneously to the surface of ferritic iron-based workpieces at temperatures usually between 773 K and 853 K [8, 31, 40]. If the chemical potentials of nitrogen and carbon imposed by the nitrocarburizing agent are sufficiently high, a compound layer typically composed of iron (carbo)nitrides such as ε-Fe$_3$(N,C)$_{1+x}$ and γ'-Fe$_4$(N,C)$_{1-z}$ develops ((possibly) eventually; see results presented in the present paper) at the surface of the workpiece [7, 33, 50]. Under certain nitrocarburizing conditions, also θ-Fe$_3$C (cementite) can form as an additional phase [31] or even as the only phase [43] in

the compound layer. The composition ranges of the relevant Fe-N-C phases are given in Table 2.1. Note that in particular the ε phase exhibits a wide range in composition.

Table 2.1: Composition ranges and crystal structure of some relevant phases in the ternary system Fe-N-C at a temperature of 853 K [15, 21].

Phase	Crystal Structure	N content [at.%]	C content [at.%]
α-Fe	Fe: bcc type, N and C in octahedral interstices	0 to 0.37	0 to 0.02
γ'-Fe$_4$N$_{1-z}$[*]	Fe: fcc type, N ordered in octahedral interstices	19.4 to 20	< 0.7
ε-Fe$_3$(N,C)$_{1+x}$[*]	Fe: hcp type, N ordered in octahedral interstices	15 to 33	0 to 8
θ-Fe$_3$C[*]	Fe: complicated orthorhombic, C in bicapped trigonal prisms	~ 0	25

[*] These phases are metastable with respect to the decomposition into iron and nitrogen and/or carbon.

The compound layer (of thickness up to several 10 µm) grown as a result of nitrocarburizing can lead to a significant improvement of mechanical (resistance to wear and friction) and chemical (resistance to corrosion) properties of the workpiece [1, 2]. Underneath the compound layer the so-called diffusion zone forms, where nitrogen and carbon are dissolved interstitially in the ferritic matrix. The diffusion zone is usually up to several 100 µm thick and induces a considerable improvement in fatigue resistance [3, 4].

Although a number of investigations on compound-layer development on pure α-iron substrates upon nitrocarburizing have been performed [14, 30, 31, 41, 51], a systematic and general description of the compound-layer evolution is still lacking. This is undoubtedly due to the complexity of the occurring microstructures which are far more complicated than in the case of pure nitriding.

Previous studies on the microstructural evolution of the compound layer growing on pure α-iron substrates upon salt-bath nitrocarburizing at 853 K [30] and upon gaseous nitrocarburizing at 848 K [14] and 853 K [41] reported the initial formation of Fe$_3$C (cementite) at the surface of the substrate, which was followed by the subsequent formation of the nitrogen-rich ε-phase. For prolonged treatment times the compound layer was only composed of either both ε and γ' [14, 30] or γ' [41]. The initial nucleation of cementite at the substrate surface was explained as a consequence of a much faster

absorption rate of carbon than that of nitrogen at the initial stage of nitrocarburizing, implying that the solubility limit of carbon in ferrite is reached faster than that of nitrogen [14, 30].

The present work aims to systematically investigate, by performing dedicated experiments with specifically prepared specimens (section 2.2), the observed initial formation of the carbon-rich phase cementite at the surface of the α-iron substrate upon nitrocarburizing as well as the subsequent evolution of the compound layer. It will be shown that all different microstructures occurring successively *within* the developing compound layer (section 2.3) can be understood on the basis of local thermodynamic equilibria at the interfaces between the solid phases formed (cf. section 2.4). In particular the relatively high nitrogen solubility in ferrite as compared to that of carbon in ferrite is shown to have an important impact on the microstructure of the developing compound layer.

2.2   Experimental

Rectangular specimens of dimensions $20 \times 25 \times 1$ mm^3 were cut from cold-rolled cast iron plates (Alfa Aesar, 99.98 wt. %), ground, polished (final stage 1 μm diamond suspension), cleaned ultrasonically in ethanol and recrystallized in hydrogen for 2 h at 973 K, followed by slow cooling. Immediately before nitrocarburizing the specimens were polished (final stage 1 μm diamond suspension) and cleaned with ethanol.

Nitrocarburizing experiments were performed at 853 K in a vertical quartz-tube furnace of 28 mm diameter. The process temperature was controlled within ± 1 K in the middle of the furnace where the specimen was placed. The nitrocarburizing atmosphere was composed of NH$_3$ (99.999 vol.%) as nitriding species, CO (99.997 vol.%) as carburizing species, H$_2$ (99.999 vol.%) and N$_2$ (99.999 vol.%) as inert gas (all gases from Westfalen AG). The flow rate of each gas component was adjusted separately by mass-flow controllers. In order to avoid significant (thermal) dissociation of ammonia and possible side reactions in the gas atmosphere (but see footnote to Table 2.2), which would affect the composition of the gas mixture, a constant overall gas-flow rate of 13.5 mm s^{-1} through the quartz-tube (calculated for the gas volume at room temperature) was chosen.

After nitrocarburizing the specimens were quenched by dropping them out of the furnace into nitrogen-flushed water.

To investigate the microstructural evolution of the compound layer upon nitrocarburizing, two series of experiments were performed in $NH_3/H_2/N_2/CO$ gas mixtures at 853 K: (i) using a constant treatment time of 4 h and a variable gas composition (cf. Table 2.2; series A) and (ii) using a variable treatment time and a constant gas composition (cf. Table 2.2; series B).

Additionally, experiments were performed using wedge-shaped specimens, obtained by dedicated grinding of original $20 \times 25 \times 1$ mm^3 specimens, leading to a linear thickness variation from 1 mm to 0.02 mm. Using such specimens and the normal rectangular $20 \times 25 \times 1$ mm^3 specimens but pre-saturated with nitrogen, the influence of nitrogen saturation of the ferrite substrate on the microstructural evolution of the compound layer could be revealed. The wedge-shaped specimens as well as the nitrogen pre-saturated rectangular specimens were nitrocarburised in a (relatively) strongly carburizing atmosphere (cf. Table 2.2; series C)[4]. The nitrogen pre-saturation was achieved by nitriding of the rectangular iron specimens for 66 h at 853 K in a NH_3 / H_2 gas mixture containing 10.9 vol.% NH_3 and 89.1 vol.% H_2. These nitriding parameters had been chosen such that a maximum solubility of nitrogen in ferrite was obtained without forming an iron-nitride compound layer [16]. After nitriding, X-ray diffraction was applied (CoK_α radiation) to verify that iron nitrides had not formed. The total nitrogen content in the pre-saturated substrate was determined by weighing of the specimen before and after nitriding [52] using a Toledo UMX2 high-precision balance. The nitrogen content in the pre-saturated samples was about 0.37 at.% which is very close to the nitrogen-solubility limit in ferrite at 853 K, which has been given in the literature as about 0.36 - 0.38 at.% [15, 18].

---

[4] The nitrocarburizing atmosphere used for series C leads to the formation of a single phase cementite layer on 1 mm thick rectangular non-saturated α-iron substrates [19, 43].

Table 2.2: Composition of the nitrocarburizing atmosphere, the corresponding nitriding potential[1] $r_N = p_{NH_3} / p_{H_2}^{3/2}$ and treatment time used for experiments of series A, B and C at 853 K.

Series	Treatment time [h]	NH$_3$ [vol.%]	H$_2$ [vol.%]	CO [vol.%]	N$_2$ [vol.%]	r_N [atm$^{-1/2}$]
A	4	13.23	57.95	20	8.82	0.30
	4	15.44	57.95	20	6.61	0.35
	4	17.64	57.95	20	4.41	0.40
	4	22.05	57.95	20	--	0.50
B	0.25	15.44	57.95	20	6.61	0.35
	0.5	15.44	57.95	20	6.61	0.35
	2	15.44	57.95	20	6.61	0.35
	4	15.44	57.95	20	6.61	0.35
	8	15.44	57.95	20	6.61	0.35
	24	15.44	57.95	20	6.61	0.35
C	4	13.23	57.95	20	8.82	0.30

[1]The nitriding potential is related to the chemical potential of nitrogen in a NH$_3$/H$_2$-containing gas mixture [7] and determines at a given temperature the iron-nitride phase in equilibrium with a purely nitriding atmosphere. In contrast to the nitriding potential, no defined carburizing potential can be given for the NH$_3$/H$_2$/CO/N$_2$ gas mixtures as applied in the present work, because the carburizing potential is hypothetically infinite [7, 43]. However, an "effective" carburizing potential prevails upon nitrocarburizing due to side reactions in the gas atmosphere [19].

The nitrocarburized specimens were cut into two pieces, which were used for optical microscopy (OM) and X-ray powder diffraction (XRPD), respectively.

The specimens for optical microscopy analysis were covered with an electrodeposited nickel layer using a Watts bath [33] at 333 K to prevent damage of the compound layer during sample preparation. Embedding (Polyfast, Struers GmbH) was followed by grinding, polishing (final stage 1 µm diamond suspension) and etching in 1 vol.% Nital containing 0.1 vol.% HCl [34]. Some cross-sections were additionally treated with a Groesbeck reagent [53] (4 g KMnO$_4$, 1 g NaOH, 1 g KOH per 100 ml H$_2$O) at 333 K, which allows phase-identification by discriminative staining of the carbon containing phases ε-Fe$_3$(N,C)$_{1+x}$ and, in particular, cementite (Fe$_3$C). The γ' phase remains unstained due to the low solubility of carbon, as indicated in Table 2.1. Optical microscopy was performed on cross-sections of specimens using a Zeiss Axiophot microscope.

X-Ray diffractograms for identification of the phases present in the compound layer were recorded from the surface region of the compound layers using a PANalytical X'Pert Multi-Purpose Diffractometer equipped with a graphite monochromator in the diffracted beam (Co-K$_\alpha$ radiation) and Bragg-Brentano geometry. To obtain better

crystallite statistics the samples were rotated around their surface normal during the measurement.

Microhardness measurements (micro-Vickers) on the specimen cross-section were carried out in the ferrite substrate directly underneath the compound layer using a Leica VMHT MOT micro-indentation system with a load of 50 gf ($\cong$ 0.49 N) and a dwell time of 10 s (higher loads occasionally caused localized cracking of the compound layer). Each hardness value presented is an average value of four measurements. The nitrogen content in ferrite (not well measurable with electron probe microanalysis; note the small nitrogen-solubility limit in ferrite of about 0.36 at.% at 853 K [15]) was determined using a linear dependence of hardness on nitrogen content in ferrite as reported in Ref. [42]. The same experimental conditions as described in Ref. [42] were used in the present work to ensure the applicability of the reported dependence of hardness on nitrogen content in ferrite.

2.3   Results

In the following, a shorthand notation for the specification of the microstructure of the compound layer is introduced. For this notation, the compound layer is divided into separate *sublayers* perpendicular to the surface normal, where each sublayer comprises a laterally homogeneous phase constitution, at least over a lateral distance of several 10 µm. In ternary systems (as the Fe-N-C system) at constant temperature and pressure, a sublayer comprising a (depth) range in composition can be composed either of a single phase or of two different phases (*single-phase* or *dual-phase* sublayers) if the phase rule is obeyed. The overall phase constitution of the compound layer can then be denoted by the sequence of sublayers (separated by "/"), starting from the surface of the material and ending at the compound layer / substrate interface. For example, an ε / $\varepsilon + \gamma$' compound layer is composed of an ε single-phase sublayer adjacent to the surface of the compound layer followed by an $\varepsilon + \gamma$' dual-phase sublayer adjacent to the ferritic substrate. Note that no specific indication is used for the α-iron substrate.

2.3.1 Influence of the nitriding potential on the compound-layer evolution; Series A

Nitrocarburizing of pure α-iron substrates at the lowest applied nitriding potential of $r_N = 0.3$ atm$^{-1/2}$ (series A) showed the formation of a closed cementite layer at the surface of the substrate (cf. Fig. 2.1a), in agreement with experiments reported in Ref. [43]. An increased nitriding potential ($r_N = 0.35$ atm$^{-1/2}$) resulted in the development of an inhomogeneous microstructure[5]. Besides a monophase cementite layer adjacent to the surface, also a complex dual-phase microstructure of intrinsically nitrogen-poor cementite and nitrogen-richer ε is present in the compound layer (cf. Figs. 2.1b-c). A reproduction of this experiment ($r_N = 0.35$ atm$^{-1/2}$) resulted again in the formation of an inhomogeneous microstructure showing, at different lateral positions, an $\varepsilon / \varepsilon + \gamma'$ double layer (Fig. 2.1d) and a θ / ε double layer (Fig. 2.1e). At one location the θ sublayer had transformed into ε in association with a locally increased thickness of the compound layer (dashed arrow in Fig. 2.1e). At still higher nitriding potentials ($r_N = 0.4$ atm$^{-1/2}$ and $r_N = 0.5$ atm$^{-1/2}$) the microstructure is composed of a laterally homogeneous $\varepsilon / \varepsilon + \gamma'$ double layer. In particular the morphology of the compound layer generated at the highest nitriding potential of $r_N = 0.5$ atm$^{-1/2}$ approaches the well-known morphology of an ε / γ' double layer obtained upon pure nitriding (Fig. 2.1g and see Ref. [54]).

---

[5] Inhomogeneous means that the phase constitution of the microstructure and thus the composition in the compound layer varies as function of the lateral position on the specimen cross section. According to the present observations, the position/height of the specimen in the furnace did not influence the distribution of the different microstructures: the linear gas flow rates in the furnace are high enough so that the effective chemical potentials of N and C are constant along the surface of the specimen during the heat treatment.
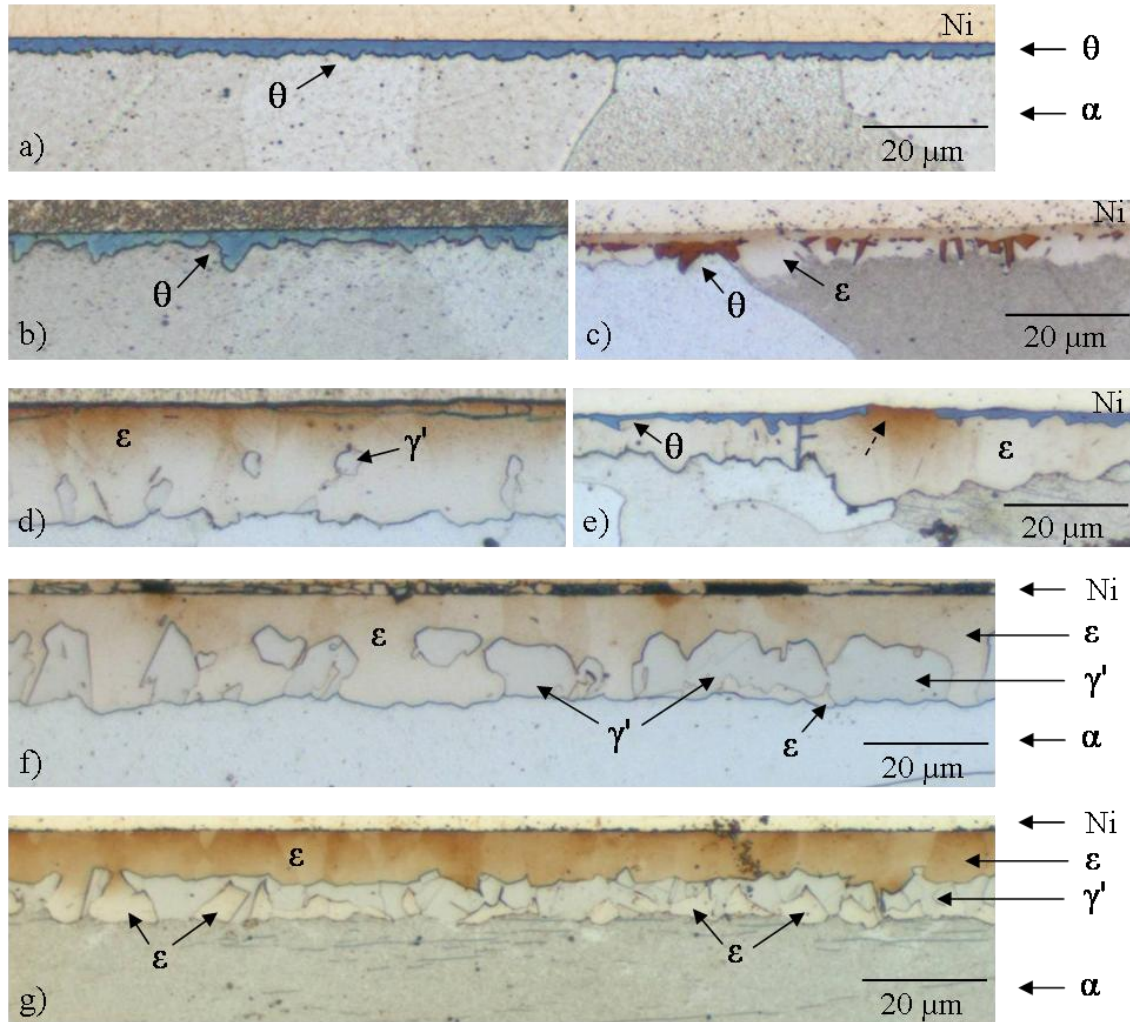
Fig. 2.1: Optical micrographs showing cross-sections (after etching with 1 vol.% Nital containing 0.1 vol.% HCl and staining with an alkaline potassium permanganate solution) of compound layers grown on α-Fe substrates by nitrocarburizing for 4 h at 853 K for various nitriding potentials (series A): (a) cementite layer, $r_N = 0.30$ atm$^{-1/2}$; (b) to (c) massive cementite layer and ε / $\theta + \varepsilon$ double layer, $r_N = 0.35$ atm$^{-1/2}$; (d) to (e) ε / $\varepsilon + \gamma'$ double layer and θ / ε double layer, $r_N = 0.35$ atm$^{-1/2}$. The dashed arrow in (e) indicates transformation of the θ sublayer into ε phase; (f) ε / $\varepsilon + \gamma'$ double layer, $r_N = 0.4$ atm$^{-1/2}$; (g) ε / $\varepsilon + \gamma'$ double layer, $r_N = 0.5$ atm$^{-1/2}$.

Evidently, the above results reveal a strong effect of the nitriding potential on the microstructural evolution of the compound layer. With increasing nitriding potential ($r_N = 0.3$ atm$^{-1/2}$ to $r_N = 0.5$ atm$^{-1/2}$), corresponding with an increasing content of nitrogen in the compound layer, the microstructure evolves from a carbon-rich and virtually nitrogen-free cementite layer to a nitrogen-rich ε / $\varepsilon + \gamma'$ double-layer.

35

2.3.2   Influence of the treatment time on the compound-layer evolution; Series B

Nitrocarburizing of pure α-iron substrates as a function of time was performed at 853 K using a nitriding potential of $r_N = 0.35$ atm$^{-1/2}$ (series B), i.e. an intermediate value of r_N with respect to the range of r_N values covered by the experiments of series A (section 2.3.1). For very short treatment times (15 min) a closed intrinsically nitrogen-poor cementite layer had developed at the surface of the substrate. Slightly longer nitrocarburizing-times (30 min) induced the formation of the nitrogen-richer ε phase in some regions at the cementite / substrate interface leading to the formation of locally confined θ / ε double-layers. After 2 h a laterally inhomogeneous microstructure was obtained: At some locations the compound layer is composed of a massive cementite layer (Fig. 2.2a), which, proceeding laterally, changes to a θ / ε double layer and to a nitrogen-richer ε / $\varepsilon + \gamma$' double layer (Fig. 2.2b). Upon continued nitrocarburizing (4 h and 8 h) the laterally inhomogeneous microstructure of the compound layer reveals an ε / $\varepsilon + \gamma$' double-layer (Fig. 2.2c) and also an $\varepsilon + \gamma$' dual-phase layer (Fig. 2.2d). After very long treatment times (24 h) the microstructure consisted of an $\varepsilon + \gamma$' dual-phase layer (Fig. 2.2e) and also of a single-phase γ' layer (Fig. 2.2f).
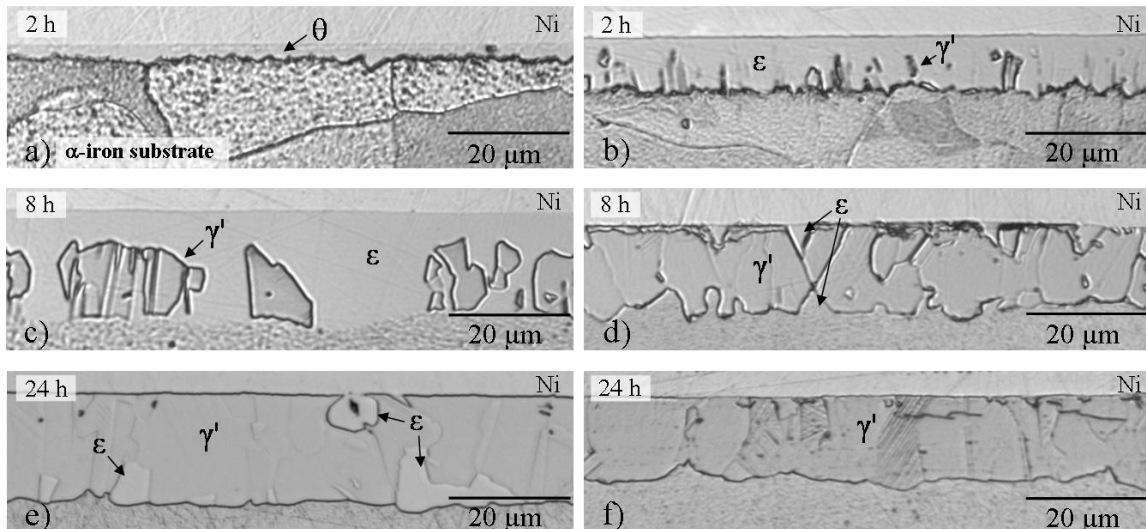

Fig. 2.2: Optical micrographs showing cross-sections (after etching with 1 vol.% Nital containing 0.1 vol.% HCl) of compound layers grown on α-Fe substrates by nitrocarburizing for various treatment times at 853 K (series B): (a) to (b) cementite layer and ε / $\varepsilon + \gamma$' double layer obtained after 2 h; (c) to (d) ε / $\varepsilon + \gamma$' double layer and $\varepsilon + \gamma$' dual-phase layer obtained after 8 h; (e) to (f) $\varepsilon + \gamma$' layer and γ' layer obtained after 24 h.

The above results show a complex time dependence of the microstructure of the compound layer. With increasing treatment time the microstructure evolves from a carbon-rich and virtually nitrogen-free cementite layer to nitrogen-richer $\varepsilon + \gamma'$ and γ' layers.

In both series (A and B) the development of the microstructure of the compound layer proceeds from a carbon-rich phase to nitrogen-rich phases. Whereas such a development for series A appears linked with an increasing value of the imposed nitriding potential, it is unclear at this stage (but see what follows), why a change in treatment time under constant nitrocarburizing conditions invokes a similar microstructural development for series B.

2.3.3   Role of nitrogen saturation of the substrate

An initially non-saturated α-iron substrate can become saturated with nitrogen during nitrocarburizing, given sufficient treatment time, i.e. a (very) thin substrate is much faster saturated with nitrogen than a thick substrate (note that the carbon solubility in the α-Fe substrate can be neglected; see Table 2.1). Against this background wedge-shaped substrates with a linear variation in thickness from 1 mm to 0.02 mm (cf. section 2.2) were used for nitrocarburizing.

Nitrocarburizing of wedge-shaped α-iron substrates for 4 h at 853 K (cf. Table 2.2, series C) showed a strong variation in the microstructure of the compound layer as a function of the substrate thickness (Fig. 2.3). After nitrocarburizing, the thick end of the specimen is covered with a massive cementite layer as shown in Fig. 2.3b (in agreement with the result for the rectangular 1 mm thick non-saturated substrate nitrocarburized under the same conditions; cf. series A, Fig. 2.1a). The formation of nitrogen-richer ε at the cementite layer / substrate interface had occurred close to the thin end of the substrate, i.e. an θ / $\theta + \varepsilon$ double layer occurs at this location (Fig. 2.3c). At the thin end of the substrate a θ / ε double layer was obtained (Fig. 2.3d). Evidently, the amount of ε in the compound layer increases from the thick end to the thin end of the substrate.
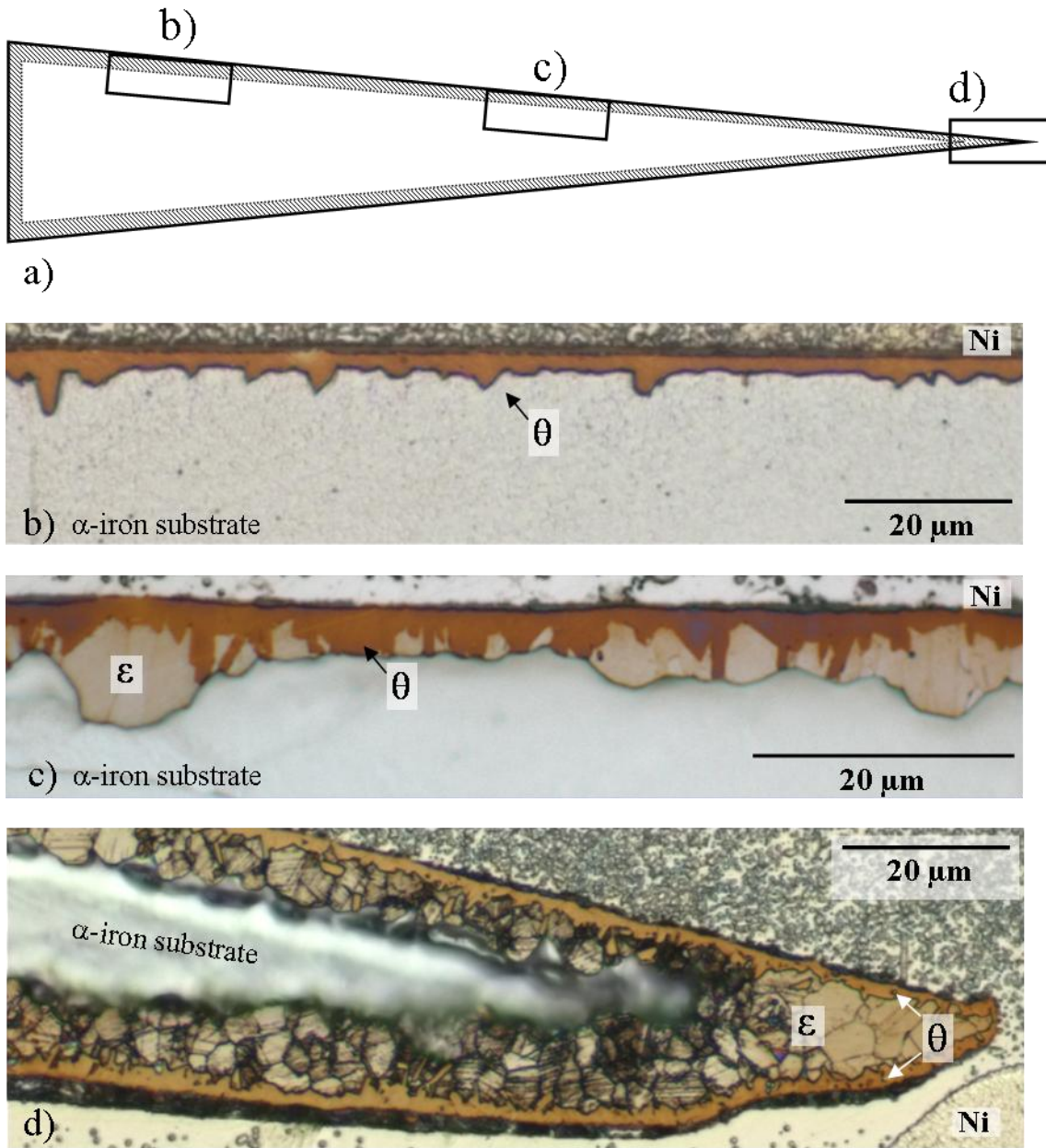
Fig. 2.3: Optical micrographs showing cross-sections (after etching with 1 vol.% Nital containing 0.1 vol.% HCl and staining with an alkaline potassium permanganate solution) of compound layers obtained on a wedge-shaped α-iron specimen by nitrocarburizing for 4 h at 853 K using a 13.23 vol.% NH_3, 57.95 vol.% H_2, 20 vol.% CO, 8.82 vol.% N_2, ($r_N = 0.30$ atm$^{-1/2}$) gas mixture: a) schematic illustration of the wedge-shaped specimen showing the lateral positions of the optical micrographs shown in b) to d); b) cementite layer at the thick end of the sample; c) θ / θ + ε double layer close to the thin end of the sample; d) θ / ε double layer at the thin end of the sample.

Nitrocarburizing of rectangular, 1 mm thick, non-saturated and nitrogen pre-saturated α-iron substrates for 4 h at 853 K (cf. Table 2.2, series C) led to the formation of strikingly

Microstructural and phase evolution of the compound layer

dissimilar microstructures of the compound layer. After nitrocarburizing of the non-saturated substrate a single-phase θ□ layer was obtained (Fig. 2.4a and see Fig. 2.1a), whereas after nitrocarburizing of the nitrogen pre-saturated substrate, a θ / ε double layer had developed (Fig. 2.4b). The corresponding X-ray diffraction patterns are given in Fig. 2.5.
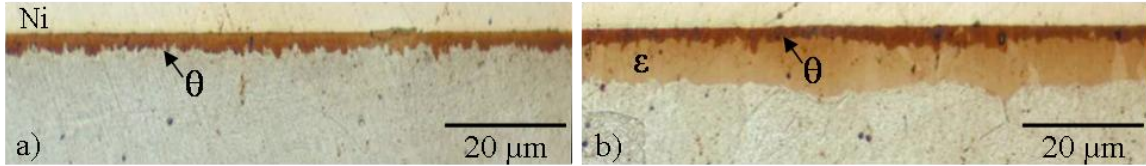

Fig. 2.4: Optical micrographs (after etching with 1 vol.% Nital containing 0.1 vol.% HCl and staining with an alkaline potassium permanganate solution) showing cross-sections of compound layers obtained by nitrocarburizing for 4 h at 853 K using a 13.23 vol.% NH$_3$, 57.95 vol.% H$_2$, 20 vol.% CO, 8.82 vol.% N$_2$, ($r_N = 0.30$ atm$^{-1/2}$) gas mixture. (a) cementite layer grown on a pure α-iron substrate, (b) θ / ε double layer grown on a nitrogen pre-saturated α-iron substrate.
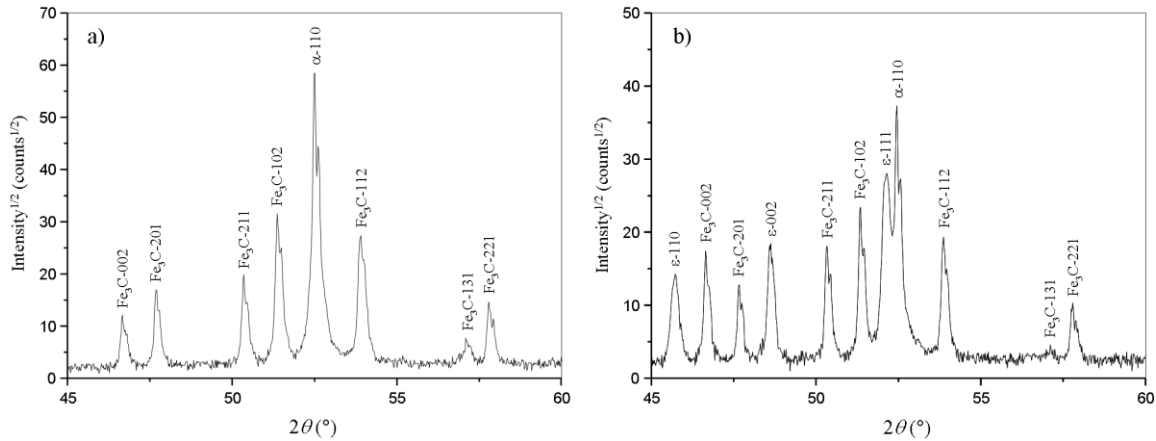
Fig. 2.5: Exemplary X-ray diffraction patterns (CoK$_\alpha$ radiation) of compound layers obtained by nitrocarburizing for 4 h at 853 K using a 13.23 vol.% NH$_3$, 57.95 vol.% H$_2$, 20 vol.% CO, 8.82 vol.% N$_2$, ($r_N = 0.30$ atm$^{-1/2}$) gas mixture. (a) cementite layer grown on a pure α-iron substrate (cf. Fig. 2.4a), (b) θ / ε double layer grown on a nitrogen pre-saturated α-iron substrate (cf. Fig. 2.4b).

To determine the degree of nitrogen saturation in the α-iron substrate, in relation to the specific microstructure of the compound layer on top of the substrate, hardness measurements were performed in the diffusion zone, at positions laterally apart, directly

underneath the compound layer, with a microstructure that varied from a carbon-rich cementite single layer to a nitrogen-rich $\varepsilon / \varepsilon + \gamma'$ double-layer (cf. Figs. 2.2a-b; rectangular specimen nitrocarburized in an 15.44 % NH_3, 57.95 % H_2, 20 % CO, 6.61 % N_2 gas mixture; series B). The results are shown in Fig. 2.6; the local nitrogen concentration in the ferrite substrate was calculated from the measured hardness values as described in section 2.2. The hardness measurements show that in the ferrite substrate underneath the compound layer, where ε is present in the microstructure, a nitrogen content of about 0.35 at.% occurs, which is practically equal to the nitrogen-solubility limit in ferrite at 853 K of about 0.36 at.% [15]. Underneath the massive cementite layer a remarkably lower nitrogen content of 0.25 at.% occurs in the ferrite substrate. The lower nitrogen content underneath the cementite layer can be ascribed to an inhibited diffusion of nitrogen through cementite as compared to the diffusion of nitrogen through iron (carbo)nitrides [14, 42, 55].
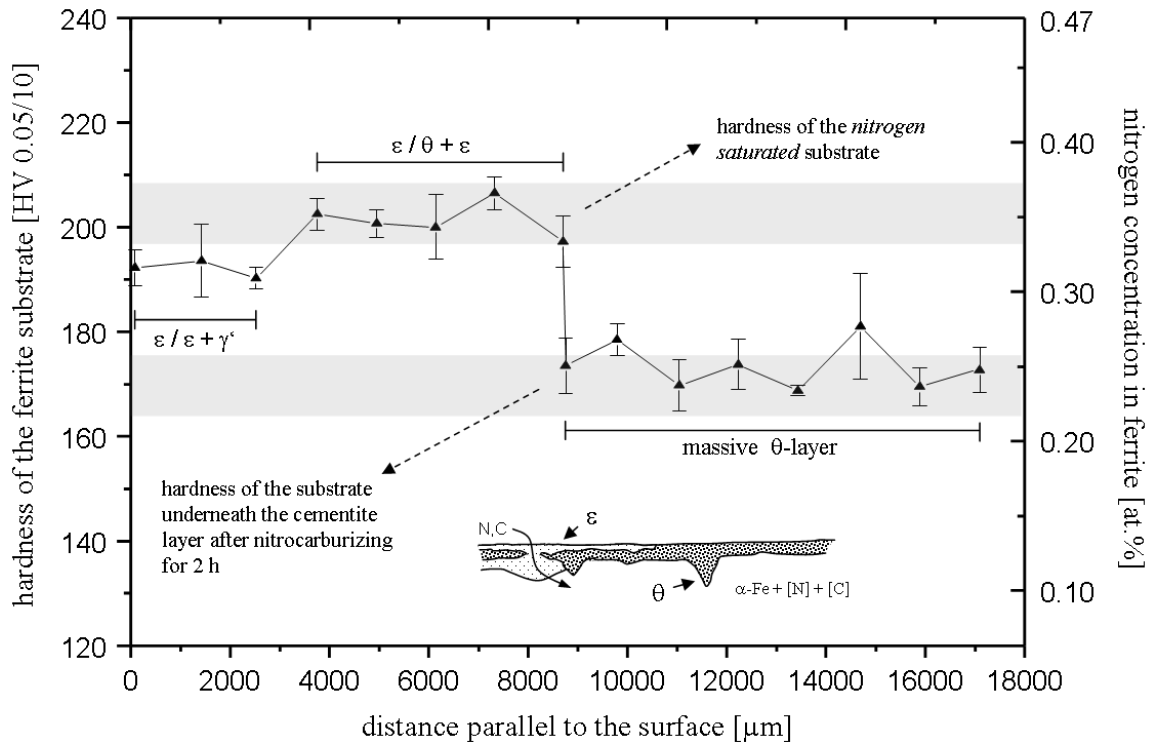
Fig. 2.6: Vickers hardness and the corresponding nitrogen concentration in the ferrite substrate directly underneath the laterally inhomogeneous compound layer obtained after nitrocarburizing using the following process parameters: 15.44 % NH_3, 57.95 % H_2, 20 % CO, 6.61 % N_2 (r_N = 0.35 atm$^{-1/2}$), 2 h and 853 K. For the inset in the bottom part of this figure see the discussion of Fig. 2.9.

2.4 Discussion

2.4.1 Kinetics: Origin of the microstructural evolution of the compound layer

As will be demonstrated in the following discussion, the time-dependent (series B) and atmosphere-dependent (series A) evolutions of the microstructure of the compound layer can be explained by assuming that local equilibria prevail at the solid-solid phase interfaces, whereas solid-gas equilibrium does not necessarily prevail at the surface of the compound layer. The time-dependent microstructural evolution of the compound layer can be caused by (i) the finite rates of nitrogen and carbon transfer from the gas phase to the α-Fe substrate (before and after compound-layer formation) and (ii) the finite thickness of the plate-like specimens used in the present experiments, implying a gradual saturation of the initially unsaturated substrate upon nitrocarburizing. As a consequence, in case of a gas atmosphere of constant composition, the microstructure of the compound layer will evolve as function of treatment time[6]. In the present case, the characteristic evolution of phases in the compound layer can be described as a consequence of the large difference of the solubilities of nitrogen and carbon in the α-iron substrate (see Fig. 2.7b) affecting the local solid-solid equilibrium at the compound layer / substrate interface. As shown in the Fe-N-C phase diagram at 853 K (Fig. 2.7b) the α-iron single-phase field exhibits a maximum solubility of 0.36 at.% for nitrogen and of 0.018 at.% for carbon [15], i.e. both solubilities differ by a factor of 20.

The phase *changes* observed at the surface of the compound layer as function of time (series B, Fig. 2.2) indicate that *at the surface* no "local equilibrium" occurs between the gas phase and the solid phase, at least not for short and intermediate treatment times. This can be discussed as follows.

The uptake of nitrogen and carbon from the nitrocarburizing gas atmosphere in the ferrite substrate is controlled by (a) the rate of NH_3 and CO dissociation (possibly

---

[6] A time-invariant phase constitution (microstructure) of the compound layer is only expected to occur for the case of a constant nitrogen and carbon concentration at the surface of the compound layer (implying local equilibrium or stationary state at the gas / solid interface) in combination with (a) a nitrogen and carbon saturated substrate or (b) an infinitely thick substrate with initially constant nitrogen and carbon content. In such cases (and assuming local equilibrium at the solid-solid interfaces in the compound layer) the so-called Boltzmann transformation can be applied to Fick's second law, implying a time-invariant diffusion path (lateral gross composition as a function of depth) and a parabolic growth of the compound-layer thickness [12, 46, 56].

catalyzed) at the substrate surface, leading to adsorbed nitrogen and carbon atoms, (b) the rate of recombination (and possibly desorption) of the adsorbed atoms and (c) the diffusion rates of, subsequently absorbed, nitrogen and carbon in the substrate away from the surface. Finite values for the nitrogen and carbon uptake imply that a local equilibrium[7], as prescribed by the chemical potentials of nitrogen and carbon, as pertaining to the composition of the nitrocarburizing atmosphere, cannot be established at once (i.e. at $t = 0$).

The rate of carbon transfer from CO gas to ferrite has been found to be much faster than the rate of nitrogen transfer from NH_3 gas [20]. It can now be concluded that the relatively low solubility of carbon in ferrite (cf. Table 2.1) in combination with the relatively fast uptake of carbon (recognizing that the diffusivities of carbon and nitrogen in α-iron do not differ much [57]) causes the ferrite substrate to be much faster saturated with carbon than with nitrogen at the early stage of nitrocarburizing[8]. Hence, at the surface of the substrate the initial formation of nitrogen-poor cementite instead of a nitrogen-richer (carbo)nitride can occur (see Fig. 2.7b, point A), although the presence of the latter phase at the surface would comply with thermodynamic equilibrium with the gas atmosphere, or with the establishment of a stationary state (see footnote 7), as suggested by the phase constitution at the surface of the compound layer after long treatment times (cf. section 2.3.2). The first observation and interpretation along these lines for the initial formation of cementite was presented in Refs. [14, 30].

Upon continued nitrocarburizing the surface-adjacent region of the substrate becomes gradually enriched with nitrogen by the continuous diffusion of nitrogen through (the grain boundaries of) the cementite layer as discussed in detail in Ref. [42]. The nucleation of ε at the cementite layer / substrate interface is then induced if the nitrogen concentration in ferrite at the layer / substrate interface exceeds a critical value (Fig. 2.7b, point B): first a local equilibrium of θ, ε and α and then, upon further nitrogen

---

[7] For example, if the recombination and desorption of adsorbed nitrogen atoms from the specimen surface cannot be neglected as compared to the rate of NH_3 dissociation, a stationary state instead of a local equilibrium occurs, i.e. the chemical potential of nitrogen in the solid at the surface of the specimen is lower than that pertaining to the nitrocarburizing atmosphere [6, 7].

[8] Even in the case of finite but about equal transfer rates of nitrogen and carbon, the solubility limit of carbon will be surpassed first as a consequence of the large difference of the solubility limits of nitrogen and carbon.

enrichment of the substrate, a local equilibrium of α and ε prevails. Note that ε can also be formed by the conversion of cementite, as first demonstrated in Ref. [58].

The role of the substrate saturation with nitrogen on the microstructural evolution of the compound layer is fully supported by the results obtained from the wedge-shaped specimens (series C; see Fig. 2.3) nitrocarburized under conditions where (initially) pure cementite layers were obtained on the usual, 1mm thick, rectangular ferrite substrates (see series A). Indeed, at the thick end of the wedge-shaped specimen, the substrate was not saturated with nitrogen after nitrocarburizing, leading to the formation of a single-phase cementite layer. At some distance away, towards the thin end (rim) of the specimen, nitrogen saturation of the substrate was reached resulting in the development of a $\theta + \varepsilon$ dual-phase layer adjacent to the substrate. At the thin end (rim) of the specimen the substrate was very fast saturated with nitrogen resulting in the formation of a θ / ε double layer (see section 2.4.3).

The effect of nitrogen saturation on the development of the microstructure of the compound layer is also confirmed by nitrocarburizing of a non-saturated, rectangular specimen and a nitrogen pre-saturated, rectangular specimen using a strongly carburizing atmosphere (series C; Fig. 2.4). The non-saturated substrate showed the formation of a massive cementite layer whereas a θ / ε double layer had developed on the nitrogen pre-saturated substrate.

The hardness measurements in the ferrite underneath a laterally inhomogeneous (θ / ε and $\varepsilon / \theta + \varepsilon$) compound layer (cf. series B, section 2.3.3; Fig. 2.6) show that the formation of ε-(carbo)nitride occurs only at locations of the layer / substrate interface where the substrate is (practically) saturated with nitrogen (for further details, see section 2.4.3).

On the basis of the above discussion, the occurrence of similar stages in the compound-layer evolution of series A (variable gas composition with constant treatment time; section 2.3.1) as compared to series B (variable treatment time with constant gas composition; section 2.3.2), can now be understood as well: the substrate becomes faster saturated with nitrogen upon applying a higher nitriding potential (cf. series A and cf. Figs. 2.1 and 2.2).

a)

b)
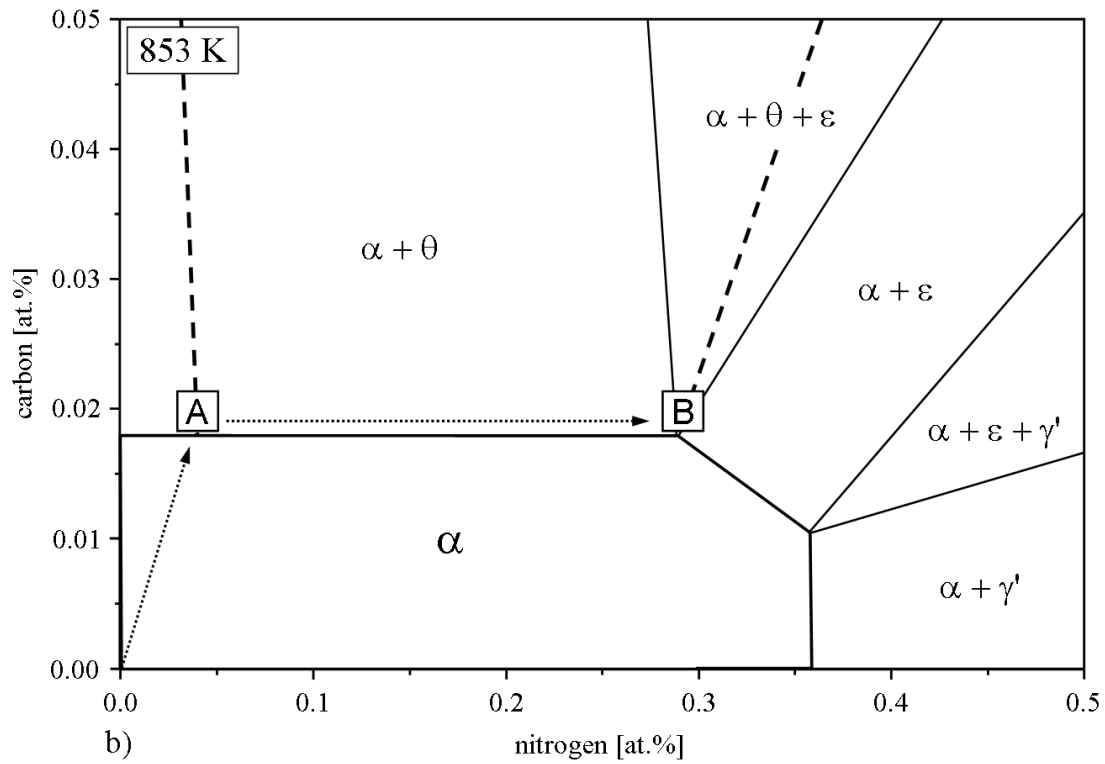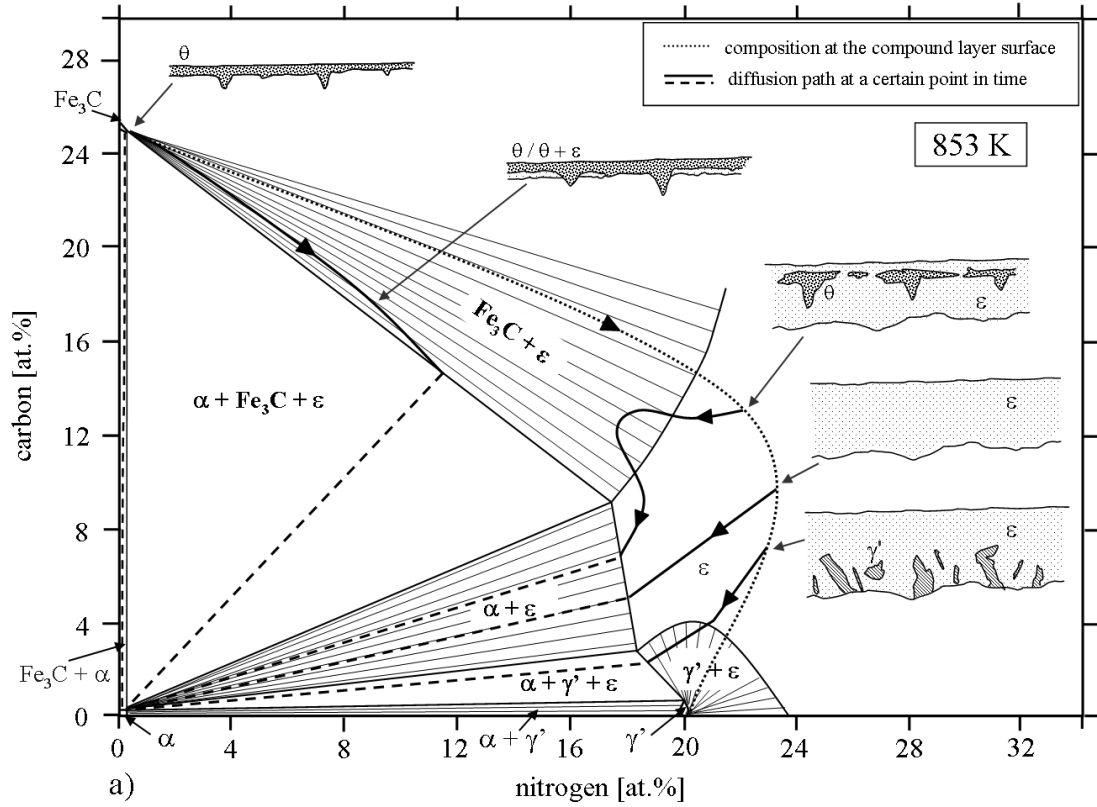
Fig. 2.7: Isothermal section of the metastable Fe-N-C phase diagram at 853 K. The time-dependent microstructural evolution of the compound layer from carbon-rich to nitrogen-rich phases upon

nitrocarburizing at 853 K is schematically illustrated by diffusion paths featuring at a given time the phase constitution and the lateral gross composition from the top to the bottom of the compound layer (solid lines with arrows for continuously changing gross composition, dashed lines for jumps in gross composition). a) Isothermal section with phase boundaries according to Ref. [41][9] showing the entire relevant range of composition. The time-dependent change of the gross composition at the surface is indicated by a dotted line with arrows. b) Iron-rich corner of the isothermal section showing the phase boundaries of the α-iron single-phase field [15]. The time-dependent change of the nitrogen and carbon content in the ferrite substrate at the surface and subsequently at the layer (cementite) / substrate (ferrite) interface upon nitrocarburizing has been schematically indicated by the dotted lines with arrows. For the points A and B see text. Within the α phase the diffusion path is not shown because the starting point (substrate surface) and the end point (substrate center) of the diffusion path change with time.

2.4.2 Thermodynamics: Microstructure and diffusion paths within the compound layer

In the following it will be shown that the observed phase constitution and interphase boundaries *within* the compound layer are in agreement with the metastable[10] ternary Fe-N-C phase diagram at 853 K [15, 21, 23, 27], i.e. "local equilibria" prevail at the interphase boundaries in the compound layer. As preparation for this discussion, the observations on the time-dependent development of the microstructure have been schematically summarized in Fig. 2.8.

---

[9] The invariant transition reaction $\gamma' + Fe_3C \rightarrow \alpha + \varepsilon$ was found to occur at a (single) temperature in the range between 833 K an 843 K, as determined by a series of experiments in Ref. [41]. However, according to calculations based on the CALPHAD database (2008) the invariant transition reaction $\alpha + \gamma' + \varepsilon \rightarrow \gamma$ would occur between 848 K and 853 K, which is not in agreement with Ref. [41] and with the here observed evolution of the compound-layer microstructure.

[10] "Metastable" because θ, ε and γ' are considered not to decompose into graphite, nitrogen gas and α-Fe as required for "stable" phase equilibria.
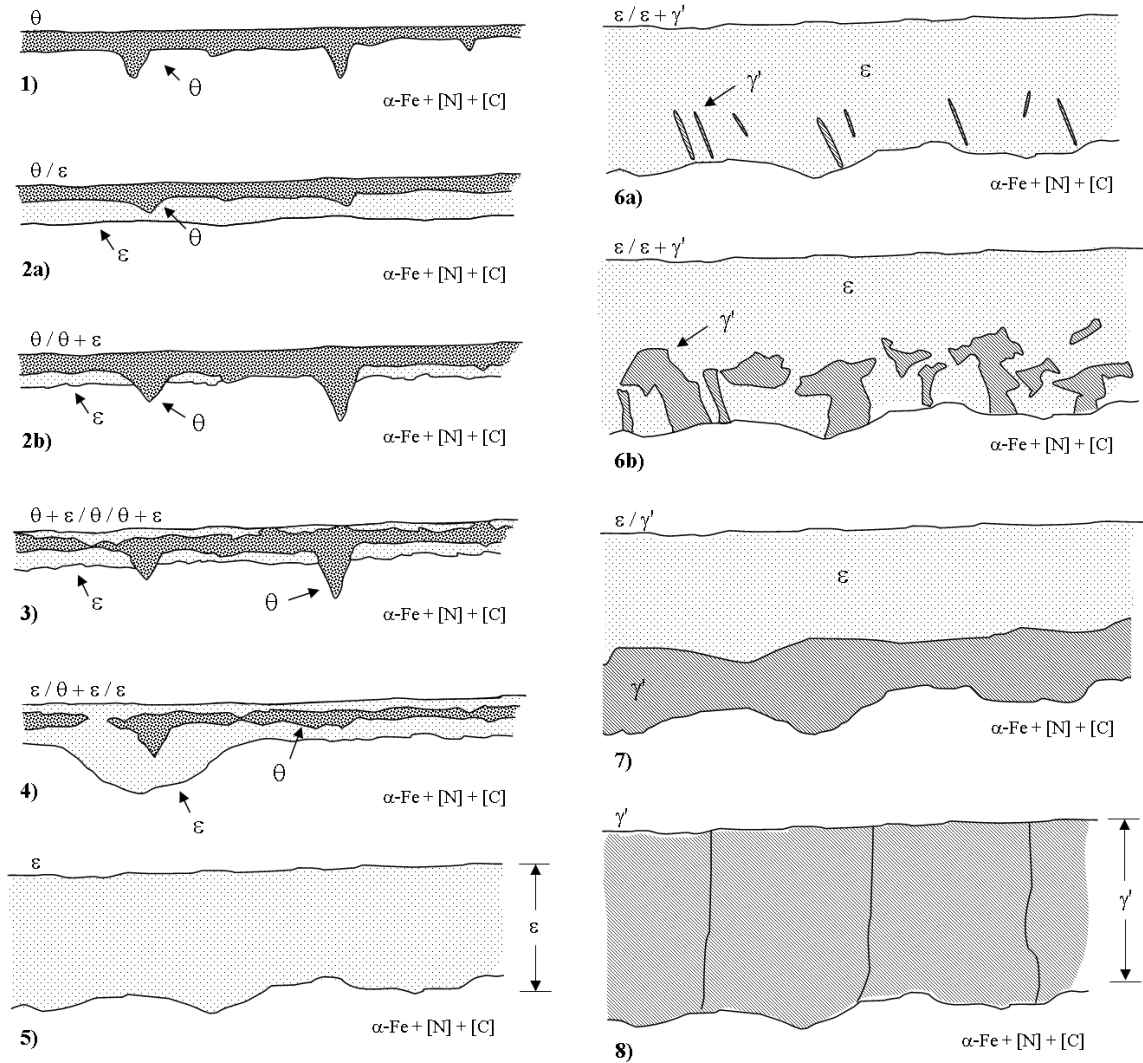
Fig. 2.8: Schematic illustration of the progressive microstructural stages of the compound-layer evolution on pure α-iron as function of time upon nitrocarburizing at 853 K. The development starts with the occurrence of a carbon-rich phase and proceeds towards nitrogen-rich phases along diffusion paths compatible with the Fe-N-C phase diagram; see Fig. 2.7a. 1) single-phase θ layer, 2a) θ / ε double layer, 2b) θ / $\theta + \varepsilon$ layer, 3) $\theta + \varepsilon$ / θ / $\theta + \varepsilon$ double layer, 4) ε / $\theta + \varepsilon$ / ε layer, 5) single-phase ε layer, 6a) ε with some γ' developing at regions close to the compound layer / substrate interface, 6b) ε / $\varepsilon + \gamma'$ double layer, 7) ε / γ' double layer, 8) single-phase γ' layer.

After the initial formation of a single-phase θ layer at the surface (stage 1) the subsequent formation of ε at the cementite layer / substrate interface occurs resulting in either a θ / ε (stage 2a) double layer or a θ / $\theta + \varepsilon$ double layer (stage 2b). Then, the amount of ε in the compound layer strongly increases by the growth of ε into the substrate and the

simultaneous conversion of cementite into ε [11] at the surface-adjacent region of the compound layer (stages 3 and 4), which development ends with the presence of a single-phase ε layer (stage 5). Next, the γ' phase is formed at the interface between the ε layer and the substrate leading to an ε / ε + γ' double layer (stages 6a,b) and then to an ε / γ' double layer (stage 7). The final stage of the compound layer development involves increasing the amount of γ' until a single-phase γ' layer results (stage 8). The occasional formation of an ε + γ' dual-phase layer (Figs. 2.2d,e) is not considered in Fig. 2.8 as a separate stage. It should be recognized that the single stages can overlap in time, as indicated by the laterally inhomogeneous nature of the microstructure of the compound layer (cf. Figs. 2.1 and 2.2 and see section 2.4.3).

In the final stage of compound-layer evolution a single-phase γ' layer is obtained (see Fig. 2.2f and stage 8 in Fig. 2.8). The γ'-phase can only contain little carbon due to its narrow composition range (see Table 2.1). So the question emerges, where the appreciable amount carbon taken up initially in the compound layer has gone to. The uptake of carbon by the α-iron substrate can be excluded due to the very small solubility limit of carbon in ferrite[12] (see Table 2.1). It is concluded that the carbon has escaped through the surface into the gas atmosphere.

Now, starting from the phase at the surface of the compound layer and its composition and ending at the α-iron substrate, different diffusion paths, representing the change of the lateral gross composition and phase constitution of the compound layer as function of depth at constant time, can be schematically indicated in the isothermal section of the ternary Fe-N-C phase diagram at 853 K for different stages of compound-layer growth. With reference to Fig. 2.8, proposals of these diffusion paths have been made in Fig. 2.7a; see the full lines with arrows (if possible the diffusion paths were simplified by straight lines). The time-dependent change in the microstructure of the compound layer implies that the diffusion path changes correspondingly during nitrocarburizing. It follows that the microstructural development as observed *within the*

---

[11] The possible conversion of cementite into ε was first reported in Ref. [58] upon nitriding of pearlitic substrates at 843 K.

[12] Moreover, as shown in Fig. 2.7, the formation of a single-phase γ' layer from a cementite and/or an ε containing compound layer is only possible if the carbon content in the α-iron substrate at the layer / substrate interface is decreased.

compound layer can be understood as a straightforward consequence of (a) the depth dependence of the gross composition at the stage of nitrocarburizing considered and (b) the thermodynamics of the Fe-N-C system, determining the solid-solid local equilibria. Consequently, kinetic constraints have not to be invoked to explain the microstructure *within the compound layer*.

A coexistence of cementite and γ' (i.e. cementite being directly in contact with γ' as reported for a temperature of *823 K* in Ref. [43]) was never observed in the present study pertaining to a temperature of *853 K*. This is in agreement with the ternary Fe-N-C phase diagram [15, 41] where a two-phase field of cementite and γ' does not exist at 853 K (cf. Fig. 2.7a). The two-phase equilibrium α + ε obtained in the microstructure of the compound layer upon nitrocarburizing of nitrogen pre-saturated substrates (series C; cf. Fig. 2.4b) clearly indicates the temperature of 853 K to be above the single temperature for the invariant reaction θ + γ' → ε + α in the Fe-N-C system, which is consistent with experimental results reported in Ref. [41], where this temperature has been claimed to lie in the range of 833 K − 843 K.

2.4.3 Kinetics: Origin of lateral inhomogeneity of the microstructure of the compound layer

Apart from the thermodynamically prescribed multiphase nature of the compound layer (see the above discussion and the diffusion paths in Fig. 2.7a), a lateral inhomogeneity of the microstructure is induced by the dramatic increase in the diffusive flux of nitrogen[13] through the compound layer at those regions, where the initially formed cementite layer has already been locally transformed into the ε phase. Nitrogen diffusion through cementite (formed in the first stage of nitrocarburizing) may vary locally depending on the local microstructure (e.g. the local presence of an initially high grain-boundary density may enhance the local flux of nitrogen through the cementite layer; cf. Ref. [19]). Consequently, along the θ / α interface a variation occurs for the time needed to attain the critical concentration of nitrogen in the substrate for the formation of ε at the

---

[13] The diffusional flux of carbon into the α-iron substrate can be neglected due to the very small solubility limit of carbon in ferrite; see Table 2.1.

θ / α interface (cf. point B in Fig. 2.7b). Upon prolonged nitrocarburizing this ε may grow from the θ / α interface through cementite to the surface of the compound layer. The growth of the ε phase may additionally occur by the conversion of θ into ε at the surface of the compound layer due to the gradually increasing chemical potential of nitrogen at the surface (cf. the discussion in section 2.4.1). Since the diffusivity of nitrogen through ε is much higher than through cementite, "short-circuit diffusion" of nitrogen through an ε "channel" becomes possible (cf. Fig. 2.9a, dashed arrow in Fig. 2.1e). Such nitrogen short-circuit diffusion, followed by a lateral diffusion of nitrogen through ε and α underneath the cementite layer will result in a laterally proceeding saturation of the substrate with nitrogen at the transformation front between θ and ε (cf. Fig. 2.6). This mechanism contributes to a laterally proceeding transformation of the cementite layer into an ε-rich compound layer (cf. Fig. 2.9b,c and see Figs. 2.1b-c, 2.1d-e, 2.2a-b and 2.2c-d). The (local) development of the ε phase at the surface of the compound layer can be observed macroscopically because the reflectivity of the cementite phase regions at the surface is higher than that of the ε phase regions.

It is noted that the thickness of the compound layer depends on the amount of cementite in the microstructure: cementite acts as a barrier for the inward diffusion of nitrogen and carbon, in particular as compared to the ε phase [8, 14, 42, 43, 54, 59]. Indeed, a retarded growth of the overall compound layer and thus a smaller compound-layer thickness was observed (also locally) for microstructures exhibiting (also locally) a high amount of cementite.
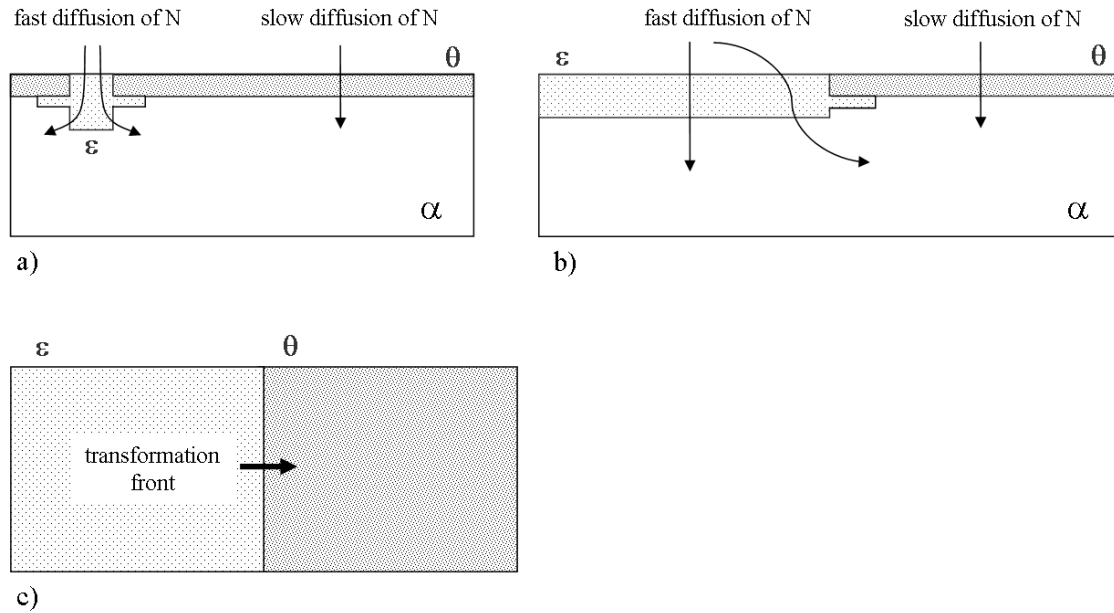
Fig. 2.9: Schematic illustration of a mechanism enhancing the lateral inhomogeneity of the microstructure of the compound layer. a) Cross-sectional view of the compound layer showing fast diffusion of nitrogen through ε at locations where the initially formed cementite layer has been locally converted into ε (the diffusion of nitrogen through cementite is comparably slow [42]). A diffusional carbon flux in the ferrite substrate is neglected due to the very small carbon solubility in ferrite. b) Following the short-circuit diffusion illustrated in a) and b) the lateral diffusion of nitrogen underneath the cementite layer leads to a lateral saturation of the substrate at the θ / ε transformation front and thus to the subsequent formation of ε, i.e. the θ / ε transformation front proceeds laterally at the specimen surface. c) Top view of the specimen shown in b).

2.5   Conclusions

1. The microstructural evolution of the compound layer developing upon nitrocarburizing of α-iron starts with the formation of carbon-rich cementite and develops into the direction of the nitrogen-richer and carbon-poorer phases ε and γ'.

2. Local equilibrium (or stationary state) conditions do *not* necessarily prevail at the gas / solid interface, at least not in the beginning of nitrocarburizing.

3. The initial formation of cementite, and the subsequent formation of ε, are the consequence of (i) a solubility of nitrogen in α-iron much larger than that of carbon and (ii) a rate of nitrogen transfer from the gas phase into the solid much lower than that of carbon, i.e. kinetics governs the developing composition and phase constitution *at* the gas / solid and compound layer / substrate interfaces.

4. Cementite acts as barrier for the inward diffusion of nitrogen. This leads to a retarded growth of the compound layer at locations where cementite is present, as well as initiates the lateral inhomogeneity of the microstructure as a consequence of "short circuit" diffusion of nitrogen through ε "channels" traversing the originally closed cementite layers.

5. Local equilibrium conditions *do* prevail within the compound layer at solid-solid phase boundaries. The change of the microstructure (phase constitution and lateral gross composition) as function of depth in the compound layer is compatible with so-called "diffusion paths" in the ternary Fe-N-C phase diagram, i.e. thermodynamics governs the microstructure *within* the compound layer. The use of diffusion paths is a powerful method to visualize the relation between the microstructure of the compound layer and (the isothermal section of) the corresponding phase diagram.

6. The courses of microstructural change of the compound layer as observed upon increasing treatment time at constant gas composition and as observed upon increasing nitriding potential at constant treatment time are identical.

7. A two-phase equilibrium $\varepsilon + \alpha$ occurs in the Fe-N-C system at 853 K as validated by the formation of θ / ε double layers on top of nitrogen pre-saturated α-iron substrates.

Chapter 3

Influence of the chemical potential of carbon on the microstructural and compositional evolution of the compound layer developing upon nitrocarburizing of α-iron

T. Woehrle[1], A. Leineweber[1], E.J. Mittemeijer[1,2]

[1]*Max Planck Institute for Metals Research, Stuttgart, Germany*
[2]*Institute for Materials Science, University of Stuttgart, Stuttgart, Germany*

Abstract

Controlled nitrocarburizing experiments were performed at 823 K and 853 K in order to systematically investigate the influence of the chemical potentials of carbon and nitrogen imposed by $NH_3/H_2/CO/CO_2/H_2O$-containing gas mixtures on the microstructural and compositional evolution of the compound layer formed on pure α-Fe substrates. The morphological evolution of the compound layer was investigated by optical microscopy. The nitrogen and carbon concentration-depth profiles in the layer were determined by electron-probe microanalysis (EPMA). Layer-growth kinetics was analysed on the basis of compound layer-thickness measurements. For a fixed chemical potential of nitrogen it was found that the microstructure and the layer-growth kinetics are strongly dependent on the chemical potential of carbon.

3.1   Introduction

Gaseous nitrocarburizing is a well-known thermochemical heat treatment process, usually performed at temperatures between 773 K and 853 K, that supplies nitrogen and carbon simultaneously to the surface of a ferritic iron or iron-based component. Provided that sufficiently high chemical potentials of nitrogen and carbon prevail in the gas atmosphere, a corrosion and wear resistant compound layer develops at the surface of the material, which can be composed of γ'-Fe_4N_{1-z} iron nitride, ε-$Fe_3(N,C)_{1+x}$ (carbo)nitrides [33, 60] and occasionally cementite θ-Fe_3C [31, 43] (cf. Fig. 3.1). The microstructure of the compound layer is influenced by both thermodynamics (local equilibria at solid-solid interfaces appear to be established, whereas this is not necessarily the case at the gas-solid interface) and kinetics (e.g. rates of uptake and diffusion of N and C; stationary state at the gas-solid interface). Not much is known about the morphological and compositional evolution of compound layers formed upon nitrocarburizing, due to a lack of systematic experiments. Such experiments are essential to understand the thermodynamics and kinetics governing the nitrocarburizing process.

The present project involves an investigation of the influence of the chemical potential of carbon on the microstructural and compositional evolution of the compound layer developing on top of pure α-iron substrates upon controlled nitrocarburizing at 823 K and 853 K in $NH_3/H_2/CO/CO_2/H_2O$-gas mixtures.
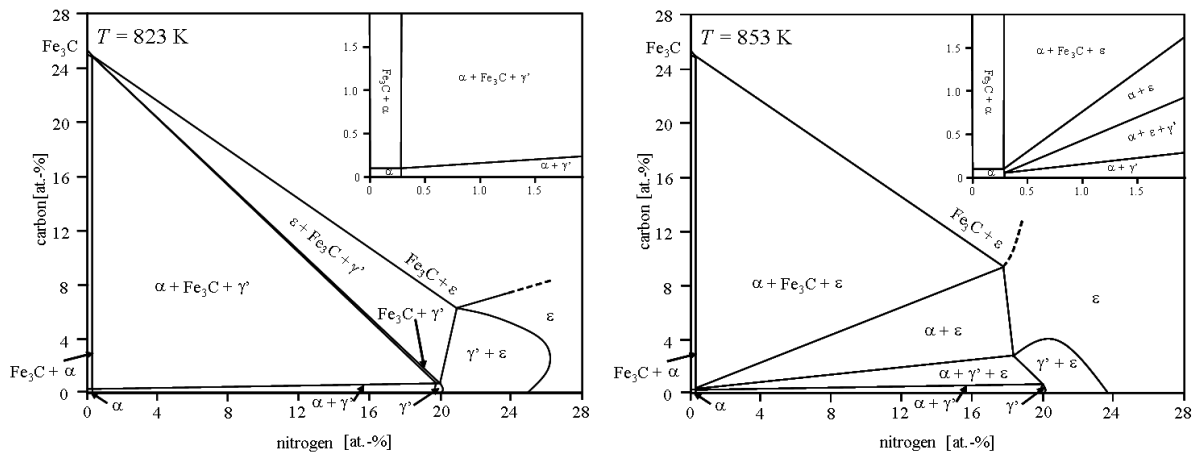
Fig. 3.1: Isothermal sections of the ternary Fe-N-C phase diagram at 823 K and 853 K. The phase boundaries have been approximated on the basis of experimental results according to the isothermal section at 773 K suggested by [21] and to the isothermal sections at 843 K – 853 K suggested by [23].

3.2   Experimental

Rectangular specimens of about $20 \times 25 \times 1$ mm³ were cut from cold-rolled iron plates (Alfa Aesar, 99.98 wt. %), recrystallized in hydrogen for 2 h at 973 K, ground, polished (final stage 1 µm diamond suspension) and cleaned ultrasonically in ethanol. The nitrocarburizing experiments were performed in a vertical quartz-tube furnace of 28 mm diameter, where the process temperature was controlled within $\pm$ 1 K. The nitrocarburizing atmosphere was composed of NH_3 (99.999 vol.%) as nitriding species, CO (99.997 vol.%) and CO_2 (99.999 vol.%) as carburizing species and evaporated H_2O. The flow rate of each gas species was adjusted separately by mass-flow controllers. To prevent significant dissociation of ammonia and side reactions in the gas atmosphere, which would affect the composition of the gas mixture, a constant overall gas-flow rate of 13.5 mm s^{-1} through the quartz-tube (calculated for gas volume at room temperature) was chosen. The gas mixtures were adjusted such that the two main carburizing reactions (the Boudouard reaction and the heterogeneous water-gas reaction) are associated with the same chemical potential of carbon [61, 62]. After nitrocarburizing the samples were quenched in nitrogen-flushed water to room temperature.

Optical microscopy was performed on cross-sections of the specimens using a Zeiss Axiophot microscope. For that purpose the specimens were covered with an electrodeposited protective nickel layer using a Watts bath to prevent destruction at the surface during sample preparation [33]. The specimens were then embedded (Polyfast, Buehler GmbH), ground, polished (final stage 1 µm diamond suspension) and etched in 1 vol.% Nital containing 0.1 vol.% HCl.

The average compound-layer thickness of the nitrocarburised specimens was determined from several light-optical micrographs of the cross sections (500x magnification) by measuring the distance from the interface with the substrate to the surface of the layer. A total number of 200 measurements were performed at each micrograph.

The nitrogen and carbon contents in the compound layer were determined by quantitative electron probe microanalysis (EPMA) on cross sections of the specimen using a Cameca SX100 microprobe equipped with five wavelength-dispersive spectrometers. For each specimen at least four line scans with a step size of 1 µm were performed perpendicular

to the surface at different locations of the compound layer. For detailed information see [43].

Two sets of nitrocarburizing experiments were performed at 823 K and at 853 K using a constant nitrogen activity[14], whereas the carbon activity[1] was varied from 0 up to 500 (cf. Table 3.1). For each temperature the nitrogen activities were within the activity range compatible with either the γ' region or the ε region of the phase diagram (cf. Fig. 3.3). The treatment time was set to 4 h.

Table 3.1: Process parameters used for controlled nitrocarburizing experiments.

Experiments	Temperature [K]	Time [h]	Nitrogen activity	Carbon activity
Set A823	823	4	626[*]	0 to 300
Set B823	823	4	417[**]	0 to 300
Set A853	853	4	553[*]	0 to 500
Set B853	853	4	415[**]	0 to 500

* Corresponds to the ε region of the phase diagram, ** Corresponds to the γ' region of the phase diagram (cf. Fig. 3.3).

3.3   Results

3.3.1   Compound-layer development upon nitrocarburizing

Nitrocarburizing experiments of set A823 yielded the formation of ε / γ'-double layers for all carbon activities applied in the gas atmosphere (cf. Fig. 3.2a). For nitrocarburizing experiments of set B823 a massive γ' layer was obtained at carbon activities in the range of $0 \leq a_C \leq 12.5$ (cf. Fig. 3.2b), whereas higher carbon activities resulted in the formation of ε / γ'-double layers (cf. Fig. 3.2c).

More complex microstructures were observed for set A853 and set B853. As for experiments of set A823, an ε / γ'-double layer had developed for set A853 up to a carbon

---

[14] The chemical potentials of nitrogen and carbon are directly related to the nitrogen and carbon activities by $\mu_i - \mu_i^0 = RT\ln(a_i)$, where $(i \in N, C)$, μ_i is the chemical potential of species i and μ_i^0 is the chemical potential of i in the reference state (the reference state is selected at the temperature concerned as nitrogen gas at 1 atm for a_N and graphite at 1 atm for a_C. The nitrogen and carbon activities obey $a_N = K_N r_N$ and $a_C = K_C r_C$, where K_N and K_C are the equilibrium constants of the nitriding and carburizing reactions and r_N and r_C are the corresponding nitriding and carburizing potentials [61].

activity of $a_C = 50$ (cf. Fig. 3.2d). Higher carbon activities ($a_C > 50$) resulted in the formation of either an $\varepsilon/\varepsilon + \gamma'$-double layer (cf. Fig. 3.2e) or an inhomogeneous microstructure composed of both ε/γ'-double layers and $\varepsilon/\varepsilon + \gamma'$-double layers. The $\varepsilon/\varepsilon + \gamma'$-double layers are characterized by interruptions of the γ'-sublayer, where the ε phase is in direct contact with the ferritic substrate (see arrows in Fig. 3.2e). Experiments of set B853 showed that a massive γ'-layer was obtained at carbon activities in the range of $0 \leq a_C \leq 15$ (cf. Fig. 3.2f), whereas at carbon activities between $a_C = 30$ and $a_C = 100$ an ε/γ'-double layer had developed (cf. Fig. 3.2g). Higher carbon activities of $a_C > 100$ resulted either in the formation of $\varepsilon/\varepsilon + \gamma'$-double layers (cf. Fig. 3.2h) or in the formation of inhomogeneous microstructures of ε/γ'-double layers (i.e. long ranges of ε/γ'-double layers without interruptions; see above) and $\varepsilon/\varepsilon + \gamma'$-double layers. The formation of cementite was not observed in any of the present experiments.
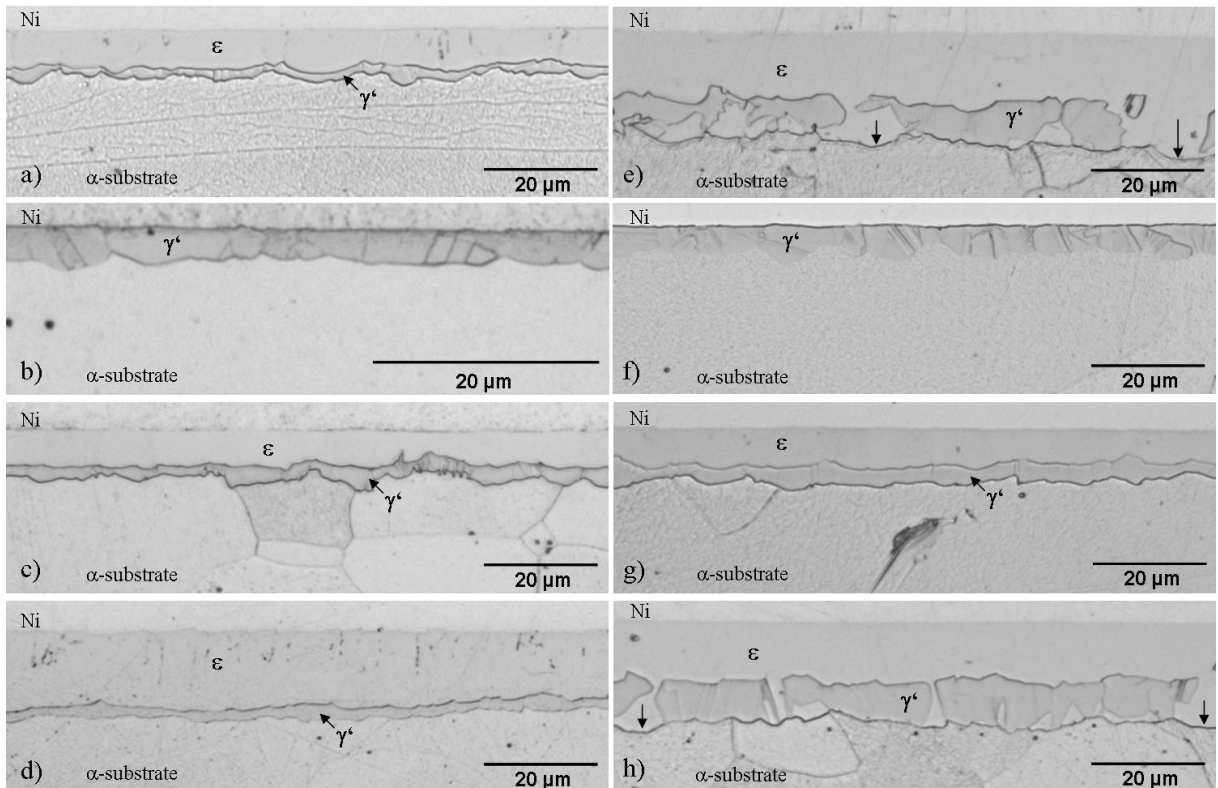
Fig. 3.2: Optical micrographs (after etching with 1 vol.% Nital containing 0.1 vol.% HCl) showing cross-sections of compound layers grown upon nitrocarburizing on α-Fe substrates for 4 h at 823 K and 853 K using a constant nitrogen activity and a variable carbon activity (cf. Table 3.1). a) set A823 with $a_C = 50$ showing an

ϵ / γ'-double layer, b) to c) set B823 with a_C = 12.5 and a_C = 50 showing a massive γ'-layer and an ϵ / γ'-double layer, respectively, d) to e) set A853 with a_C = 50 and a_C = 500 showing an ϵ / γ'-double layer and an ϵ / ϵ + γ'-double layer, respectively, f) to h) Set B853 with a_C = 15, a_C = 50 and a_C = 500 showing a massive γ'- layer, an ϵ / γ'-double layer and an ϵ / ϵ + γ'-double layer, respectively. The arrows in e) and h) indicate the presence of ϵ / α-iron substrate interfaces.

The solid phases obtained in contact with the nitrocarburizing atmosphere at the compound-layer surface have been presented superimposed on isothermal sections of the ternary Fe-N-C phase diagram as a function of the nitrogen and carbon activities at 823 K and 853 K in Fig. 3.3. Evidently, the phases formed at the compound-layer surface in many cases appear not to represent equilibrium with the gas atmosphere.
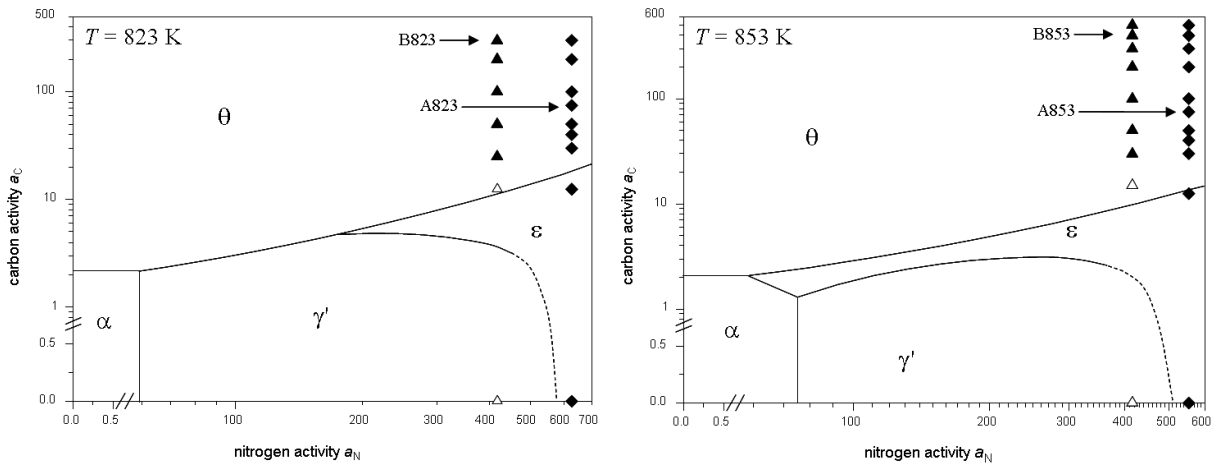
Fig. 3.3: Isothermal sections of the ternary Fe-N-C phase diagram as function of nitrogen and carbon activities at 823 K and 853 K. Solid lines were obtained by thermodynamic calculations according to the procedure described in [15]. Dashed lines were drawn to comply with the phase boundaries presented in [18]. Solid points represent the formation of ϵ at the compound-layer surface and open points represent the formation of γ' at the compound-layer surface.

3.3.2   Layer-growth kinetics

The compound-layer thickness after treatment times of 4 h is shown in Fig. 3.4 as function of the carbon activity, at constant nitrogen activity, for all sets of nitrocarburizing experiments. The thickness of single-phase, γ'-layers decreases as the carbon activity increases (see Figs. 3.4b and 3.4d at a_C < 25). For the case of ϵ / γ'-double layers, the thickness of the ϵ sublayer increases, the thickness of the γ' sublayer decreases and the total layer thickness increases with increasing carbon activity up to a_C = 50. An almost constant

total layer thickness is reached at $a_C > 50$. For the case of $\varepsilon / \varepsilon + \gamma$'-double layers (cf. Figs. 3.2e and 3.2h) a strongly increased total layer thickness occurs, as compared to the case of ε / γ'-double layers, which is in particular evident for compound layers showing an inhomogeneous (i.e. mixed ε / γ'- and $\varepsilon / \varepsilon + \gamma$'-double layers; cf. section 3.3.1) microstructure (see data connected by dashed lines in Fig. 3.4c). It follows from Fig. 3.4a to Fig. 3.4d that the general tendencies of the sub- and total layer thickness as function of the carbon activity are the same in all sets of experiments, albeit the microstructures vary distinctly.
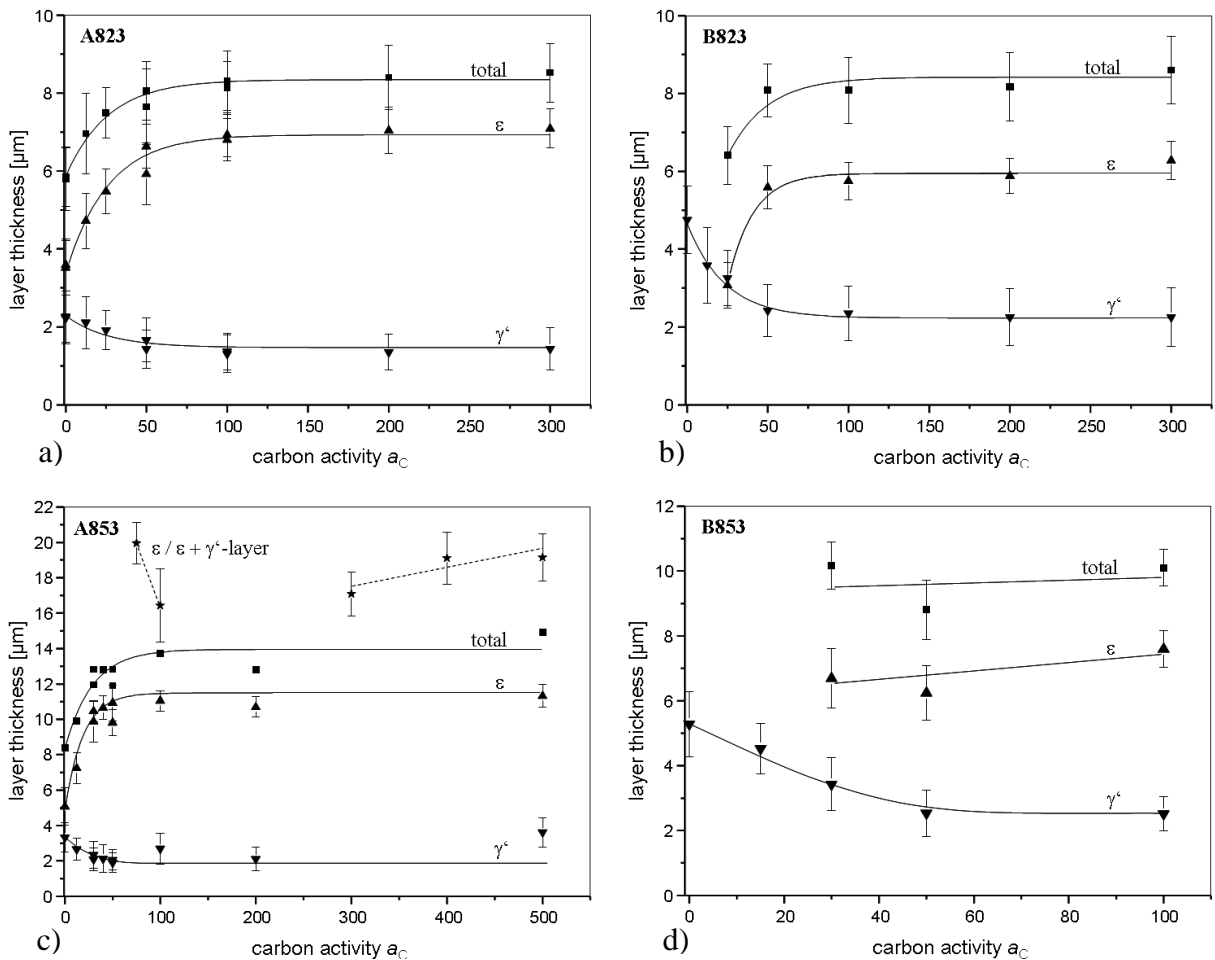
Fig. 3.4: Thickness of the total compound layer, the ε sublayer and the γ' subayer as function of carbon activity as obtained for the nitrocarburizing experiments of a) set A823, b) set B823, c) set A853 and d) set B853. The treatment time was 4 h and the nitrogen activity was kept constant according to Table 3.1. The solid and dashed lines have been drawn to guide the eye and indicate general trends in the compound-layer thickness as function of the carbon activity. The dashed lines indicate layer thicknesses obtained for $\varepsilon / \varepsilon + \gamma$'-double layers (see text).

3.3.3   Compositional evolution

The average contents of nitrogen and carbon in the ε-phase at the surface of the compound layer are shown as function of carbon activity for the experiments of set A823 in Figure 3.5. Increasing the carbon activity in the gas atmosphere leads to an increase of the carbon content and to a decrease of the nitrogen content at the compound-layer surface, while the total atomic content of interstitial (N and C) remains practically constant. This suggests a substitution of nitrogen by carbon upon increasing the carbon activity: within the range of adjusted carbon activities ($0 \leq a_C \leq 300$), the amount of nitrogen decreases from 25.3 at.% to 21.0 at.%, whereas the amount of carbon increases from 0 at.% to about 4.3 at.%. The total content of interstitials (N + C) is around 25.3 at.%.
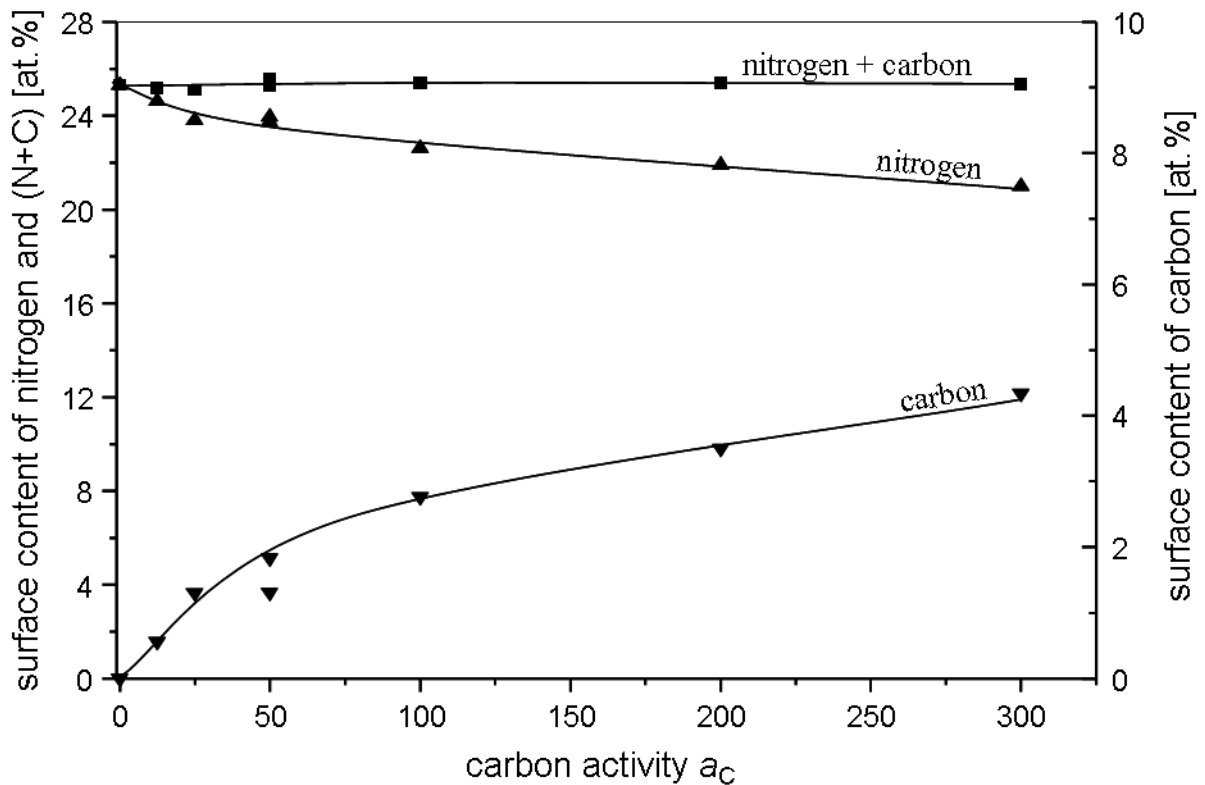
Fig. 3.5: Nitrogen and carbon contents in the ε phase at surface of the compound layer as determined by EPMA for the experiments of set A823. Solid lines have been drawn to guide the eye.

3.4 Discussions

3.4.1 Solid-gas phase equilibria – Microstructural and compositional evolution at the compound-layer surface

As predicted by the Lehrer diagram [16], pure nitriding experiments ($a_C = 0$) resulted in the formation of γ' at the compound-layer surface for the sets B823 and B853 and the formation of ε at the compound-layer surface for the sets A823 and A853 (cf. Fig. 3.3). These results are compatible with the possible establishment of local equilibrium between the nitriding atmosphere and the Fe-N solid phases at the surface of the compound layer. Considering the nitrocarburizing experiments of sets B823 and B853 ($a_C > 0$), the development of ε on top of γ' occurs upon exceeding a critical carbon activity a_C in the gas atmosphere. This minimum carbon activity is $12.5 < a_C < 25$ for set B823 and $15 < a_C < 30$ for set B853 (cf. Fig. 3.3). The tendency to favour ε over γ' with increasing a_C in the nitrocarburizing atmosphere is in qualitative agreement with isothermal sections of the ternary Fe-N-C phase diagram calculated on the basis of the approach by [15] (other assessments [21] yield qualitatively similar results). However, the quantitative, experimentally determined critical a_C values for the "γ' $\rightarrow$ ε transition" at the compound-layer surface are considerably higher than predicted (for the applied a_N values; cf. Fig. 3.3, Figs. 3.2c and 3.2d). Moreover, no cementite was found at the compound-layer surface, not even at very high carbon activities of $a_C = 500$, although the thermodynamic calculations indicate that the critical carbon activity for the formation of cementite is in-between $a_C = 8$ and $a_C = 20$ for the conditions applied in the experiments. Here it is noted that nitrocarburizing experiments performed at 848 K in $NH_3/H_2/CO/CO_2$-gas mixtures as reported in [14] resulted in the formation of cementite at a relatively low carbon activity of $a_C = 2.9$ for treatment times of 35 min to 240 min.

In case of genuine gas-solid equilibrium established at the specimen surface, not only the phases (ε or γ' or cementite) but also the nitrogen and carbon contents in the respective phases at the compound-layer surface should systematically reflect the nitrogen and carbon activities imposed by the nitrocarburizing gas atmospheres. The above discussed differences between the experimental results for the phases and their composition at the surface of the compound layer and the corresponding data calculated for prevalence of

thermodynamic equilibrium may suggest that a stationary state rather than a local equilibrium has been established at the gas-atmosphere / specimen-surface interface.

The experiments of set A823 show that for a constant a_N, the carbon content in ε at the compound-layer surface increases, at the expense of the nitrogen content, as a_C increases (cf. Fig. 3.5). This "substitution" effect is consistent with experimental results obtained by gaseous nitrocarburizing of thin iron foils in $NH_3/H_2/CO/CO_2$ gas mixtures at 843 K [63] and with thermodynamic calculations according to [15].

3.4.2 Solid-solid phase equilibria – Microstructural evolution and growth kinetics of the compound layer

The nitrocarburizing experiments resulted in three different types of microstructures: massive γ'-layers (Fig. 3.2b), ε / γ'-double layers (Fig. 3.2a) and $\varepsilon / \varepsilon + \gamma'$-double layers (Fig. 3.2e). The first two microstructures can be also obtained upon pure nitriding, whereas the third microstructure can only be obtained upon nitrocarburizing. All observed microstructures of the compound layer are compatible with the occurrence of local equilibrium at the solid phase – solid phase interfaces.

The formation of $\varepsilon / \varepsilon + \gamma'$-double layers occurred by nitrocarburizing at $T = 853$ K (sets A853 and B853) and not at $T = 823$ K (sets A853 and B853). These observations can be understood as a consequence of the invariant transition reaction $\gamma' + \theta \rightarrow \alpha + \varepsilon$ at a critical temperature T_{In} of about 833 K $< T_{In} <$ 843 K [41]: the invariant reaction indicates the existence of a two-phase equilibrium of α and ε at $T > T_{In}$, implying the possible occurrence of ε / α interfaces (compatible with local equilibria in the solid state) as observed at the interface of $\varepsilon / \varepsilon + \gamma'$-double layers and the α-iron substrate at a temperature of 853 K, but not at 823 K.

The development of microstructures composed of $\varepsilon / \varepsilon + \gamma'$-double layers appears to be promoted by an increase in a_C (at $a_C > 50$ for sets A853 and B853), thus in association with an increasing carbon content in the compound layer, which is compatible with the nitrogen and carbon concentration range of the $\alpha + \varepsilon$ phase boundary in the ternary Fe-N-C phase diagram at 853 K (Fig. 3.1).

The microstructure of the compound layer influences the compound-layer growth kinetics

(cf. Fig. 3.4). The transition from a single-phase γ'-layer to an ε / γ'-layer by exceeding a critical a_C (at constant a_N), leads to a strongly increased growth rate of the compound layer, which is ascribed to a higher intrinsic diffusivity of N and C in ε as compared to γ'. The increase of the total ε / γ'-layer thickness approaches a plateau for $a_C > 50$. The highest growth rate was found upon (local) transition from an ε / γ'-double layer microstructure to an ε / ε + γ'-double layer microstructure, resulting in regions of the compound layer where the ε phase extends over the whole layer. At such regions, the ε phase provides a fast diffusion path for the interstitials N and C from the surface directly to the compound-layer / substrate interface, by by-passing the γ' phase, which acts as a barrier for the inward diffusion of nitrogen and carbon.

3.5 Conclusion

1. At a given temperature and treatment time, the microstructural evolution of the compound layer developing upon nitrocarburizing on pure α-iron substrates is governed by the chemical potentials of nitrogen and carbon in the gas atmosphere. Stationary states may prevail at the compound-layer / gas-atmosphere interface; local equilibria may occur at the solid phase - solid phase interfaces within the compound layer.

2. As indicated by the ternary Fe-N-C phase diagram, for nitrogen activities corresponding to γ' phase formation upon nitriding of pure iron, the formation ε on top of γ' is induced by imposing a carbon activity exceeding a critical value in the nitrocarburizing atmosphere, thus causing the formation of ε / γ' double layers.

3. The formation of ε / ε + γ'-double layers was only observed at 853 K and at very high carbon activities and can be explained by the occurrence of an invariant transition reaction γ' + θ → α + ε at a critical temperature T_{In} (833 K < T_{In} < 843 K).

4. Layer-growth kinetics strongly depend on the phase composition of the compound layer. The slowest growth rates occur for compound layer composed of massive γ'. The ε / γ'-

double layers and in particular the $\varepsilon / \varepsilon + \gamma$'-double layers show much higher growth rates.

5. Increasing the carbon activity in the gas atmosphere leads to a decrease in the nitrogen content and an increase in the carbon content in the ε phase$\square$ at the compound-layer surface. The overall interstitial, atomic content of N and C remains almost constant, implying a substitution of nitrogen by carbon.

Chapter 4

Multicomponent interstitial diffusion in and thermodynamic characteristics of the interstitial solid solution ε-Fe$_3$(N,C)$_{1+x}$; nitriding and nitrocarburizing of pure α-iron

T. Woehrle[1], A. Leineweber[1], E.J. Mittemeijer[1,2]

[1]*Max Planck Institute for Intelligent Systems (formerly Max Planck Institute for Metals Research), Heisenbergstraße 3, D-70569 Stuttgart, Germany*
[2]*Institute for Materials Science, University of Stuttgart, Stuttgart, Germany*

Abstract

A series of gas nitriding and gas nitrocarburizing experiments was performed at 823 K to investigate the growth kinetics of ε-Fe$_3$(N,C)$_{1+x}$ / γ'-Fe$_4$N$_{1-z}$ -double layers on pure α-iron substrates. The growth rate and composition of the (sub)layers were determined by (sub)layer-thickness measurements using light optical microscopy and electron-probe microanalyses (EPMA), respectively. Models for the growth of bilayers into a substrate, controlled by the interstitial diffusion of two elements (N and C), were applied to the experimental data to determine the intrinsic diffusion coefficients of N and C in ε-Fe$_3$(N,C)$_{1+x}$ as well as the self-diffusion coefficient of N in γ'-Fe$_4$N$_{1-z}$. For ε-Fe$_3$(N,C)$_{1+x}$ it was found that the four components of the diffusion matrix, D_{NN}^ε, D_{CC}^ε, D_{NC}^ε and D_{CN}^ε, are all positive. The significant values of the off-diagonal diffusivities D_{NC}^ε and D_{CN}^ε indicate profound interaction of both interstitial species. Thereby, additional information is obtained about the thermodynamic properties of the ε phase in the ternary Fe-N-C system.

4.1 Introduction

Diffusion-controlled processes and phase transformations in material systems are of great technological importance, e.g. solid-state reactions in solder joints, microelectronics, and thermochemical surface treatments. The scientific interest in diffusion processes derives from the aspiration to comprehend the relation between the thermodynamics and the kinetics of matter.

In particular fundamental understanding of *multicomponent* diffusion phenomena is essential for the development and optimization of high performance materials. In most cases, the driving force for diffusion is given by the gradients of the chemical potentials (= partial Gibbs energies) of all diffusing components, which are related to the corresponding concentration gradients in the phases in which diffusion takes place [12, 29, 64-66].

Most of the published works on diffusion in ternary systems concern substitutional solid solutions [12, 64]. Compared to diffusion in ternary *substitutional* solid solutions, until now only a few studies have been conducted on diffusion in ternary *interstitial* solid solutions composed of one substitutional and two interstitial species. The evaluation of diffusion kinetics, i.e. the assessment of the intrinsic diffusion coefficients, provides information about the thermodynamic properties of a multicomponent phase.

A specific case of diffusion in interstitial solid solutions occurs upon gas nitriding and gas nitrocarburizing of iron and iron-based alloys, usually performed at temperatures between 823 K and 853 K. During these processes nitrogen or nitrogen and carbon diffuse into the surface of a ferritic workpiece. Sufficiently high chemical potentials of nitrogen or nitrogen and carbon imposed by the nitriding/nitrocarburizing atmosphere lead to an iron(carbo)nitride compound layer growing at the surface of the workpiece. The compound layer is typically composed of the iron(carbo)nitrides ε-Fe$_3$(N,C)$_{1+x}$, with a relatively wide homogeneity range, and γ'-Fe$_4$(N,C)$_{1-z}$, with a relatively narrow composition range close to the ideal stoichiometric composition of Fe$_4$N (see section 4.4.2) [7, 33, 51]. Moreover, under certain nitrocarburizing conditions, the formation of θ-Fe$_3$C (cementite) can occur [31, 43]. Because of its wide homogeneity range the ε-Fe$_3$(N,C)$_{1+x}$ phase serves as an excellent model system to study the thermodynamics of multicomponent interstitial solid solutions. The thermodynamics and the growth kinetics

of ε-Fe$_3$(N,C)$_{1+x}$ (usually in association with the simultaneous growth of γ'-Fe$_4$(N,C)$_{1-z}$) have been subject of a number of investigations [14, 15, 21, 23, 30, 31, 38, 50, 51, 54]. Nevertheless, until now, quantitative data on the interstitial diffusivities of N and C in ε have not been determined. Such data, once available, can be used to (in)validate the thermodynamic models of the ε phase, in particular in view of such contradictory descriptions for ε-Fe$_3$(N,C)$_{1+x}$ given in Refs. [15] and [21].

In the present work, the growth kinetics of γ' single layers and of ε / γ' double layers, obtained by, respectively, gas nitriding and gas nitrocarburizing of pure α-iron substrates at 823 K, have been investigated to expose the thermodynamics of interstitial solid solutions in the ternary Fe-N-C system. Experimentally determined layer-growth kinetics and concentration-depth profiles have been used to calculate the four intrinsic diffusion coefficients in the ε phase, D_{kj}^{ε} with $(k, j \in \mathrm{N,C})$. It follows that in particular the "off-diagonal" diffusion coefficients $D_{\mathrm{NC}}^{\varepsilon}$ and $D_{\mathrm{CN}}^{\varepsilon}$ are significant and thus reveal the pronounced thermodynamic interaction of N and C in the ε-Fe$_3$(N,C)$_{1+x}$ phase. The results have been compared with different thermodynamic descriptions of the ε-Fe$_3$(N,C)$_{1+x}$ phase determined on the basis of assessments of the Fe-N-C system [15, 21].

4.2   Experimental

Rectangular α-iron samples of dimensions $20 \times 25 \times 1$ mm³ were cut from cold-rolled iron plates (Alfa Aesar, 99.98 wt. %), ground, polished (final stage 1 µm diamond suspension), cleaned ultrasonically in ethanol and, finally, recrystallized for 2 h at 973 K in a hydrogen gas flow of 200 ml·min^{-1}. Immediately before the nitriding /nitrocarburizing process, the specimens were polished (final stage 1 µm diamond suspension) and cleaned in ethanol.

For gas nitriding/nitrocarburizing a vertical quartz-tube furnace of 28 mm diameter was used [62]. The specimen was placed in the middle of the furnace by a quartz fibre. The furnace temperature of 823 K was controlled within ± 1 K. The composition of the gas atmosphere was adjusted by separate mass-flow controllers for

NH_3 as nitriding species, CO and CO_2 as carburizing species, N_2 as inert gas, H_2 and evaporated H_2O (all gases from Westfalen AG with a purity of 99.999 vol.%, except CO with a purity of 99.997 vol.%). The overall linear gas-flow rate through the quartz tube was 13.5 mm$\cdot$s^{-1} (calculated for the gas volume at room temperature) in order to prevent significant ammonia dissociation and side reactions in the gas atmosphere, which would affect the composition of the gas mixture. The gas-supply lines were heated to 393 K to avoid the formation of ammonium bicarbonate upon nitrocarburizing. After the heat treatment the specimens were quenched in nitrogen-flushed water.

The nitrided/nitrocarburized samples were cut into three pieces for investigation by optical microscopy, X-ray diffraction (XRD) analysis and electron-probe microanalysis (EPMA).

For optical microscopy and EPMA analysis the specimens were covered with an electrodeposited protective nickel layer using a Watts bath [33] at 333 K to avoid mechanical damaging of the surface layer during sample preparation. The specimens were then embedded (Polyfast, Struers GmbH), ground, polished (final stage 1 µm diamond suspension) and etched in 1 vol.% Nital containing 0.1 vol.% HCl [34].

Optical microscopy was performed at a Zeiss Axiophot microscope. The thicknesses of the entire compound layer and the sublayers were determined separately from at least four (mostly six) light-optical micrographs of cross sections (500x magnification) of the specimens investigated by measuring the distance from the interface to the surface of the layer at 200 laterally equidistant positions.

The nitrogen- and carbon-content depth profiles in the compound layer were determined simultaneously by quantitative electron probe microanalysis (EPMA) performed on cross sections of the specimens using a Cameca SX100 microprobe equipped with five wavelength-dispersive spectrometers. For each specimen at least three (mostly five) line scans with a step size of 1 µm were performed perpendicular to the surface at different locations of the compound layer. In order to remove carbon contaminations on the cross-sectional surface an air jet was used before the measurement: oxygen was blowed for 40 seconds onto the cross section at the position of the focused electron beam. To determine the elemental concentrations, the intensities of the characteristic N-K_α, C-K_α and Fe-K_α radiations excited by an incident 10 keV-electron

beam were measured simultaneously at each measurement point. The data were compared to the K_α intensities of N, C and Fe obtained, for the same measurement conditions, from standard specimens of γ'-Fe$_4$N$_{1-z}$, θ-Fe$_3$C and α-Fe. The concentrations of N, C and Fe were calculated from the corresponding intensity ratios applying the $\Phi(\rho z)$ approach [67].

For phase identification X-ray diffractometry was applied using a PANalytical X'Pert Mulit-Purpose Diffractometer equipped with a graphite monochromator in the diffracted beam (Co-K$_\alpha$ radiation) and Bragg-Brentano geometry. The specimens were rotated around their surface normal during the measurement to obtain better crystallite statistics.

Four series of nitriding/nitrocarburizing experiments were performed to investigate the growth kinetics and composition of ε / γ'-double layers during nitriding and nitrocarburizing at 823 K as function of treatment time and as function of the carbon activity[15] (at constant nitrogen activity) in the gas atmosphere. The nitrocarburizing experiments were performed in an NH$_3$/H$_2$/N$_2$/CO$_2$/CO/H$_2$O gas mixture, whereas for pure nitriding an NH$_3$/H$_2$/N$_2$ gas mixture was applied. The nitrocarburizing atmospheres were designed such that the two main carburizing reactions, the Boudouard reaction and the heterogeneous water-gas reaction, are associated with the same chemical potential of carbon [62]. The corresponding nitrogen and carbon activities have been calculated as described in Ref. [62]. The process parameters have been given in Table 4.1 (detailed information about the gas composition is given in the Appendix B).

Series A1 and A2 were performed to examine the growth kinetics of ε / γ'double-layers upon gas nitriding and gas nitrocarburizing at a nitrogen activity of $a_N = 636$ and a carbon activity of $a_C = 0$ and $a_C = 50$, respectively.

Series B1 and B2 were conducted to investigate the influence of the carbon activity a_C in the gas atmosphere on the growth kinetics and composition of ε / γ' double

---

[15] The chemical potentials of nitrogen and carbon in the nitriding/nitrocarburizing atmosphere are directly related to the corresponding activities by the equation $\mu_k = \mu_k^0 + RT\ln(a_k)$, where $k \in \{N, C\}$, μ_k is the chemical potential of species k and μ_k^0 is the chemical potential of k in the reference state (nitrogen gas at 1 atm for a_N and graphite at 1 atm for a_C, at the temperature concerned).

layers upon nitrocarburizing at nitrogen activities of $a_N = 636$ and $a_N = 417$, respectively. The treatment time was 4 h and the carbon activity was varied from $a_C = 0$ to $a_C = 300$.

Table 4.1: Process parameters used for nitriding and nitrocarburizing at 823 K.

experiments	temperature [K]	nitrogen activity a_N*	carbon activity a_C	treatment time [h]
series A1	823	636	0	0-6
series A2	823	636	50	0-8
series B1	823	636	0-300	4
series B2	823	417	0-300	4

* Pure nitriding ($a_C = 0$) using a nitrogen activity of $a_N = 417$ at 823 K would result in the formation of a γ' iron-nitride surface layer, whereas at $a_N = 636$ the formation of an ε/γ' double layer would occur [16].

4.3 Modeling of interstitial diffusion for growing ε / γ' double layers

Modeling of the diffusion of N and C in ε and γ' for the case of the growth of ε / γ'-double layers on α-Fe plates is based on the following assumptions: (i) the surface and all interfaces of the ε / γ'-double layer are planar and parallel to each other; (ii) the ε / γ' double layer prevails during the whole nitrocarburizing process, e.g. intermediate cementite formation does not occur (see Ref. [60]); (iii) as shown in Ref. [38] the volume of the unit cell per iron atom of all phases (ε, γ' and α) can be taken approximately equal and independent of the N and C contents. Hence, within this approximation, the overall volume of the specimen does not change significantly upon nitriding/nitrocarburizing; (iv) the N and C contents at both sides of the ε / γ' interface and at both sides of the γ' / α interface are constant and compatible with so-called local thermodynamic equilibrium[16]; (v) the concentration-depth profiles of N and C in ε-$Fe_3(N,C)_{1+x}$ are linear (see results in section 4.4.2); (vi) the γ' phase has an ideal stoichiometric composition of Fe_4N with a N content of 20 at.%, i.e. the concentration gradient in the γ' (sub)layer is taken zero. However, the chemical potential gradient of N over the γ' phase is taken into account; (vii) the solubilities of C in α-Fe and in γ' are very low and can thus be neglected

---

[16] Even for local equilibrium, for example at the ε/γ' interface, the position of the diffusion path [10, 11, 59] of N and C in ε (see section 4.4.2; Fig. 4.7) and the corresponding concentrations $c_N^{\varepsilon/\gamma'}$ and $c_C^{\varepsilon/\gamma'}$ in ε at the ε/γ' interface are not necessarily constant and may change as a function of time according to the tie-lines in the ε+γ' two-phase region of the Fe-N-C phase diagram. The concentration variations at all interfaces of the compound layer, assumed to experience local thermodynamic equilibrium, are, however, assumed to be very slow and thus, for example, $c_N^{\varepsilon/\gamma'}$ and $c_C^{\varepsilon/\gamma'}$ in ε at the ε/γ' interface are practically independent of time.

(compare Fig. 4.6); (viii) the intrinsic diffusion coefficients D_{kj}^{ε} with ($k, j \in$ N,C) are independent of concentration (see section 4.5.2); (ix) the iron atoms in the compound layer and in the substrate are immobile at the nitriding/nitrocarburizing temperature of 823 K. Thus, the intrinsic diffusion coefficient of iron is $D_{\text{Fe}}^{\phi} \approx 0$, where $\phi \in \{\varepsilon, \gamma', \alpha\}$; (ix) the intrinsic diffusion coefficients D_{kj}^{ε} with $(k, j \in$ N,C$)$ are taken independent of concentration (see section 4.5.2).

In contrast with other works [37, 59], it was taken into account that the α-iron substrate is continuously saturated with nitrogen upon nitriding and nitrocarburizing under the applied conditions as indicated by numerical calculations, i.e. after a treatment time of 4 h at 823 K (pertaining to series B1 and B2) an α-iron substrate of 1 mm thickness contains (only) 87% of the maximum possible nitrogen content in α (after 9 h at 823 K: 99%).

The intrinsic diffusion coefficients can be evaluated applying a model for the diffusion-controlled growth of a bilayer into a substrate. Such a model has been presented in Ref. [54] for modeling the growth kinetics of ε / γ' double layers upon pure nitriding.

The growth of an ε / γ' double-layer into an α-iron substrate upon nitrocarburizing can be described by the shift of the interfaces, ε / γ' and γ'/ α, due to a difference in the diffusive fluxes of interstitial species arriving at an interface and the diffusive fluxes of interstitial species away from that interface. The resulting flux balance equations at the shifting ε/γ'and γ'/α interfaces are given by [38, 54]

$$\varepsilon/\gamma': \quad v^{\varepsilon/\gamma'}\left(c_k^{\varepsilon/\gamma'} - c_k^{\gamma'/\varepsilon}\right) = J_k^{\varepsilon/\gamma'} - J_k^{\gamma'/\varepsilon} \tag{4.1}$$

$$\gamma'/\alpha: \quad v^{\gamma'/\alpha}\left(c_k^{\gamma'/\alpha} - c_k^{\alpha/\gamma'}\right) = J_k^{\gamma'/\varepsilon} - J_k^{\alpha/\gamma'} \tag{4.2}$$

where $c_k^{I/II}$ is the concentration of species k $(k \in$ N,C$)$ in phase I at the interface between I and II $\left(I, II \in \{\varepsilon, \gamma', \alpha\}\right)$ expressed as a quantity per unit volume, $J_k^{I/II}$ is the flux of k

in phase *I* at the interface *I/II* and $v^{I/II}$ is the growth rate of the *I/II* interface. Note that the boundary condition (vii) implies that the fluxes of C in γ' and in α are zero, i.e. $J_C^{\gamma'/\varepsilon} = J_C^{\gamma'/\alpha} = J_C^{\alpha/\gamma'} = 0$ (cf. Fig. 4.1).

In order to maintain the concentration-depth profile in a (sub)layer during layer growth a certain amount of solute has to be consumed, which leads to a decrease in the diffusive flux of the interstitial species from one interface of the (sub)layer to the other interface of the (sub)layer. Adopting a linear concentration-depth profile (see assumption (v)) the following flux balance equations hold for the growing ε-sublayer [54]

$$\frac{1}{2} v^{\varepsilon/\gamma'} \left(c_k^{\varepsilon/gas} - c_k^{\varepsilon/\gamma'} \right) = J_k^{\varepsilon/gas} - J_k^{\varepsilon/\gamma'}. \tag{4.3}$$

The amount of nitrogen required to maintain the (N) concentration-depth profile in the γ' sublayer is zero since the γ' phase is assumed to be ideal stoichiometric, i.e. $c_N^{\gamma'/\varepsilon} = c_N^{\gamma'/\alpha}$ and thus $J_N^{\gamma'/\varepsilon} - J_N^{\gamma'/\alpha} = 0$ (cf. Eq. (4.3)). As a consequence, the flux of N in γ' at the ε/γ' interface is equal to the flux of N in γ' at the γ'/α interface, $J_N^{\gamma'/\varepsilon} = J_N^{\gamma'/\alpha}$, implying quasi-steady state diffusion[17] of N in γ', i.e. at a given time the flux of N through the γ' sublayer is independent of the position.

The four intrinsic diffusion coefficients D_{kj}^{ε} can then be obtained from Eqs. (4.1) to (4.4) on the basis of values for the diffusive fluxes of $J_N^{\alpha/\gamma'}$, $J_N^{\varepsilon/gas}$, $J_C^{\varepsilon/gas}$ and $J_N^{\gamma'/\varepsilon}$, which can be obtained from experimental data (see what follows in section 4.4.3). However, a complication arises since the α-Fe substrate has a finite thickness of $L^{\alpha} = 1$ mm and is thus gradually saturated with nitrogen upon nitrocarburizing (see above). Consequently, the concentration-depth profiles of N and C in the sublayers of the compound layer as well as the (sub)layer growth rates are *not* invariant to $\lambda = x/\sqrt{t}$

---

[17] Quasi-steady state diffusion of N in γ' was confirmed by numerical calculations [68] for a γ' (sub)layer growing into a ferrite substrate, after lifting the constraint of a constant (stoichiometric) composition of γ' as assumed in the present paper, and is attributed to the very small composition range of γ' iron nitride and the large concentration difference between the γ' sublayer and the α-iron substrate.

(=Boltzmann transformation[18]), where x is the depth in a sublayer and t is the treatment time. As a consequence, the change in the thicknesses of both sublayers S^ε and $S^{\gamma'}$, at constant temperature, is not necessarily parabolic (see section 4.4.1).

The flux of nitrogen in a plate-like α-Fe substrate of finite thickness L^α during growth of a compound layer of a very small thickness as compared to L^α (i.e. the partial transformation of the substrate into a compound layer during layer growth can be neglected) can be calculated for the case of a constant intrinsic diffusion coefficient of nitrogen, D_N^α, and a constant nitrogen concentration in the substrate at the layer/substrate interface, $c_N^{\alpha/\gamma'}$. It holds that [54, 56]

$$J_N^{\alpha/\gamma'} = \frac{4D_N^\alpha c_N^{\alpha/\gamma'}}{L^\alpha} \cdot \sum_{n=1}^{\infty} \exp\left(-\frac{D_N^\alpha \pi^2 t (2n-1)^2}{\left(L^\alpha\right)^2} \right), \tag{4.4}$$

where t is the treatment time and the well-established intrinsic diffusion coefficient of N in α at 823 K is taken from Ref. [57] as $D_N^\alpha = 1.3 \times 10^{-11}$ m^2·s^{-1}. The nitrogen content in α at the α/γ' interface is calculated from the data in Ref. [15] as 0.316 at.%. For a treatment time of 4 h (as used for series B1 and B2) and $L^\alpha = 1$ mm (see section 4.2) it follows that $J_N^{\alpha/\gamma'} = 3.61 \times 10^{-6}$ mol·m^{-2}s^{-1}.

For the case of quasi-steady state diffusion of N through the γ' sublayer (see above and footnote 17), the flux $J_N^{\gamma'/\alpha}$ can be associated with a generalized form of Fick's 1st law as follows [68, 69][19]

---

[18] The Boltzmann transformation $\lambda = x/\sqrt{t}$ [56] can only be applied for the extreme cases of a nitrogen pre-saturated substrate or an infinitely thick substrate provided that the surface concentrations of N and C in ε are constant. Under these boundary conditions the diffusion process is invariant to $\lambda = x/\sqrt{t}$ (i.e. the boundary conditions can be expressed in terms of $\lambda = x/\sqrt{t}$) and the equations for the concentration profile can be expressed in terms of error functions as shown in Refs. [12, 38].

[19] In contrast with e.g. the ε phase, with a wide composition range, the very narrow composition range of N in γ' cannot be easily determined experimentally. As compared to the nitrogen-content variation, the nitrogen-activity range over the γ' (sub)layer is not small and can straightforwardly be derived from nitriding experiments [70]. For that reason the flux equation for γ' is related here to the self-diffusion coefficient and the nitrogen-activity range over the γ'-phase (cf. Eq. (4.5)).

$$J_N^{\gamma'/\alpha} = J_N^{\gamma'/\varepsilon} = D_N^{\gamma'*} \frac{c_N^{\gamma'} \Delta \ln a_N^{\gamma'}}{S^{\gamma'}}, \tag{4.5}$$

where $D_N^{\gamma'*}$ is the self-diffusion coefficient of N in γ', $S^{\gamma'}$ is the thickness of the γ'-sublayer, $c_N^{\gamma'}$ is the nitrogen concentration in γ' and $\Delta \ln a_N^{\gamma'} = \ln a_N^{\gamma'/\varepsilon} - \ln a_N^{\gamma'/\alpha}$ is the difference in the natural logarithm of the nitrogen activity in γ' at the γ'/ε interface and at the γ'/α interface.

For the ε-phase, the flux $J_k^{\varepsilon/gas}$ can be related with the intrinsic diffusion coefficients D_{kj}^ε $(k, j \in \text{N,C})$. Adopting linear concentration-depth profiles in the ε-sublayer (cf. assumption (v)) and assuming D_{kj}^ε to be independent of concentration (cf. assumption (ix) and see section 4.5.2), the flux of N in ε at the surface of the compound layer can be obtained from Fick's 1st law as [29, 71]

$$J_k^{\varepsilon/gas} = \sum_{j=\{N,C\}} J_{kj}^\varepsilon = \sum_{j=\{N,C\}} D_{kj}^\varepsilon \frac{c_j^{\varepsilon/gas} - c_j^{\varepsilon/\gamma'}}{S^\varepsilon}, \tag{4.6}$$

where the intrinsic diffusion coefficients D_{kj}^ε are related to the flux of the component k caused by the concentration gradients of component k and component j, i.e. J_{kj}^ε. Equation (4.6), with its composition-independent D_{kj}^ε together with the linear nature of the concentration depth profile, might seem to imply, upon first view, quasi-steady state diffusion of N and C in ε. In contrast, however, to the γ' phase (cf. footnote 17), the fluxes of N and C in ε decrease from the surface of the ε sublayer to the ε/γ' interfaces in order to maintain the corresponding concentration-depth profiles upon layer growth, i.e. $J_k^{\varepsilon/gas} \neq J_k^{\varepsilon/\gamma'}$ (cf. Eq. (4.3)).
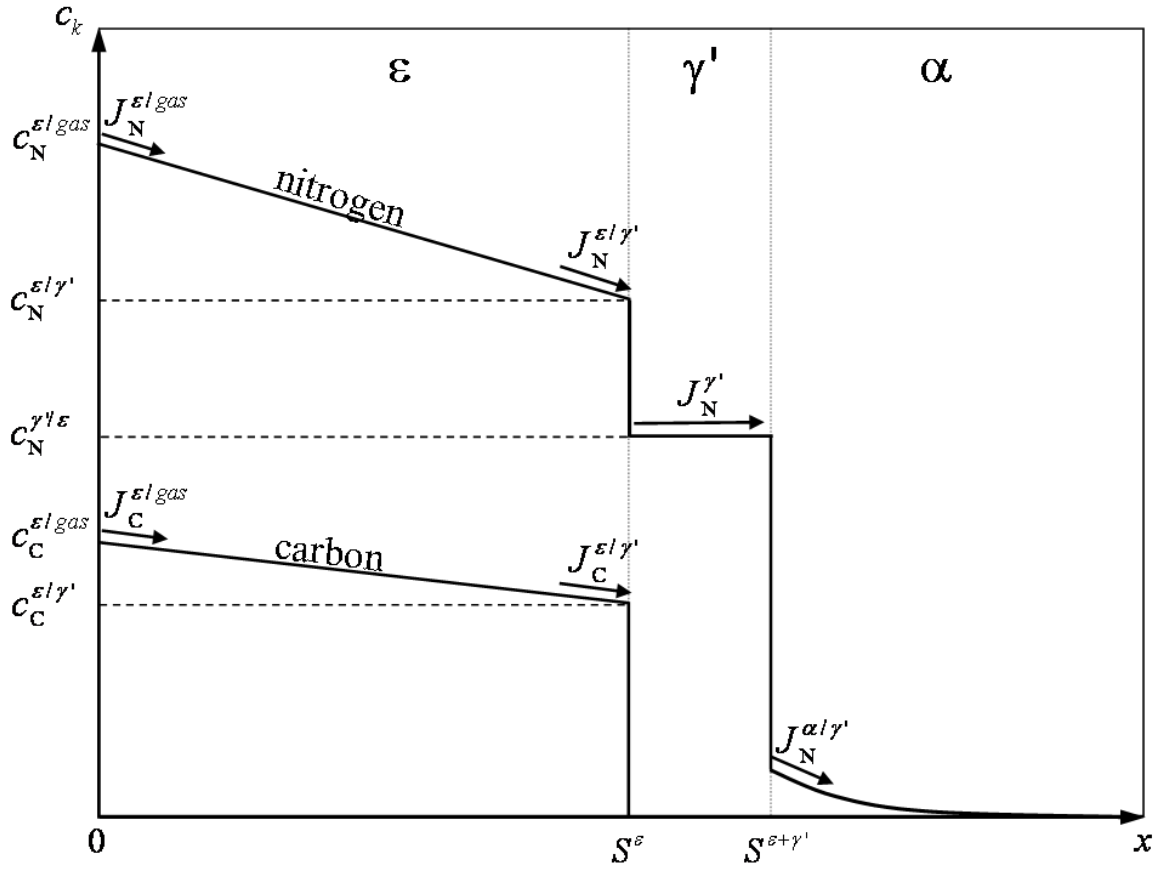
Fig. 4.1: Schematic concentration-depth profiles of nitrogen and carbon for the growth of an ε / γ' double layer into an α-Fe substrate. The diffusive fluxes of N and C at the ε / γ' interface and the γ' / α interface have been indicated. The C contents in γ' and α have been set to nil, i.e. $J_C^\gamma = 0$ and $J_C^\alpha = 0$.

4.3.1 Relation between intrinsic diffusion coefficients and thermodynamic properties

The intrinsic diffusion coefficients D_{kj}^ε are related to the thermodynamics of the ε-Fe$_3$(N,C)$_{1+x}$ phase by the so-called thermodynamic factors $\vartheta_{kj}^\varepsilon$ with $(k, j \in N, C)$. It holds that [29, 65, 72]

$$D_{kj}^\varepsilon = D_k^{\varepsilon *} \frac{c_k^\varepsilon}{RT} \frac{\partial \mu_k^\varepsilon}{\partial c_j^\varepsilon} = D_k^{\varepsilon *} \vartheta_{kj}^\varepsilon, \qquad (4.7)$$

where $D_k^{\varepsilon*}$ is the self-diffusion coefficient of component k, R is the gas constant, T is the absolute temperature and μ_k^ε is the chemical potential of component k in ε. For the present case $(k, j \in \{N,C\})$ equations (4.7) can be represented by a "diffusion matrix" as follows

$$
\begin{bmatrix} D_{NN}^\varepsilon & D_{NC}^\varepsilon \\ D_{CN}^\varepsilon & D_{CC}^\varepsilon \end{bmatrix} = \begin{bmatrix} D_N^{\varepsilon*} & 0 \\ 0 & D_C^{\varepsilon*} \end{bmatrix} \cdot \begin{bmatrix} \dfrac{c_N^\varepsilon}{RT} \dfrac{\partial \mu_N^\varepsilon}{\partial c_N^\varepsilon} & \dfrac{c_N^\varepsilon}{RT} \dfrac{\partial \mu_N^\varepsilon}{\partial c_C^\varepsilon} \\ \dfrac{c_C^\varepsilon}{RT} \dfrac{\partial \mu_C^\varepsilon}{\partial c_N^\varepsilon} & \dfrac{c_C^\varepsilon}{RT} \dfrac{\partial \mu_C^\varepsilon}{\partial c_C^\varepsilon} \end{bmatrix},
\tag{4.8}
$$

where D_{kj}^ε $(k = j)$ are the diagonal components and D_{kj}^ε $(k \neq j)$ are the off-diagonal components of the "diffusion matrix". It holds that $\partial \mu_N^\varepsilon / \partial c_C^\varepsilon = \partial \mu_C^\varepsilon / \partial c_N^\varepsilon$ [12] implying the same algebraic sign for D_{NC}^ε and D_{CN}^ε. The off-diagonal components reflect the influence of the thermodynamic interaction of different species on the diffusion process leading to diffusional cross effects. In ternary solid-state systems the off-diagonal components are frequently found to have a non-negligible influence on the diffusion process [12]. A measure for the significance of these interactions of diffusional species on the diffusion process is given by (cf. Eq. 4.7) [12, 65]

$$
D_{kj}^\varepsilon / D_{kk}^\varepsilon = \vartheta_{kj}^\varepsilon / \vartheta_{kk}^\varepsilon,
\tag{4.9}
$$

Note that Eq. (4.9) represents a purely thermodynamic quantity.

4.4   Experimental results and evaluation of diffusion data

4.4.1   Layer thicknesses and growth rates of ε / γ' double layers

The nitriding experiments of series A1 ($a_N = 636$) resulted in the formation of a massive γ'-layer after 0.5 h, whereas for treatment times in the range of 1 h to 6 h an ε / γ'-double layer was obtained (cf. Figs. 4.2a-c). In contrast, the nitrocarburizing

experiments of series A2 ($a_N = 636$, $a_C = 50$) showed the formation of ε / γ'-double layers for all treatment-times in the range of 0.5 h to 8 h (cf. Figs. 4.2d-f). For the nitrocarburizing experiments of series B1 ($a_N = 636$, $a_C = 0$-300, $t = 4$ h), the development of massive ε / γ' double layers was observed for all carbon activities in the range of $a_C = 0$ to $a_C = 300$ [51]. At a decreased nitrogen activity of $a_N = 417$ (series B2) a massive γ'-layer was obtained for carbon activities in the range of $0 \leq a_C \leq 12.5$, whereas higher carbon activities resulted in the formation of ε / γ'-double layers [51]. The measured layer thicknesses for all nitriding/nitrocarburizing experiments of series A and B are presented in Fig. 4.3 and Fig. 4.4, respectively. The influence of the carbon activity at a given nitrogen activity on the growth kinetics of ε / γ'- double layers (series B1 and B2) has already been discussed in Ref. [51]. In the present work the thickness data are used to determine the layer-growth rates $v^{\varepsilon/\gamma'}$ and $v^{\gamma'/\alpha}$, which are needed to evaluate the diffusion coefficients D_{kj}^{ε} and $D_N^{\gamma'*}$ (see section 4.4.3).
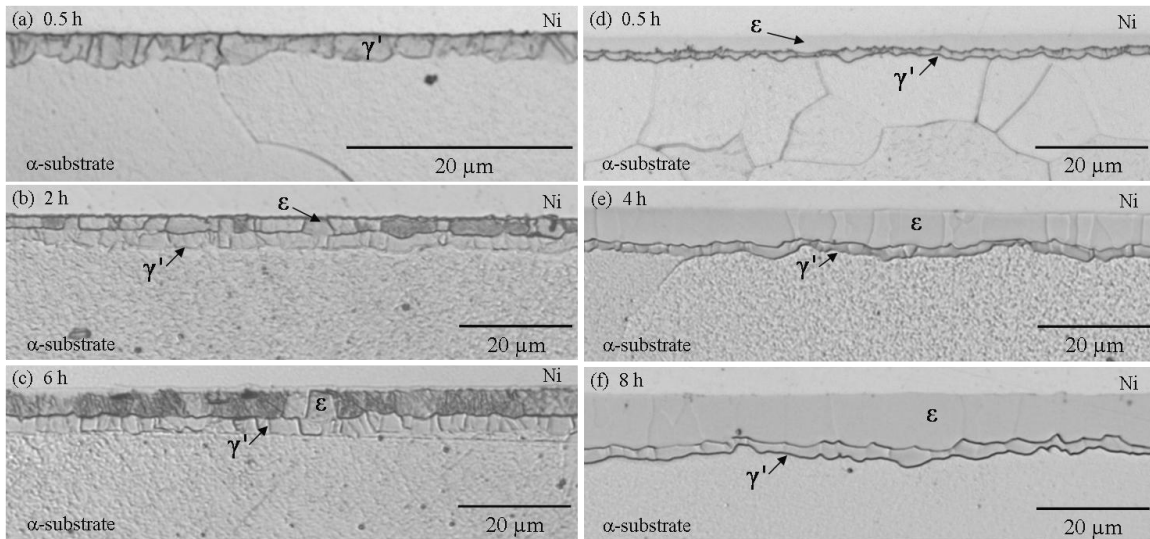

Fig. 4.2: Optical micrographs after etching with 1 vol.% Nital containing 0.1 vol.% HCl showing cross-sections of compound layers obtained on α-Fe substrates after nitriding and nitrocarburizing for different treatment times at 823 K. a) to c) massive γ' layer and ε / γ'-double layers formed during nitriding; series A1 ($a_N = 636$, $a_C = 0$). d) to f) ε / γ'-double layers formed during nitrocarburizing; series A2 ($a_N = 636$, $a_C = 50$).
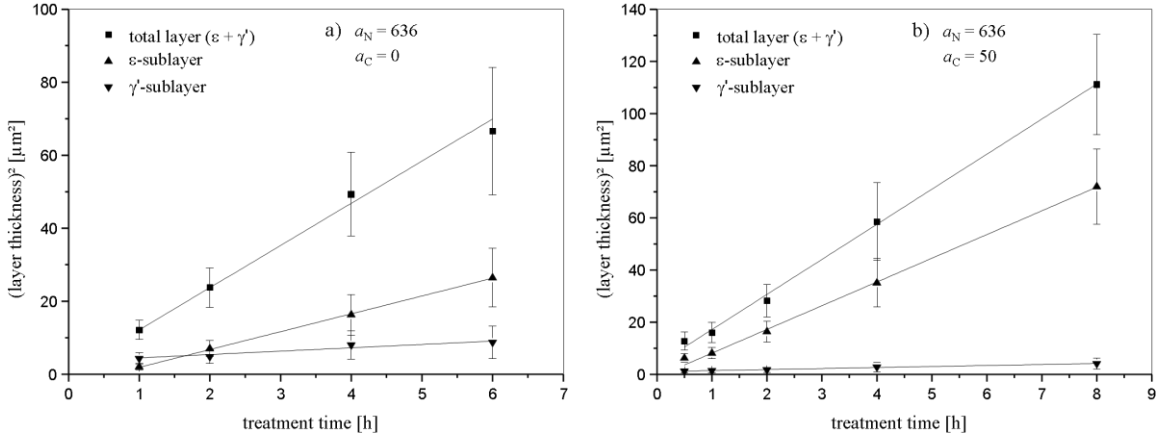
Fig. 4.3: Squared thickness of the $\varepsilon\,/\,\gamma'$-double layer and the sublayers as function of time (a) for pure nitriding (series A1, $a_C = 0$) and (b) for nitrocarburizing (series A2, $a_C = 50$) performed at 823 K. The straight lines drawn have been obtained by least-squares fitting of Eq. (4.10) to the experimental data.
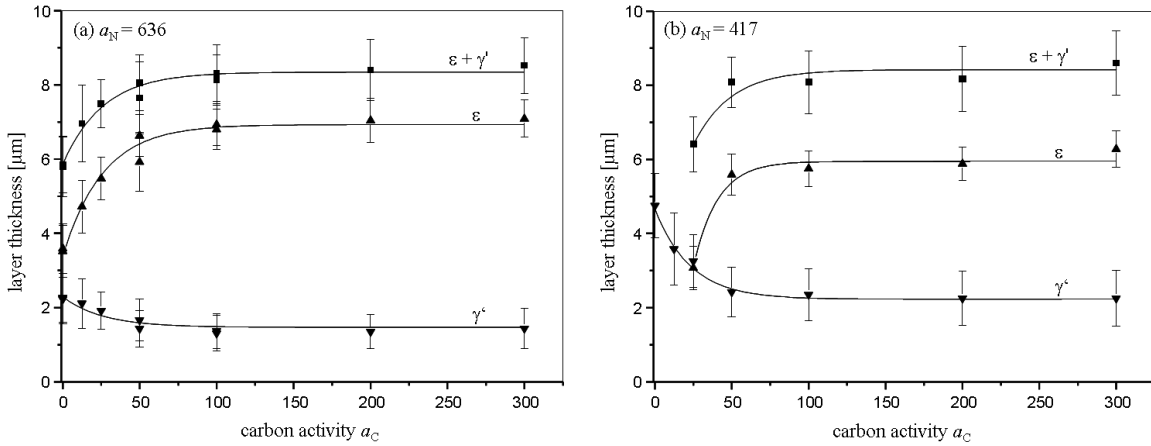
Fig. 4.4: Thickness of the $\varepsilon\,/\,\gamma'$-double layer, the ε-sublayer and the γ'-sublayer as function of the carbon activity for nitrocarburizing during 4 h at 823 K and for a nitrogen activity of (a) $a_N = 636$ (series B1) and (b) $a_N = 417$ (series B2), respectively. The solid lines have been drawn to guide the eye.

For the nitriding/nitrocarburizing experiments of series A1 and A2 the time-dependent growth of ε / γ'-double layers can be well described by a modified parabolic growth law according to (cf. Fig. 4.3)

$$S_I^2 = k^I t + S_{0,I}^2 \qquad\qquad (4.10)$$

where S_I is the thickness of the (sub)layer $I \in \{\varepsilon, \gamma', \varepsilon+\gamma'\}$, k^I is the parabolic growth-rate constant, t is the treatment time and $S_{0,I}^2$ is the hypothetical, initial squared layer thickness at $t = 0$. The occurrence of a purely parabolic growth of the compound layer for $t \downarrow 0$ implying $S_I^2 = k^I t$ would only be expected for the case of a nitrogen pre-saturated substrate (not the case here) and the immediate formation of a closed nitride/nitrocarbide layer (see also footnote 18).

Table 4.2: Experimentally determined parabolic growth-rate constants k^I and hypothetical, initial squared layer thicknesses $S_{0,I}^2$ for the growth of ε / γ'-double layers on α-Fe upon nitriding (series A1; $a_N = 636$, $a_C = 0$) and nitrocarburizing (series A2; $a_N = 636$, $a_C = 50$) at 823 K. The values were determined by least-squares fitting of Eq. (4.10) to the experimental data (cf. Fig. 4.3).

treatment	layer I	k^I [m²/s]	$S_{0,I}^2$ [m²]
pure nitriding	ε	$1.35 \cdot 10^{-15}$	$-2.85 \cdot 10^{-12}$
	γ'	$2.71 \cdot 10^{-16}$	$3.27 \cdot 10^{-12}$
	ε + γ'	$3.07 \cdot 10^{-15}$	$1.97 \cdot 10^{-12}$
nitrocarburizing	ε	$2.49 \cdot 10^{-15}$	$-2.53 \cdot 10^{-13}$
	γ'	$1.09 \cdot 10^{-16}$	$9.83 \cdot 10^{-13}$
	ε + γ'	$3.73 \cdot 10^{-15}$	$3.65 \cdot 10^{-12}$

The values for k^I and $S_{0,I}^2$ were determined by least-squares fitting of Eq. (4.10) to the experimental data given in Fig. 4.3 and have been summarized in Table 4.2.

The observation of $S_{0,\varepsilon}^2 < 0$ (cf. Table 4.2) indicates an incubation time for the formation of ε-nitride, which is compatible with the observation of *only* a massive γ' layer after the short nitriding time of $t = 0.5$ h (series A1; see above). The observation of $S_{0,\gamma'}^2 > 0$ can be explained by the formation of an only incomplete γ' layer at the

beginning of nitriding and nitrocarburizing, leaving parts of the ferrite substrate still in direct contact with the gas atmosphere and thus allowing additional fast "bypass diffusion" of N through the ferrite substrate to the growing γ' grains [43, 54].

The discussed initial stages of layer growth (see above) together with the nitrogen saturation of the ferrite substrate proceeding during the treatment (see section 4.3) imply that the real layer-growth kinetics are only approximately parabolic. Evidently, the modified parabolic growth law (Eq. 4.10) can be faithfully adopted in the following for the calculation of the growth rates $v^{\varepsilon/\gamma'}$ and $v^{\gamma'/\alpha}$. It holds that

$$v^{\varepsilon/\gamma'} = \frac{dS_\varepsilon}{dt} = \frac{k^\varepsilon}{2\sqrt{k^\varepsilon t + S_{0,\varepsilon}^2}} \qquad (4.11)$$

$$v^{\gamma'/\alpha} = \frac{dS_{\varepsilon+\gamma'}}{dt} = \frac{k^{\varepsilon+\gamma'}}{2\sqrt{k^{\varepsilon+\gamma'}t + S_{0,\varepsilon+\gamma'}^2}} . \qquad (4.12)$$

For series B1 and B2 the (sub)layer thicknesses S_ε^2 and $S_{\varepsilon+\gamma'}^2$ (cf. Fig. 4.4) were only determined at $t = 4$ h. The corresponding growth-rate constants k^ε and $k^{\varepsilon+\gamma'}$ were calculated from Eq. (4.10) using the same values of $S_{0,\varepsilon+\gamma'}^2$ and $S_{0,\varepsilon}^2$ as determined experimentally for series A2 (see discussion above). Further, in order to obtain a value for the growth-rate constant $k^{\gamma'}$ of the γ' single layer formed during pure nitriding for 4 h at $a_N = 417$ (series B2), the measured thickness $S_{\gamma'}^2$ (cf. Fig. 4.4) was used in combination with $S_{0,\gamma'}^2$ as determined during pure nitriding at $a_N = 636$ (series A1), by applying Eq. (4.10). The thus resulting growth-rate constants for series B1 and B2 and the corresponding layer-growth rates obtained from Eqs. (4.11) and (4.12) have been given in Table 4.3.

Table 4.3: Growth-rate constants (cf. Eq. 4.10), and layer-growth rates (cf. Eqs. (4.11) and (4.12)) using the experimental layer thicknesses after a treatment time of 4 h (cf. Fig. 4.4) and the values of the initial layer thicknesses as determined experimentally from series A2 for $a_C > 0$ and series A1 for $a_C = 0$ (cf. Table 4.2). Only those values needed for further calculations have been given.

series	a_N	a_C	growth constants (10^{-15} m²/s)			growth rates (10^{-10} m²/s)	
			$k^{\varepsilon+\gamma'}$	k^ε	$k^{\gamma'}$	$v^{\varepsilon/\gamma'}$	$v^{\gamma'/\alpha}$
A1, B1[a]	636	0	3.07	1.35	--	1.66	2.26
B1	636	12.5	3.11	1.72	--	1.82	2.23
B1	636	25	3.64	2.26	--	2.06	2.43
A2, B1[a]	636	50	3.73	2.49	--	2.16	2.46
B1	636	100	4.55	3.51	--	2.53	2.74
B1	636	200	4.65	3.62	--	2.57	2.77
B1	636	300	4.79	3.67	--	2.59	2.81
B2	417	0	--	--	1.34	--	1.41
B2	417	25	2.60	--	--	--	2.03
B2	417	50	4.23	--	--	--	2.63
B2	417	100	4.28	--	--	--	2.65
B2	417	200	4.38	2.58	--	2.19	2.68
B2	417	300	4.88	2.92	--	2.32	2.84

[a] These values of the growth-rate constants were obtained directly from experiments of series A and have already been given in Table 4.2.

4.4.2 Concentration-depth profiles in ε / γ' double layers

The concentration-depth profiles of N and C in the grown ε / γ'-double layers were determined by EPMA for the nitriding/nitrocarburizing experiments of series B1 and B2. It was found that, within experimental accuracy, the N and C concentration-depth profiles in the ε-sublayer can all be considered to be linear, as exemplarily shown in Fig. 4.5. Consequently, the concentration-depth profiles in ε can be completely characterized by the N and C contents at the surface and the ε / γ' interface, $c_j^{\varepsilon/gas}$ and $c_j^{\varepsilon/\gamma'}$ with $j \in \{N,C\}$. Values for these surface/interface contents were obtained by least-squares fitting of straight lines to the experimental concentration-depth profiles in the ε-sublayer and their subsequent extrapolation to the surface and at the ε / γ' interface (cf. Fig. 4.5). Average values of the N and C surface/interface contents were determined from at least

three (mostly five) measured concentration-depth profiles and have been listed in Table 4.4. These N and C surface/interface contents were used together with the experimental growth rates $v^{\varepsilon/\gamma'}$ and $v^{\gamma'/\alpha}$ to calculate the intrinsic diffusion coefficients D_{ij}^{ε} (see section 4.4.3).
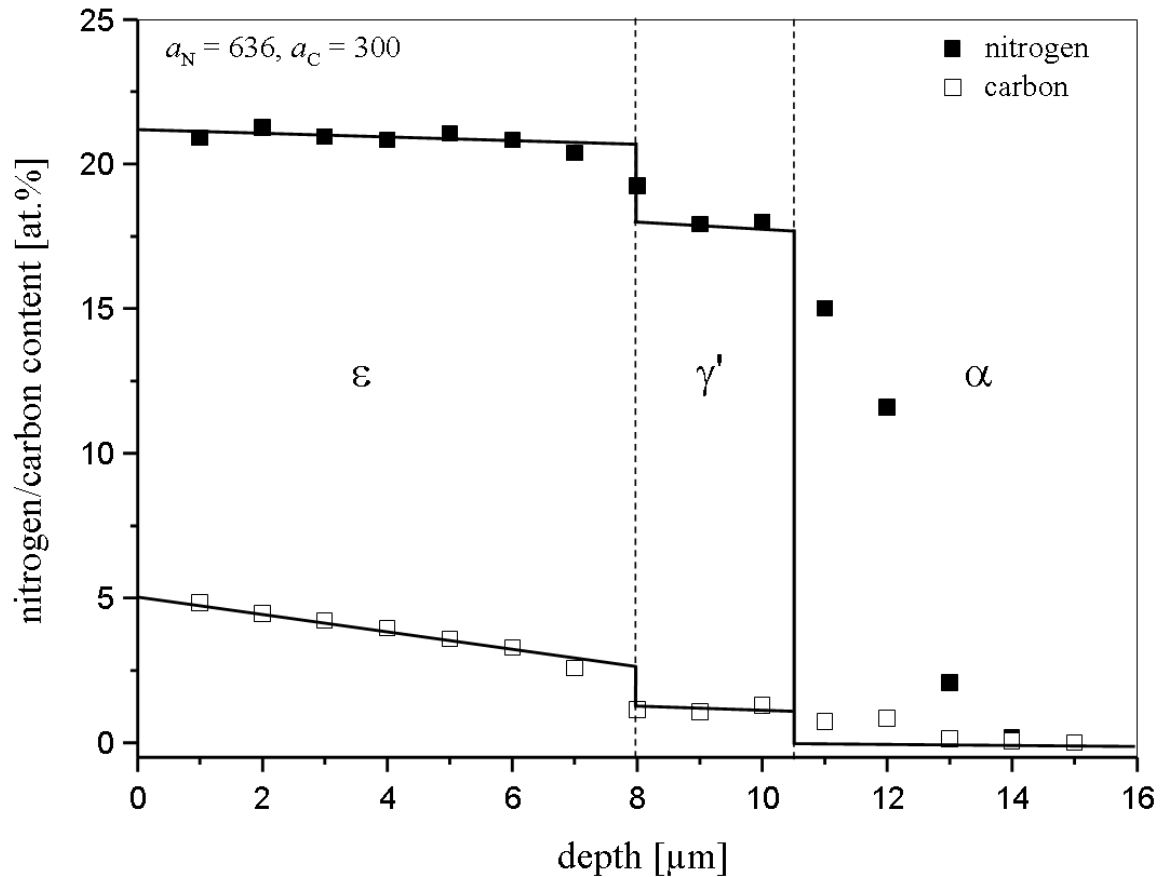
Fig. 4.5: Concentration-depth profiles of nitrogen and carbon as determined by EPMA in an ε/γ'-double layer obtained after nitrocarburizing for 4 h at 823 K with $a_N = 636$ and $a_C = 300$ (series B1). The solid lines were obtained by least-squares fitting of straight lines to the experimental data. Extrapolation of these straight lines in the ε sublayer to the surface and the ε/γ' interface led to values for $c_j^{\varepsilon/gas}$ and $c_j^{\varepsilon/\gamma'}$ with $j \in \{N,C\}$.

Table 4.4: Nitrogen and carbon contents, in the ε sublayer, at the surface and at the ε / γ'-interface, as determined by EPMA, after nitriding and nitrocarburizing for 4 h at 823 K. The nitrogen- and carbon-content values in the ε sublayer are averages obtained from at least three (mostly five) measured concentration-depth profiles (cf. section 4.4.2).

series	a_N	a_C	surface $c_N^{\varepsilon/gas}$ [at.%]	surface $c_C^{\varepsilon/gas}$ [at.%]	ε/γ' interface $c_N^{\varepsilon/\gamma'}$ [at.%]	ε/γ' interface $c_C^{\varepsilon/\gamma'}$ [at.%]
A1, B1	636	0	25.3 ± 0.2	0.0	24.3 ± 0.6	0.0
B1	636	12.5	24.6 ± 0.4	0.6 ± 0.2	24.1 ± 0.2	0.5 ± 0.1
B1*	636	25	24.0 ± 0.2	1.4 ± 0.3	22.7 ± 0.2	1.2 ± 0.1
A2, B1	636	50	--	--	--	--
B1	636	100	--	--	--	--
B1*	636	50	23.9 ± 0.3	2.0 ± 0.4	22.3 ± 0.3	1.7 ± 0.2
B1*	636	100	22.7 ± 0.2	2.9 ± 0.4	21.3 ± 0.2	2.4 ± 0.3
B1*	636	200	22.0 ± 0.3	3.7 ± 0.3	20.9 ± 0.3	2.9 ± 0.2
B1*	636	300	21.1 ± 0.3	4.7 ± 0.5	20.7 ± 0.3	3.0 ± 0.3
B2	417	0	--	--	--	--
B2	417	12.5	--	--	--	--
B2	417	25	--	--	--	--
B2	417	50	--	--	--	--
B2	417	100	--	--	--	--
B2*	417	200	20.6 ± 0.2	4.8 ± 0.3	20.2 ± 0.2	3.5 ± 0.2
B2*	417	300	19.7 ± 0.1	6.1 ± 0.1	19.6 ± 0.1	4.3 ± 0.2

* Experiments of these series were used to determine the values of D_{ij}^{ε} with $i,j \in \{N, C\}$.

As follows from the linearity of the concentration-depth profiles in ε the corresponding "diffusion paths" [11] in ε can be given by straight lines connecting the N and C contents at the surface and the ε / γ' interface (cf. Table 4.4). The thus resulting diffusion paths in the ε sublayers are presented in a proposed schematic isothermal section of the ternary Fe-N-C phase diagram at 823 K in Fig. 4.6. The diffusion paths shift along the ε / $\varepsilon + \gamma$' phase boundary towards higher carbon contents upon increasing carbon activity in the gas atmosphere. Strikingly, the nitrogen-concentration gradient in the ε-sublayer decreases, while the carbon-concentration gradient increases with increasing carbon activity in the gas atmosphere, i.e. the diffusion path changes from a horizontal line at $a_C = 0$ to an almost vertical line at $a_C = 300$.
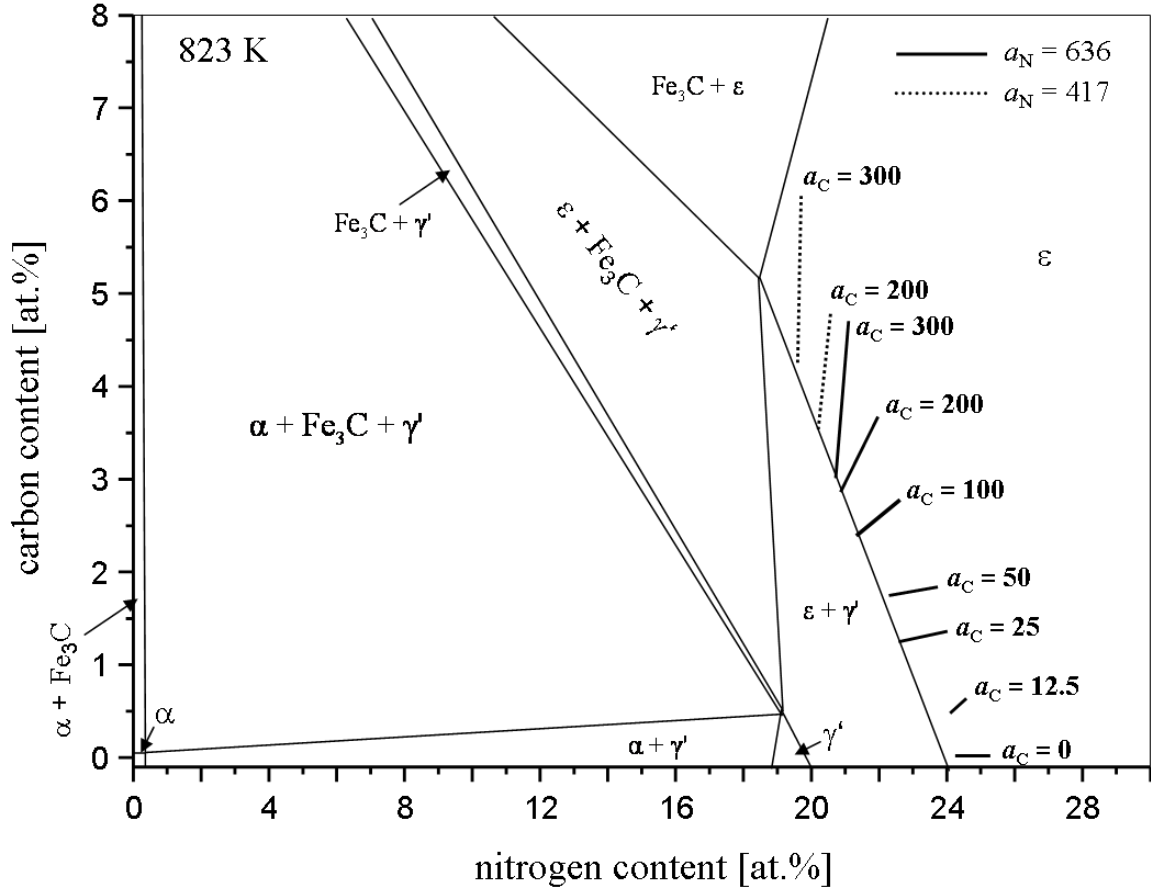
Fig. 4.6: Presentation of the observed diffusions paths of N and C, determined by EPMA, in ε sublayers formed upon nitriding and nitrocarburizing for 4 h at 823 K (series B1 and B2) in the proposed isothermal section of the ternary Fe-N-C phase diagram at 823 K.

4.4.3 The diffusion coefficients $D_N^{\gamma'*}$ and $D_{kj}^{\varepsilon}\left(k, j \in \mathrm{N,C}\right)$ as well as the activity change over the γ' phase

A. Nitriding

The nitriding experiments of series A1 and B2 were used to determine the diffusion coefficients of N in γ' and ε.

The self-diffusion coefficient $D_N^{\gamma'*}$ was directly calculated from Eq. (4.2) and Eqs. (4.4) and (4.5) on the basis of the experimental values for $v^{\gamma'/\alpha}$ and $S^{\gamma'}$ obtained by pure nitriding at $a_N = 636$ and $a_N = 417$ (series A1 and B2; cf. Tables 4.3-4.4 and

Figure 4.4), respectively. The needed values of the N activities in γ' ($a_N^{\gamma'/\varepsilon}$ and $a_N^{\gamma'/\alpha}$) and of the N content in α ($c_N^{\alpha/\gamma'}$) were calculated from available thermodynamic data under the assumption of local thermodynamic equilibria at the surface and the interface of the γ' (sub)layer and all interfaces of the ε / γ' double layer [7] (cf. Table 4.5). For the nitriding experiments of series A1 the self-diffusion coefficient of N in γ' was then obtained as $D_N^{\gamma'*} = 5.4 \times 10^{-16}$ m$^2 \cdot$s^{-1} at 823 K. The nitriding experiments of series B2 gave $D_N^{\gamma'*} = 7.6 \times 10^{-16}$ m$^2 \cdot$s^{-1} at 823 K.

The intrinsic diffusion coefficient D_N^ε was directly calculated by substitution of Eqs. (4.2) to (4.4) and Eq. (4.6) into Eqs. (4.1), using the experimental values for $c_N^{\varepsilon/gas}$, $v^{\varepsilon/\gamma'}$, $v^{\gamma'/\alpha}$ and S^ε of series A1 given in section 4.4.2 (cf. Tables 4.2-4.4 and Figure 4.4). The needed values for the nitrogen content in ε at the ε / γ' interface and the N contents in γ' and in α at the γ' / α interface were taken from Table 4.5 (the N content in ε at the ε / γ' interface was calculated from thermodynamic data (cf. Table 4.5) since the experimental value could not be assessed with sufficient accuracy by EPMA). For experiments of series A1 the intrinsic diffusion coefficient of N in ε was then obtained as $D_N^\varepsilon = 1.9 \times 10^{-14}$ m$^2 \cdot$s^{-1} at 823 K.

Table 4.5: Nitrogen contents/activities at the surface and interfaces of ε / γ' double layers and of single γ' layers for *pure* nitriding of α-Fe at 823 K with $a_N = 636$ and $a_N = 417$, respectively, calculated using available thermodynamic data for local equilibria at the surface and the interfaces [7].

position	calculated c_N [at.%]	calculated a_N
ε/gas-surface	25.43	636
γ'/gas-surface	19.92	417
ε/γ'-interface	24.04	517
γ'/ε-interface	19.95	517
γ'/α-interface	19.58	84
α/γ'-interface	0.32	84

B. Nitrocarburizing

The nitrocarburizing experiments of series A2, B1 and B2 were used to evaluate the intrinsic diffusion coefficients D_{kj}^ε of N and C in ε. The substitution of Eqs. (4.2) to (4.4)

and Eqs. (4.6) into Eqs. (4.1) yields two flux-balance equations for the shifting ε / γ' interface with the four unknowns $D_{\text{NN}}^{\varepsilon}$, $D_{\text{NC}}^{\varepsilon}$, $D_{\text{CC}}^{\varepsilon}$ and $D_{\text{CN}}^{\varepsilon}$. Hence, using experimental data for $c_k^{\varepsilon / gas}$, $c_k^{\varepsilon / \gamma'}$, $v^{\varepsilon / \gamma'}$, $v^{\gamma' / \varepsilon}$ and S^{ε} (cf. Tables 4.2 to 4.4 and Figure 4.4), the four diffusion coefficients D_{kj}^{ε} can be calculated from the two flux balance equations for at least two combinations of a_{N} and a_{C} pertaining to the gas atmosphere. The needed values for $c_{\text{N}}^{\gamma' / \varepsilon}$, $c_{\text{N}}^{\gamma' / \alpha}$ and $c_{\text{N}}^{\alpha / \gamma'}$ were taken from Table 4.5. A fitting procedure was applied for the four intrinsic diffusion coefficients, taking into account the layer-growth kinetic data and the values of $c_k^{\varepsilon / gas} - c_k^{\varepsilon / \gamma'}$ $(k \in \text{N,C})$ as obtained for seven combinations of a_{N} and a_{C} (i.e. for seven different gas atmospheres) simultaneously (with $a_{\text{C}} \geq 25$; see footnote of Table 4.4). The intrinsic diffusion coefficients $D_{\text{NN}}^{\varepsilon}$, $D_{\text{NC}}^{\varepsilon}$, $D_{\text{CC}}^{\varepsilon}$ and $D_{\text{CN}}^{\varepsilon}$ were then obtained by the minimization of the sum of squared differences between the fluxes $J_k^{\varepsilon / gas}$ $(k \in \text{N,C})$ as calculated from Eqs. (4.1) (no data for D_k^{ε} is needed) and those as calculated from Eqs. (4.6) using estimated values for D_k^{ε}. The experimental data for the case $a_{\text{N}} = 636$ and $a_{\text{C}} = 12.5$ (series B1) were not included in the evaluation because the small concentration changes from $c_{\text{N}}^{\varepsilon / gas}$ to $c_{\text{N}}^{\varepsilon / \gamma'}$ and from $c_{\text{C}}^{\varepsilon / gas}$ to $c_{\text{C}}^{\varepsilon / \gamma'}$ over the layer (cf. Table 4.4), in combination with the experimental inaccuracy, led to relatively large errors of the concentration gradients. The thus determined values of the intrinsic diffusion coefficients D_{kj}^{ε} at 823 K have been given in Table 4.6.

Table 4.6: Intrinsic diffusion coefficients D_{kj}^{ε} at 823 K as determined by simultaneous fitting to the experimental data for different combinations of a_{N} and a_{C} (i.e. for different gas atmospheres) simultaneously (cf. section 4.4.3).

Diffusion coefficients (10^{-15} m²/s)			
$D_{\text{NN}}^{\varepsilon}$	$D_{\text{NC}}^{\varepsilon}$	$D_{\text{CC}}^{\varepsilon}$	$D_{\text{CN}}^{\varepsilon}$
21.2	19.6	3.6	0.85

Using the values of D_{kj}^{ε} as determined by fitting, the fluxes $J_{kj}^{\varepsilon / gas}$ in ε at the surface of the compound layer can be calculated as function of the carbon activity in the gas atmosphere by application of Eq. (4.6). For the case of series B1 the results are shown in Fig. 4.7.
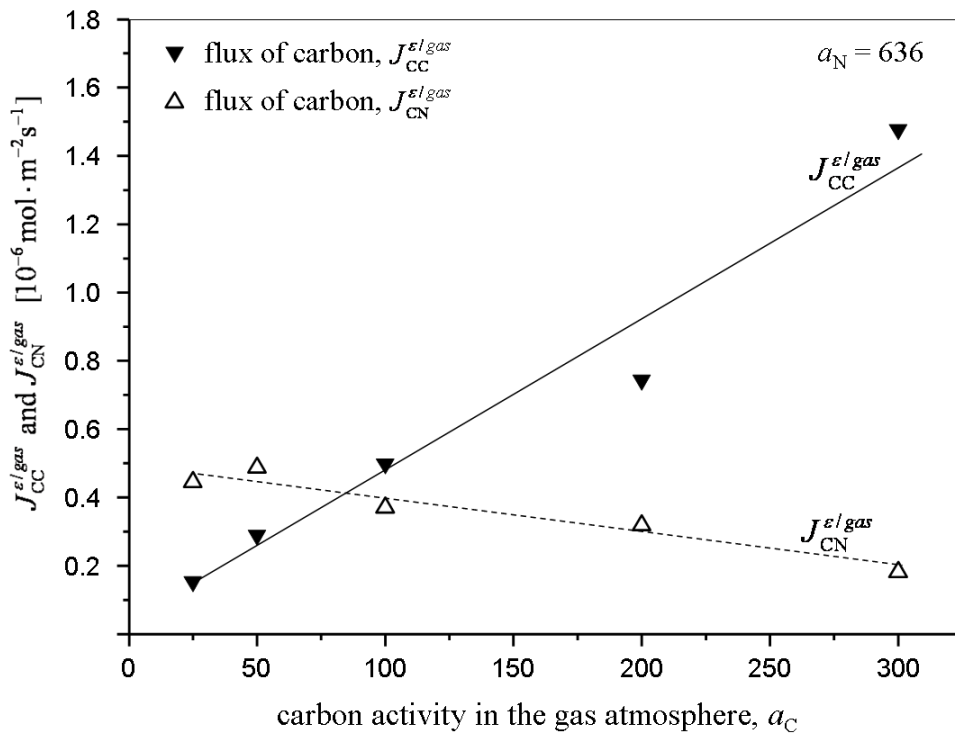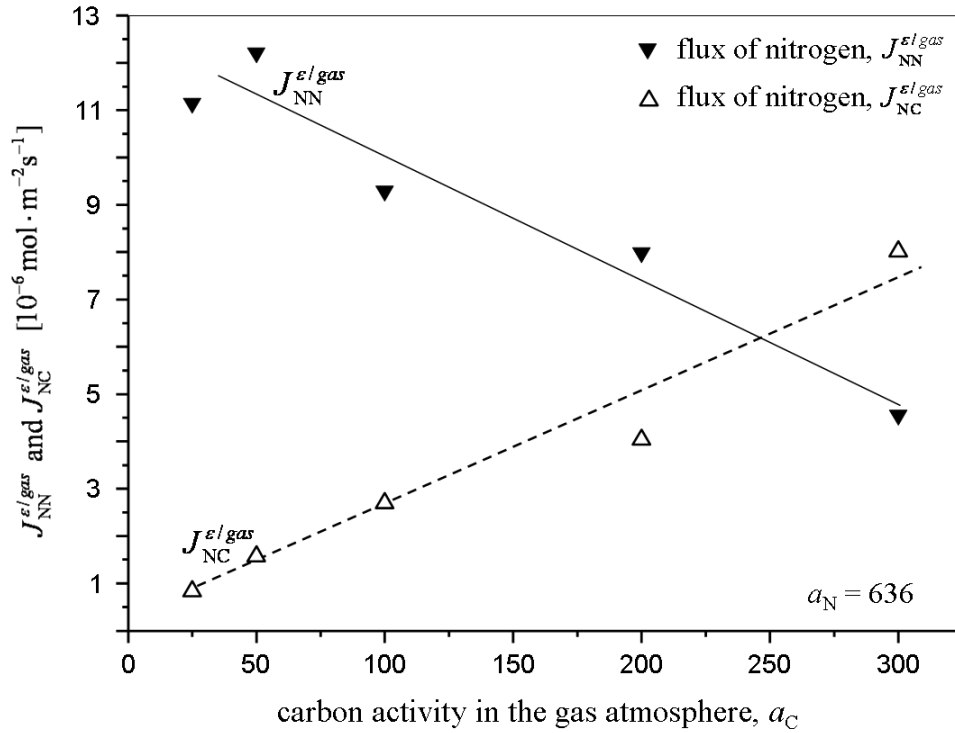
Fig. 4.7: Interstitial diffusion fluxes of N and C in ε at the compound-layer surface as function of a_C, as calculated from Eq. (4.6) using the intrinsic diffusion coefficients D_{kj}^{ε} as determined by fitting (Table 4.6)

and the experimental results for series B1 as given in Table 4.4 (pertaining to a nitrocarburizing time of 4 h at 823 K). The solid and the dashed lines have been drawn to guide the eye.

The nitrogen activity in γ' at the ε/γ' phase boundary, $a_N^{\gamma'/\varepsilon}$, was obtained from Eqs. (4.2), after substitution of Eq. (4.4) and (4.5), using the experimental data obtained for $v^{\gamma'/\alpha}$, $S^{\gamma'}$ and $D_N^{\gamma'*}$ (cf. series A1, B1 and B2; see Tables 4.2-4.3 and Figure 4.4) and using the calculated value for the N activity at the γ'/α phase boundary $a_N^{\gamma'/\alpha}$ (cf. Table 4.5), which is taken independent of the C content. These results for the nitrogen activity at the ε / γ' phase boundary in the ternary Fe-N-C system, $a_N^{\varepsilon/\gamma'}$, have been plotted in Fig. 4.8 as function of the carbon activity a_C as imposed by the nitrocarburizing atmosphere.
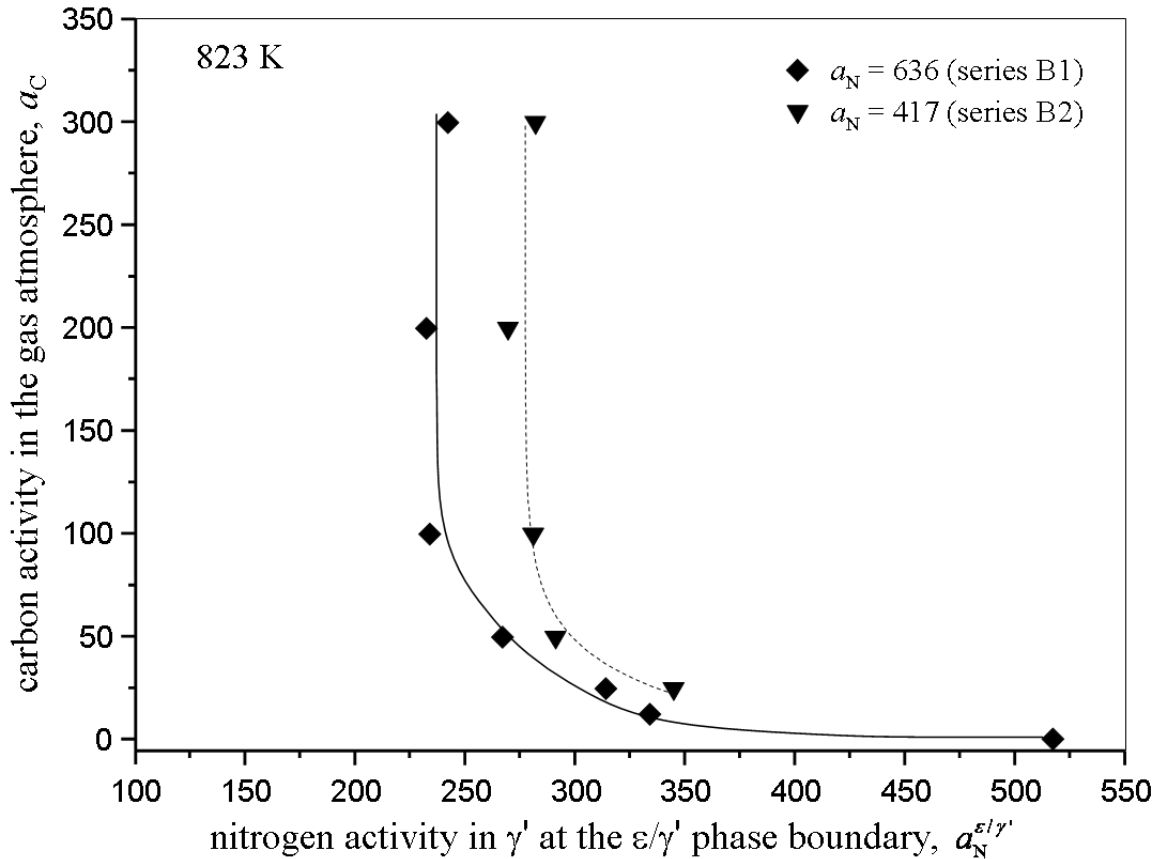
Fig. 4.8: Nitrogen activity in γ' at the ε/γ' phase boundary as function of the carbon activity a_C imposed by the nitrocarburizing atmosphere for $a_N = 636$ (series B1) and $a_N = 417$ (series B2), respectively. The solid and the dashed lines have been drawn to guide the eye.

4.5   Discussion

4.5.1   Diffusion coefficients of nitrogen in γ' and nitrogen and carbon in ε

The values of the self-diffusion coefficient of nitrogen in the γ'-sublayer determined at 823 K in this study as $D_N^{\gamma'*} = 5.4 \times 10^{-16}$ m^{2}s^{-1} (series A1) and $D_N^{\gamma'*} = 7.6 \times 10^{-16}$ m^{2}s^{-1} (series B2) agree well with the values calculated for 823 K from the temperature dependences of $D_N^{\gamma'*}$ as presented in Refs. [54, 59], i.e. $D_N^{\gamma'*} = 6.0 \times 10^{-16}$ m^{2}s^{-1} [54] and $D_N^{\gamma'*} = 6.7 \times 10^{-16}$ m^{2}s^{-1} [59]. The modest difference in these values is probably caused by the experimental inaccuracy inherent to the experimental determination of the layer thicknesses (cf. section 4.4.1).

The intrinsic diffusion coefficient of N in the ε-sublayer determined at 823 K in this study as $D_N^{\varepsilon} = 1.9 \times 10^{-14}$ m^{2}s^{-1} (series A1) is in reasonable agreement with the values calculated for 823 K from the temperature dependences of D_N^{ε} as presented in the literature, i.e. $D_N^{\varepsilon} = 2.4 \times 10^{-14}$ m^{2}s^{-1} [73] and $D_N^{\varepsilon} = 2.9 \times 10^{-14}$ m^{2}s^{-1} [74]. A direct comparison of the values determined in the present work with those from the literature is, however, difficult since D_N^{ε} (i) varies as a function of N concentration and (ii) strongly depends on the accuracy of the determined N content at the surface and at the ε/γ' interface. Moreover, the temperature dependence of D_N^{ε} given in Ref. [74] pertains to $848 \text{ K} < T < 1003 \text{ K}$ and thus had to be extrapolated to the lower temperature of 823 K.

The ternary intrinsic diffusion coefficient of nitrogen in ε determined from the nitrocarburising experiments of series B1 and B2 as $D_{NN}^{\varepsilon} = 2.1 \times 10^{-14}$ m^{2}s^{-1} at 823 K differs only slightly from the value of $D_N^{\varepsilon} = 1.9 \times 10^{-14}$ m^{2}s^{-1} obtained from the nitriding experiments (series A1; see above)), which suggests a weak concentration dependence of the intrinsic diffusion coefficient D_{NN}^{ε} on the N and C contents. The values of the ratios $D_{NC}^{\varepsilon} / D_{NN}^{\varepsilon} = 0.93$ and $D_{CN}^{\varepsilon} / D_{CC}^{\varepsilon} = 0.23$ imply that the off-diagonal diffusion coefficients have pronounced influence on the fluxes of nitrogen and carbon through the ε-sublayer. Indeed, as shown in Fig. 4.7, at a high carbon activity of $a_C = 300$ the carbon-

concentration gradient is able to drive the inward diffusion of N ($J_{NC}^{\varepsilon} > J_{NN}^{\varepsilon}$), since the nitrogen-concentration gradient is comparably low (cf. Fig. 4.6). A similar effect can occur for the inward diffusion of carbon at low carbon activities of $a_C < 100$, where the flux of carbon J_C^{ε} is mainly due to the contribution J_{CN}^{ε} carried by the concentration gradient of nitrogen in ε. The variation of the fluxes $J_{kj}^{\varepsilon}(k, j \in N,C)$ with increasing a_C is reflected by the change of the diffusion path in ε as shown in Fig. 4.6.

4.5.2 Thermodynamics of ε-Fe$_3$(N,C)$_{1+x}$ and γ'-Fe$_4$N$_{1-z}$ in the ternary Fe-N-C system

The distinct values of the off-diagonal diffusion coefficients D_{NC}^{ε} and D_{CN}^{ε} indicate significant thermodynamic interactions of the interstitial species N and C in the ε phase. These interactions express themselves as entropy and enthalpy effects on the thermodynamic factors $\vartheta_{kj}^{\varepsilon}$.

A thermodynamic model describing the Gibbs energy of the ε phase in the ternary Fe-N-C system can be based on the Hillert-Staffansson approach[20], i.e. a subregular solid solution model [15, 21, 39] (see Appendix). On that basis the thermodynamic factors $\vartheta_{kj}^{\varepsilon}$ were calculated (cf. Table 4.7) employing the two assessments of the ternary Fe-N-C system presented in Ref. [15] and Ref. [21], respectively. For the calculations, a representative composition of interstitials in the ε-sublayer was chosen as 22.15 at.% N and 2.58 at.% C, which corresponds to the average N and C contents obtained for all ε sublayers of series B1 for $a_C \geq 25$, as determined by EPMA (cf. section 4.4.2). The sublattice models for the ε-Fe$_3$(N,C)$_{1+x}$ phase proposed in Ref. [15] and in Ref. [21] are $(Fe)_1(N,C,Va)_1$ and $(Fe)_2(N,C,Va)_1$, respectively, where "Va" denotes the vacancies on the sublattice concerned.

The experimentally determined intrinsic diffusion coefficients D_{kj}^{ε} can now be related to the thermodynamic descriptions of the ε phase by considering the ratios

---

[20] Other thermodynamic models of the ε phase such as the Gorsky-Bragg-Williams approach were only derived for the binary Fe-N system [75, 76].

$D_{kj}^{\varepsilon} / D_{kk}^{\varepsilon} = \vartheta_{kj}^{\varepsilon} / \vartheta_{kk}^{\varepsilon}$ (cf. Eq. 4.9). The ratios $\vartheta_{NC}^{\varepsilon} / \vartheta_{NN}^{\varepsilon}$ and $\vartheta_{CN}^{\varepsilon} / \vartheta_{CC}^{\varepsilon}$ calculated according to the thermodynamic assessment given in Ref. [15] are positive and of the same order as the experimental values determined in the present work (cf. Table 4.7). The same ratios calculated from the thermodynamic data given in Ref. [21] are negative owing to the negative values calculated for $\vartheta_{NC}^{\varepsilon}$ and $\vartheta_{CN}^{\varepsilon}$, implying negative values for D_{NC}^{ε} and D_{CN}^{ε}. Such negative off-diagonal diffusion coefficients D_{NC}^{ε} and D_{CN}^{ε} were also presented in Ref. [38] for modeling the growth of ε / γ'-double layers upon nitrocarburizing at 848 K. However, the experimental results in the present work (see the evaluation made in section 4.4) clearly demonstrate that negative values for D_{kj}^{ε} $(k \neq j)$ are inconsistent with the experimentally determined diffusion paths and layer-growth rates. Evidently, the (sub)regular parameters presented in Refs. [21] and [38], describing the thermodynamic interaction of N and C in the ε phase, are wrong.

Unfortunately, a direct fit of the (sub)regular model parameters, pertaining to either the $(\text{Fe})_1 (\text{N,C,Va})_1$ sublattice model [15] or the $(\text{Fe})_2 (\text{N,C,Va})_1$ sublattice model [21], to the experimental data given in the present work, taking into account the concentration dependence of $\vartheta_{kj}^{\varepsilon}$ as described by the Hillert-Staffansson approach for ε (see Appendix), was impossible. This is due to strong correlations of the fitted parameters and, possibly, not sufficiently precisely determined values for the average N and C concentrations resulting from the different values of a_N and a_C. Nevertheless, all evaluations very robustly led to positive values for D_{kj}^{ε} $(k \neq j)$.

According to the Hillert-Staffansson approach for the Gibbs energy of the ε phase negative values of the off-diagonal thermodynamic factors $\vartheta_{NC}^{\varepsilon}$ and $\vartheta_{CN}^{\varepsilon}$ can only occur if the excess enthalpy term in Eq. (A2) and Eq. (A4) (see Appendix A) is negative and sufficiently (absolutely) large to overcompensate the positive contribution due to the configurational entropy term. Positive values of $\vartheta_{kj}^{\varepsilon}$ $(k \neq j)$, as observed in this work, can only occur for positive or small negative terms of the excess enthalpy.

The assumption of concentration independent D_{NN}^{ε}, D_{NC}^{ε} and D_{CC}^{ε}, made in the present work (for D_{CN}^{ε}, see below), appears reasonable considering the modest variation

of the corresponding thermodynamic factors as function of N and C concentration, as calculated according to the thermodynamic description for ε as given in Ref. [15] for the various average N and C contents per ε sublayer of series B1 and B2 (see Table 4.8). As already indicated in the literature [54, 59] $D_k^{\varepsilon^*}\left(k \in \mathrm{N,C}\right)$ may depend on concentration, which has not been considered in the above evaluation. The influence of $D_k^{\varepsilon^*}$ on the concentration dependence of $D_{\mathrm{NN}}^{\varepsilon}$, $D_{\mathrm{NC}}^{\varepsilon}$ and $D_{\mathrm{CC}}^{\varepsilon}$ could not be evaluated on the basis of the experimental data, because $D_k^{\varepsilon^*}$ and $\vartheta_{kj}^{\varepsilon}$ cannot be determined separately without knowing the actual concentration dependence of the thermodynamic factor.

The values of $\vartheta_{\mathrm{CN}}^{\varepsilon}$ calculated according to Ref. [15] (cf. Table 4.8) imply a strong concentration dependence of $D_{\mathrm{CN}}^{\varepsilon}$ (apart from the role of $D_k^{\varepsilon^*}$; see above), which can be estimated as follows. As shown in section 4.3.1, the off-diagonal diffusion coefficients are given by $D_{\mathrm{NC}}^{\varepsilon} = D_{\mathrm{N}}^{\varepsilon^*}\dfrac{c_{\mathrm{N}}^{\varepsilon}}{RT}\dfrac{\partial\mu_{\mathrm{N}}^{\varepsilon}}{\partial c_{\mathrm{C}}^{\varepsilon}}$ and $D_{\mathrm{CN}}^{\varepsilon} = D_{\mathrm{C}}^{\varepsilon^*}\dfrac{c_{\mathrm{C}}^{\varepsilon}}{RT}\dfrac{\partial\mu_{\mathrm{C}}^{\varepsilon}}{\partial c_{\mathrm{N}}^{\varepsilon}}$ (cf. Eq. 4.7), with $\partial\mu_{\mathrm{N}}^{\varepsilon}/\partial c_{\mathrm{C}}^{\varepsilon} = \partial\mu_{\mathrm{C}}^{\varepsilon}/\partial c_{\mathrm{N}}^{\varepsilon}$. Thus, assuming $D_{\mathrm{N}}^{\varepsilon^*} \approx D_{\mathrm{C}}^{\varepsilon^*}$ and recognizing that the relative change of the average nitrogen content in the ε phase in the range $0 \leq a_{\mathrm{C}} \leq 300$ (series B1 and B2) is small as compared to the relative change of the carbon content (cf. Table 4.4), it follows that the concentration dependence of $D_{\mathrm{CN}}^{\varepsilon}$ is much larger than that for $D_{\mathrm{NC}}^{\varepsilon}$. In any case, the flux due to the $J_{\mathrm{CN}}^{\varepsilon}$ term is expected to be small as compared to the flux due to the $J_{\mathrm{CC}}^{\varepsilon}$ term (cf. Fig. 4.7). Therefore, neglecting a variation of $D_{\mathrm{CN}}^{\varepsilon}$ with concentration in the evaluation given in section 4.4.3 will not have a large effect on the values determined for the diffusion coefficients $D_{\mathrm{NN}}^{\varepsilon}$, $D_{\mathrm{NC}}^{\varepsilon}$ and $D_{\mathrm{CC}}^{\varepsilon}$.

From the diffusion data of nitrogen in γ' obtained in this work it follows that the nitrogen activity in γ' at the ε/γ' phase boundary decreases with increasing carbon activity in the gas atmosphere (Fig. 4.8). This result is in qualitative agreement with calculated potential phase diagrams based on the Hillert-Staffanson approach for ε and γ' [14, 27, 40].

Table 4.7: Thermodynamic factors $\vartheta_{kj}^{\varepsilon}$ at 823 K obtained from the thermodynamic description of the ε phase given in the Appendix and the thermodynamic data in Ref. [15] and Ref. [21], respectively, using a constant composition of 22.15 at.% N and 2.58 at.% C in ε, which corresponds to the average N and C contents obtained from the EPMA measurements of all ε sublayers of series B1 with $a_C \geq 25$. The experimental values of this work for $D_{kj}^{\varepsilon} / D_{jk}^{\varepsilon} \left(= \vartheta_{kj}^{\varepsilon} / \vartheta_{jk}^{\varepsilon} \right)$ have been calculated from the data in Table 4.6.

reference	$\vartheta_{NN}^{\varepsilon}$	$\vartheta_{NC}^{\varepsilon}$	$\vartheta_{CC}^{\varepsilon}$	$\vartheta_{CN}^{\varepsilon}$	$\vartheta_{NC}^{\varepsilon} / \vartheta_{NN}^{\varepsilon}$	$\vartheta_{CN}^{\varepsilon} / \vartheta_{CC}^{\varepsilon}$
This work	---	---	---	---	0.93	0.23
Ref. [15]	5.70	2.52	1.48	0.29	0.44	0.20
Ref. [21]	5.39	-3.70	2.13	-0.43	-0.69	-0.20

Table 4.8: Thermodynamic factors $\vartheta_{kj}^{\varepsilon}$ at 823 K obtained from the thermodynamic description of the ε phase as given in the Appendix and the thermodynamic data in Ref. [15] using the experimental average nitrogen and carbon contents per ε sublayer of series B1 and B2 as determined by EPMA.

series	a_N	a_C	average N content in ε [at.%]	average C content in ε [at.%]	$\vartheta_{NN}^{\varepsilon}$	$\vartheta_{NC}^{\varepsilon}$	$\vartheta_{CC}^{\varepsilon}$	$\vartheta_{CN}^{\varepsilon}$
B1	636	25	23.36	1.29	6.04	2.73	1.24	0.15
B1	636	50	23.08	1.86	6.03	2.71	1.35	0.22
B1	636	100	22.01	2.64	5.63	2.48	1.49	0.30
B1	636	200	21.42	3.26	5.45	2.38	1.61	0.36
B1	636	300	20.91	3.85	5.32	2.31	1.72	0.43
B2	417	200	20.40	4.16	5.07	2.18	1.75	0.44
B2	417	300	19.64	5.15	4.91	2.07	1.93	0.54

4.6 Conclusions

1. A modified parabolic growth law well describes the (sub)layer-growth kinetics of ε/γ' double layers upon both nitriding and nitrocarburizing of pure ferritic iron.

2. The nitrogen and carbon concentration-depth profiles in the ε sublayer could be well described by linear functions. The nitrogen-concentration gradient in the ε sublayer decreases, while the carbon-concentration gradient increases with increasing carbon activity of the nitrocarburizing atmosphere.

3. From single values of the sublayer-growth rates, (i) the self-diffusion coefficient of nitrogen in γ'-Fe$_4$N$_{1-z}$ at 823 K was evaluated as $D_N^{\gamma'*} = 5.4 - 7.6 \times 10^{-16}$ m^{2}s^{-1} and (ii) the

intrinsic diffusion coefficient of nitrogen in ε-Fe$_3$N$_{1+x}$ at 823 K was obtained as $D_\text{N}^\varepsilon = 1.9 \times 10^{-14}$ m^{2}s^{-1}.

4. By fitting to a set of values for the sublayer-growth rates, obtained for various combinations of the nitrogen and carbon activity imposed by the nitrocarburizing atmosphere, the four intrinsic diffusion coefficients of nitrogen and carbon in ε-Fe$_3$(N,C)$_{1+x}$ were determined at 823 K as $D_\text{NN}^\varepsilon = 2.1 \times 10^{-14}$ m$^2 s^{-1}$, $D_\text{NC}^\varepsilon = 2.0 \times 10^{-14}$ m$^2 s^{-1}$, $D_\text{CC}^\varepsilon = 3.6 \times 10^{-15}$ m$^2 s^{-1}$ and $D_\text{CN}^\varepsilon = 8.5 \times 10^{-16}$ m$^2 s^{-1}$. The off-diagonal diffusion coefficients, $D_{kj}^\varepsilon \ (k \neq j)$, are positive and have a strong influence on the diffusive fluxes of N and C in ε and can thus not be neglected for modeling the growth of ε/γ' double layers upon nitrocarburizing of pure α-iron.

5. The ratios of the off-diagonal and diagonal diffusivities, $D_\text{NC}^\varepsilon / D_\text{NN}^\varepsilon$ and $D_\text{CN}^\varepsilon / D_\text{CC}^\varepsilon$, which are equal to the corresponding ratios of the so-called thermodynamic factors, imply significant thermodynamic interaction of both interstitial elements on the same sublattice. The intrinsic diffusion coefficients D_{kj}^ε provide additional information on the thermodynamic properties of the ε phase, which can be used for an accurate assessment of the ternary Fe-N-C system.

Appendix A

According to the Hillert-Staffansson approach [24], the ε phase can be conceived as an interstitial subregular solid solution of formula unit $\left(\text{Fe}\right)_a \left(\text{N,C,Va}\right)_c$ composed of two separate sublattices: one substitutional sublattice with a number of a sites per formula unit occupied by Fe and an interstitial sublattice with a number of c sites per formula unit occupied by N, C and vacancies (Va). The number of sites per formula unit assumed in the literature for the ε phase is $a = 1$, $c = 1$ according to Ref. [15] and $a = 1$, $c = 1/2$ according to Ref. [21], i.e. the site fractions of component k (N, C) in the interstitial sublattice, y_k^ε, given in Ref. [15] and Ref. [21] differ by a factor of 2.

The thermodynamic factors, $\vartheta_{kj}^{\varepsilon}$, can be calculated from the Gibbs energy per formula unit, $G_{\mathrm{m}}^{\varepsilon}$, [15, 21] as

$$\vartheta_{kj}^{\varepsilon} = \frac{y_k}{RT}\frac{\partial^2 G_{\mathrm{m}}^{\varepsilon}}{\partial y_k \partial y_j} = \frac{y_k}{cRT}\frac{\partial \mu_k^{\varepsilon}}{\partial y_j} \quad \text{with } k,j \in (\text{N, C}). \tag{A1}$$

It thus is obtained that

$$\vartheta_{\text{NN}}^{\varepsilon} = \left[\frac{1-y_{\text{C}}^{\varepsilon}}{(1-y_{\text{N}}^{\varepsilon}-y_{\text{C}}^{\varepsilon})} - \frac{2y_{\text{N}}^{\varepsilon}\left[{}^{0}L_{\text{Fe:N,Va}}^{\varepsilon} + 3\left(2y_{\text{N}}^{\varepsilon}+y_{\text{C}}^{\varepsilon}-1\right){}^{1}L_{\text{Fe:N,Va}}^{\varepsilon} \right]}{RT} \right] \tag{A2}$$

$$\vartheta_{\text{NC}}^{\varepsilon} = \left[\frac{y_{\text{N}}^{\varepsilon}}{(1-y_{\text{N}}^{\varepsilon}-y_{\text{C}}^{\varepsilon})} - \frac{y_{\text{N}}^{\varepsilon}\Delta L^{\varepsilon}}{cRT} \right] \tag{A3}$$

$$\vartheta_{\text{CC}}^{\varepsilon} = \left[\frac{1-y_{\text{N}}^{\varepsilon}}{(1-y_{\text{N}}^{\varepsilon}-y_{\text{C}}^{\varepsilon})} - \frac{2y_{\text{C}}^{\varepsilon}\left(y_{\text{N}}^{\varepsilon}{}^{1}L_{\text{Fe:N:Va}}^{\varepsilon} + {}^{0}L_{\text{Fe:C:Va}}^{\varepsilon} \right)}{cRT} \right] \tag{A4}$$

$$\vartheta_{\text{CN}}^{\varepsilon} = \left[\frac{y_{\text{C}}^{\varepsilon}}{(1-y_{\text{N}}^{\varepsilon}-y_{\text{C}}^{\varepsilon})} - \frac{y_{\text{C}}^{\varepsilon}\Delta L^{\varepsilon}}{cRT} \right], \tag{A5}$$

where $\Delta L^{\varepsilon} = \left[{}^{0}L_{\text{Fe:N:Va}}^{\varepsilon} + 2\left(3y_{\text{N}}^{\varepsilon}+y_{\text{C}}^{\varepsilon}-1\right){}^{1}L_{\text{Fe:N:Va}}^{\varepsilon} \right] + {}^{0}L_{\text{Fe:C:Va}}^{\varepsilon} - {}^{0}L_{\text{Fe:N:C}}^{\varepsilon}$, y_k^{ε} is the site fraction of component k in the interstitial sublattice, ${}^{0}L_{\text{Fe:N:Va}}^{\varepsilon}$ and ${}^{0}L_{\text{Fe:C:Va}}^{\varepsilon}$ are the regular solid solution parameters and ${}^{1}L_{\text{Fe:N:Va}}^{\varepsilon}$ is the subregular solid solution parameter. The first term of the thermodynamic factor $\vartheta_{kj}^{\varepsilon}$ given at the right-hand side of Eqs. (A2) to (A5) represents the contribution of the configurational entropy and the second term represents the contribution of the excess enthalpy, describing the non-ideality of the system, i.e. the interaction of nitrogen and carbon. The (sub)regular parameters can be obtained on the basis of an assessments of the ternary Fe-N-C system [15, 21, 39]. Note that the thermodynamic model assumed in Ref. [21] provides a more distinct contribution of the configurational entropy to the thermodynamic factor as compared to the model used in Ref. [15].

Note that also for ideal systems (then the (sub)regular parameters and thus the excess enthalpy is zero) with a wide composition range, the off-diagonal thermodynamic factors can be significant due to the configurational entropy i.e. $\vartheta_{kj}^{\varepsilon} / \vartheta_{kk}^{\varepsilon} = y_k^{\varepsilon} / \left(1 - y_j^{\varepsilon}\right)$, reflecting the geometrical interaction of nitrogen and carbon. It holds that $\vartheta_{kj}^{\varepsilon} \left(k \neq j\right) \to 0$ for $y_k^{\varepsilon} \to 0$, which, obviously, is not the case for the diagonal components.

Appendix B

The gas composition used for the nitriding and nitrocarburizing experiments of series A1, A2, B1 and B2 has been given in Table I. These gas compositions as claimed to impose specific combinations of a_N and a_C at 823 K, were calculated as described in Ref. [62].

Table I: Composition of the nitriding / nitrocarburizing gas atmosphere used for the nitriding and nitrocarburizing experiments of series A1, A2, B1 and B2 at 823 K.

series	a_N	a_C	NH_3 [vol.%]	H_2 [vol.%]	CO [vol.%]	CO_2 [vol.%]	H_2O [vol.%]
A1, B1	636	0	16.0	22.35	--	--	--
B1	636	12.5	16.0	22.35	27.07	28.16	6.46
B1	636	25	16.0	22.35	34.57	22.97	4.10
A2, B1	636	50	16.0	22.35	42.11	17.04	2.50
B1	636	100	16.0	22.35	48.77	11.43	1.45
B1	636	50	20.0	25.94	37.76	13.70	2.60
B1	636	100	20.0	25.94	43.48	9.09	1.50
B1	636	200	20.0	25.94	47.76	5.48	0.82
B1	636	300	20.0	25.94	49.56	3.93	0.57
B2	417	0	20.0	34.37	--	--	--
B2	417	12.5	20.0	34.37	21.01	16.97	7.66
B2	417	25	20.0	34.37	26.86	13.87	4.90
B2	417	50	20.0	34.37	32.51	10.16	2.96
B2	417	100	20.0	34.37	37.26	6.67	1.70
B2	417	200	20.0	34.37	40.72	3.98	0.93
B2	417	300	20.0	34.37	42.15	2.85	0.64

Chapter 5

The shape of nitrogen concentration-depth profiles in γ'-Fe$_4$N$_{1-z}$ layers growing on α-Fe substrates; the thermodynamics of γ'-Fe$_4$N$_{1-z}$

T. Woehrle[1], A. Leineweber[1], E.J. Mittemeijer[1,2]

[1]*Max Planck Institute for Intelligent Systems (formerly Max Planck Institute for Metals Research), Heisenbergstraße 3, D-70569 Stuttgart, Germany*

[2]*Institute for Materials Science, University of Stuttgart, Stuttgart, Germany*

Abstract

An unusual, concave curvature is observed in experimental nitrogen concentration-depth profiles in the surface region of γ'-Fe$_4$N$_{1-z}$ layers obtained upon nitriding of pure iron at 823 K (550 °C) and 843 K (570 °C). It can be shown by simulation of nitrogen concentration-depth profiles in γ'-layers, adopting the thermodynamic Wagner-Schottky approach applied to γ'-Fe$_4$N$_{1-z}$, that this concave character is due to the strong concentration dependence of the Gibbs energy of the γ'-phase, which is counter-intuitive in recognition of the very small homogeneity range of γ' iron nitride. Thereby, for γ'-layers with low porosity, a previous suggestion ascribing the concave shape to the additional uptake of nitrogen through porous grain-boundary channels is rendered less likely.

5.1 Introduction

Nitriding is a widely applied thermochemical surface treatment for iron and iron-based alloys (usually performed at temperatures between 823 K (550 °C) and 853 K (580 °C)) by which nitrogen is supplied to the surface region of a workpiece [5, 8, 61, 77]. During nitriding a compound layer typically composed of the iron nitrides ε and/or γ' can be formed at the surface of the material [7, 33]. Underneath the compound layer a diffusion zone develops in the ferrite matrix, in which nitrogen is interstitially dissolved. Both, the compound layer and the diffusion zone can lead to significant improvement of the mechanical and chemical properties of the material due to structural and chemical changes in the nitrided region [1-3, 78]. The control of the nitriding process strongly depends on the accuracy of the thermodynamic models of the solid phases involved, in particular of the ε and the γ' phases in the Fe-N system [15, 21-23, 76, 79]. Such thermodynamic data are not only suitable to describe solid-gas and solid-solid phase equilibria but can also be used to determine the driving forces of N diffusion-controlled reactions in the solid state, which are essential to understand the rate of the associated kinetic processes [7, 38].

In the binary system Fe-N the γ'-Fe_4N_{1-z} phase has a very narrow homogeneity range close to the ideal stoichiometric composition of Fe_4N with a maximum nitrogen content of 20 at.% [18]. The nitrogen atoms in Fe_4N (face-centered cubic arrangement of iron atoms) occupy one-quarter of all available octahedral interstitial sites in the iron substructure by a specific long-range ordering (LRO) such that, in the conventional unit cell, the octahedral site of the position (1/2, 1/2, 1/2) is preferentially occupied by nitrogen atoms and the octahedral sites of the positions (1/2, 0, 0), (0, 1/2, 0) and (0, 0, 1/2) are preferentially unoccupied; see Fig. 5.1 [76, 80-84]. Note that the translation lattice becomes primitive due to this long-range ordering of nitrogen, leading to the designated space-group symmetry $Pm\overline{3}m$.
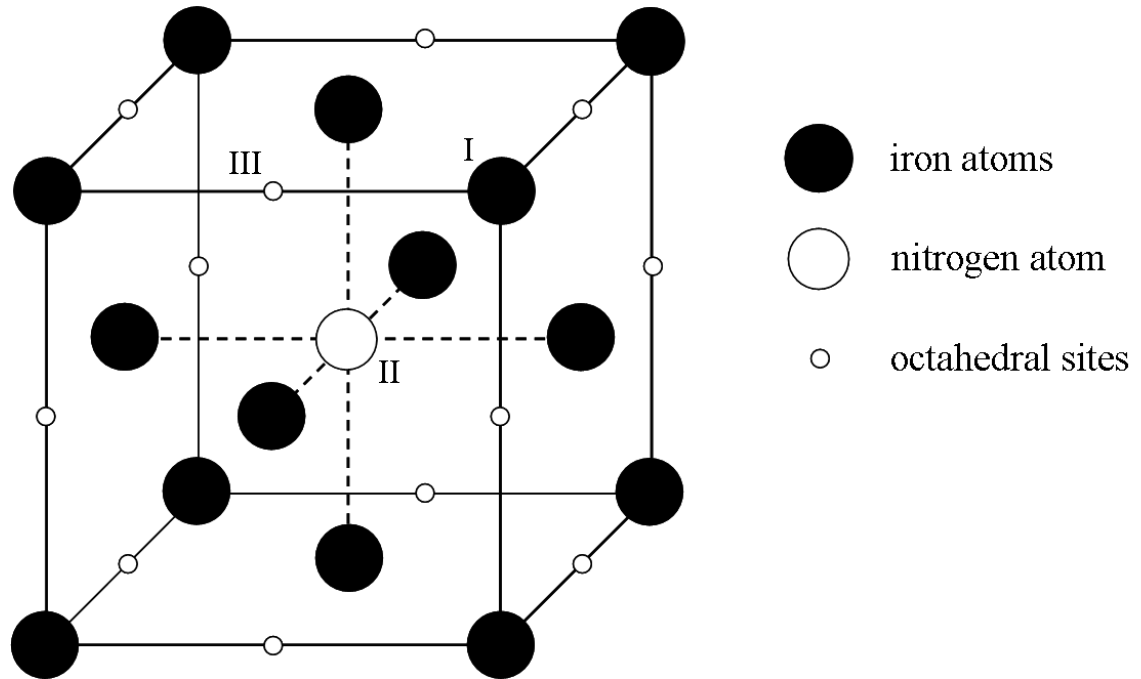
Fig. 5.1: Crystal structure of γ'-Fe$_4$N$_{1-z}$ exhibiting a face-centered cubic arrangement of iron atoms. The nitrogen atoms preferentially occupy octahedral sites of type II at (1/2, 1/2, 1/2) positions, whereas the octahedral sites of type III at positions (1/2, 0, 0), (0, 1/2, 0) and (0, 0, 1/2) are preferentially unoccupied.

A first thermodynamic description of the γ'-phase was proposed by Wagner and Schottky on the basis of variations of the configurational entropy by the occurrence of defects in the atomic ordering [85]. Further models for the γ' phase are given by the Langmuir-type approach [86], the Gorsky-Bragg-Williams approach [86] and the Hillert-Staffansson approach (compound-energy formalism) [21, 59], cf. section 5.2.3. In accordance with these thermodynamic approaches, the γ'-phase can be described as an interstitial solid solution $Fe_4^I(N^{II}, Va^{II})_1(N^{III}, Va^{III})_3$ composed of three separate sublattices [59, 69], one main sublattice occupied by iron and two interstitial sublattices occupied by nitrogen (N) and vacancies (Va), where the subscript II denotes the mainly occupied octahedral sites ("ordered sublattice") and the subscript III denotes the mainly unoccupied octahedral sites ("disordered sublattice").

In the case of *hypo-stoichiometric* γ'-Fe$_4$N$_{1-z}$ (i.e. with a N content smaller than 20 at.%; $z > 0$), the site fraction of nitrogen, y_N, will ideally (at $T = 0$ K (-273 °C)) be $y_N^{II} < 1$ in the "ordered sublattice" and $y_N^{III} = 0$ in the "disordered sublattice" i.e. the

composition is modified by "N vacancies" as constitutional defects on sublattice II. In contrast, for (hypothetical) *hyper-stoichiometric* γ'-Fe$_4$N$_{1-z}$ (i.e. with a N content larger than 20 at.%; $z < 0$) at $T = 0$ K (-273 °C) occupancies of $y_N^{II} = 1$ and $y_N^{III} > 0$ will occur, i.e. the composition is modified by "N interstitials" as constitutional defects on sublattice III. Moreover, in both cases (hypo-stoichiometric and hyper-stoichiometric γ'-Fe$_4$N$_{1-z}$), the formation of additional thermal defects given by $y_N^{III, th}$ and $y_{Va}^{II, th}$ can occur at $T > 0$ K (-273 °C) (even at the ideal stoichiometric composition Fe$_4$N) by the transfer of nitrogen atoms from sublattice II to sublattice III resulting in an increase in the configurational entropy. The number of thermal defects is determined by thermodynamic equilibrium and varies as function of temperature.

The extent of the homogeneity range of γ' has been investigated by various authors [83, 84, 87-97]. A considerable number of experimental results indicate the γ'-Fe$_4$N$_{1-z}$ to be *hypo-stoichiometric* [84, 88, 91, 92, 95, 97]. The formation of *hyper-stoichiometric* γ'-Fe$_4$N$_{1-z}$ has been observed in Refs. [83, 87, 89, 90, 92-94, 96]. However, the latter data appear to be unreliable as shown by thermodynamic analyses [84, 86, 95]. Hence, the γ'-phase is hypo-stoichiometric, e.g. the formation of ε-iron nitride phase is more favorable than exceeding the stoichiometric composition in γ'[21]. Indeed, all of the more recent experimental studies (see above) on the extent of the homogeneity range of the γ' phase confirm this conclusion.

Until now, numerous analytical and numerical calculations have been performed on the basis of the above-mentioned thermodynamic descriptions of γ'-Fe$_4$N$_{1-z}$ in order to model the growth kinetics of γ'-layers during gaseous nitriding of pure α-Fe [38, 54, 59, 73, 98, 99]. Furthermore, as a particular aspect of such studies, the defect mechanism of nitrogen diffusion in γ' has been analyzed by several authors [69, 70, 100]. However, none of these studies was focused on the nitrogen concentration-depth profile in γ'-layers.

The present work was motivated by the strikingly concave shape of the nitrogen concentration-depth profiles in the surface region of γ'-Fe$_4$N$_{1-z}$ layers formed on α-Fe substrates upon gaseous nitriding, as determined by X-ray diffraction analyses [44, 101]

---

[21] The observation of seemingly hyperstoichiometric γ' may be ascribed to systematic experimental errors such as the detection of adsorbed nitrogen at the specimen surface [84].

(cf. Figure 5.3a-c). The concave character of the concentration-depth profiles had been ascribed to the occurrence of porosity[22] in the surface-adjacent region of the compound layer, which allows direct contact of γ' at some depth of the layer with the nitriding atmosphere leading to an additional uptake of nitrogen. Thus, the concentration-depth profiles as expected for non-porous compound layers will be distorted.

A nitrogen concentration-depth profile in γ' based on numerical calculations was presented by Belmonte et al. [98]. Until now, such calculated concentration-depth profiles have not been compared with experimental data.

In the present work, it will be demonstrated that the observed concave shape of the nitrogen concentration-depth profiles can be explained by the strong concentration-dependence of the intrinsic diffusion coefficient of nitrogen in γ'-Fe$_4$N$_{1-z}$, in particular close to the ideal stoichiometric composition Fe$_4$N. This (specific) concentration dependence of the intrinsic diffusion coefficient can be shown to be a direct consequence of the thermodynamics of the γ' phase.

5.2   Theoretical background

5.2.1   Concentration variables

Three different concentration variables for nitrogen to be applied in the present work are introduced below.

The *atomic ratio* $u_N^{(\gamma')}$ denotes the number of nitrogen atoms divided by the number of iron atoms in Fe$_4$N$_{1-z}$ as exhibited by the chemical formula

$$\text{Fe}_4\text{N}_{4u_N^{(\gamma')}} = \text{FeN}_{u_N^{(\gamma')}} \tag{5.1}$$

implying $4u_N^{(\gamma')} = 1 - z$, i.e. for ideal stoichiometric Fe$_4$N it holds that $u_N^{(\gamma')} = 1/4$.

---

[22] Porosity is caused by the metastability of the γ' phase with respect to pure iron and molecular nitrogen gas at normal nitriding temperature and pressure, leading to the precipitation of N$_2$ gas, predominantly at grain boundaries in the surface adjacent region of the compound layer layer [69, 101, 102].

The *molar concentration* $c_N^{(\gamma')}$, as used to model diffusion processes on the basis of conventional forms of Fick's laws can be related to $u_N^{(\gamma')}$ by

$$c_N^{(\gamma')} = \frac{u_N^{(\gamma')}}{N_{Av} V^{(\gamma')}},$$
(5.2)

where N_{Av} is Avogadro's number and $V^{(\gamma')}$ represents the volume of the unit cell of γ' per iron atom.

The atomic ratio $u_N^{(\gamma')}$ can be expressed in terms of the *site fractions* of nitrogen on the interstitial sublattices II and III by recognizing that, per iron atom, there is one octahedral site II and there are three octahedral sites III. It follows

$$u_N^{(\gamma')} = \frac{1}{4} y_N^{II} + \frac{3}{4} y_N^{III}.$$
(5.3)

5.2.2   Modeling of nitrogen diffusion in the γ' phase

The following assumptions have been made for modeling the time and temperature dependences of the layer thickness and of the nitrogen concentration-depth profiles in γ'-layers growing on α iron: (i) The volume of the unit cell of a phase ϕ (i.e. γ' and α) per iron atom $V^{(\phi)}$ is independent of the nitrogen concentration; (ii) The surface of the compound layer and the layer/substrate interface are planar and parallel; (iii) The nitrogen concentrations in γ' at the compound-layer surface $c_N^{\gamma'/gas}$ and at the layer/substrate interface $c_N^{\gamma'/\alpha}$ are constant and determined by local thermodynamic equilibrium. These equilibrium concentrations have been calculated from thermodynamic data of the Fe-N system [7, 86] for the nitriding conditions applied (cf. Table 5.1). The experimentally determined nitrogen concentrations at the gas/γ' interface and at the γ'/α interface are in good agreement with the calculated values (cf. Table 5.2) confirming the practical establishment of local equilibrium at both sides of the γ' layer; (iv) The α-Fe

substrate is saturated with nitrogen yielding a net flux of nitrogen in ferrite equal to nil. The nitrogen concentration in a saturated α-Fe substrate is 0.36 at.% at 843 K (570 °C) and 0.29 at.% at 823 K (550 °C) [15]; (v) The γ' layer is immediately formed at the start of nitriding and covers the whole substrate; (vi) The growth of the compound layer is controlled by the inward diffusion of nitrogen, resulting in a parabolic growth law[23] as given by the expression $\xi^{(\gamma')} = k^{(\gamma')}\sqrt{t}$, where $\xi^{(\gamma')}$ is the layer thickness, $k^{(\gamma')}$ is the parabolic growth constant and t is the treatment time.

For one-dimensional diffusion the flux of nitrogen in γ', $J_N^{(\gamma')}$, obeys Fick's first law

$$J_N^{(\gamma')} = -D_N^{(\gamma')}\left(\frac{\partial c_N^{(\gamma')}}{\partial x}\right)_{p,T}, \qquad (5.4)$$

where $D_N^{(\gamma')}$ is the intrinsic diffusion coefficient of N in γ', which may depend on the nitrogen concentration, x is the depth coordinate along which diffusion takes place and $c_N^{(\gamma')}$ is the concentration of N at depth x expressed as a quantity per unit volume. The depth x is measured from the surface of the compound layer where $x = 0$. The diffusion of iron atoms in γ' can be neglected at the nitriding temperatures, i.e. $D_{Fe}^{(\gamma')} \approx 0$.

Fick's first law (cf. Eq. (5.4)) can be conceived as the result of adopting the gradient of the chemical potential as the driving force for diffusion. For crystalline phases where the diffusion of a species occurs by a vacancy mechanism of atoms jumping into neighboring vacant lattice sites, e.g. as for nitrogen in γ', it holds that [69, 72]

$$J_N^{(\gamma')} = -y_{Va}^{(\gamma')}c_N^{(\gamma')}M_N^{(\gamma')}\left(\frac{\partial \mu_N^{(\gamma')}}{\partial x}\right)_{p,T}, \qquad (5.5)$$

---

[23] The parabolic growth law is expected to be exactly valid in the case of local equilibrium at both interfaces of the layer and either a completely nitrogen-saturated α-iron substrate or an initially unsaturated substrate of infinite thickness. In the following the case of a fully nitrogen-saturated substrate will be adopted because of the relatively fast saturation of the up to 2 mm thick α-iron substrates at the nitriding conditions applied (cf. Table 5.1).

where $y_{Va}^{(\gamma')}$ is the fraction of vacant sites, in the sublattice where diffusion takes place, $M_N^{(\gamma')}$ is the atomic mobility, $\mu_N^{(\gamma')}$ is the chemical potential of nitrogen in γ', T is the absolute temperature and p is the pressure.

The combination of Eq. (5.4) and Eq. (5.5) yields an expression for the concentration dependence of the intrinsic diffusion coefficient as

$$D_N^{(\gamma')} = y_{Va}^{(\gamma')} M_N^{(\gamma')} c_N^{(\gamma')} \left(\frac{\partial \mu_N^{(\gamma')}}{\partial c_N^{(\gamma')}} \right)_{p,T} = D_N^{(\gamma')*} \varphi_N^{(\gamma')}, \tag{5.6}$$

with

$$\varphi_N^{(\gamma')} = \frac{c_N^{(\gamma')}}{RT} \left(\frac{\partial \mu_N^{(\gamma')}}{\partial c_N^{(\gamma')}} \right)_{p,T}, \tag{5.7}$$

where $D_N^{(\gamma')*} = y_{Va}^{(\gamma')} M_N^{(\gamma')} RT$ [24] is the self-diffusion coefficient of N in γ', R is the gas constant and $\varphi_N^{(\gamma')}$ is the so-called thermodynamic factor, which relates the intrinsic diffusion coefficient to the self-diffusion coefficient. The thermodynamic factor $\varphi_N^{(\gamma')}$ can be evaluated from the thermodynamic description of the γ'-phase, as shown in section 5.2.3. Note that the thermodynamic factor can only be assumed to be constant for ideal solid solutions or diluted solid solutions obeying Henry's law.

As suggested in a couple of works involving diffusion of nitrogen in γ' iron-nitride [54, 59, 98], the self-diffusion coefficient $D_N^{(\gamma')*}$ is in the following assumed to be independent of concentration, implying that $y_{Va}^{(\gamma')}$ is constant. Two scenarios can lead to that situation: (a) Close to the stoichiometric composition Fe$_4$N the thermal vacancies (superscript "th") on sublattice II are the predominant type of vacancies as compared to the constitutional vacancies (superscript "cst") [69]: $y_{Va}^{II,cst} \ll y_{Va}^{II,th}$. The concentration of

---

[24] The self-diffusion coefficient normally is written as $D_N^{(\gamma')*} = M_N^{(\gamma')\prime} c_N^{(\gamma')}$, where $M_N^{(\gamma')\prime} = y_{Va}^{(\gamma')} M_N^{(\gamma')}$.

thermal vacancies is assumed to be independent of concentration and determined by thermodynamic equilibrium, i.e. $y_{\mathrm{Va}}^{\mathrm{II,th}}$ is constant over the γ' layer. Considering diffusion in both interstitial sublattices II and III, the self-diffusion coefficient of nitrogen in γ' can be obtained from Eq. (5.6) as $D_{\mathrm{N}}^{(\gamma')*} = y_{\mathrm{Va}}^{\mathrm{II,th}} M_{\mathrm{N}}^{(\gamma')} RT$ [69] [25]; (b) the diffusion of nitrogen mainly occurs in the "disordered" sublattice III, where $y_{\mathrm{Va}}^{\mathrm{III}} \approx 1$ [59], leading to $D_{\mathrm{N}}^{(\gamma')*} = y_{\mathrm{Va}}^{\mathrm{III}} M_{\mathrm{N}}^{(\gamma')} RT$ (cf. Eq. (5.6)).

The nitrogen concentration-depth profile in a γ' layer growing on the surface of an α-Fe substrate can be obtained from Eq. (5.4) under the constraint of the prevailing boundary conditions (i) to (vi). As proposed in Refs. [59, 69], quasi-steady state diffusion[26] of nitrogen through the growing γ'-layer is assumed during nitriding, i.e. at a given time the diffusive flux of nitrogen $J_{\mathrm{N}}^{(\gamma')}$ is constant throughout the γ'-layer and its instantaneous value depends only on the actual layer thickness $\xi^{(\gamma')}$.

Calculation of the concentration-depth profiles under quasi-steady state conditions is based on integration of Eq. (5.4) as follows

$$J_{\mathrm{N}}^{(\gamma')} \int_{0}^{x} dx = \int_{c_{\mathrm{N}}^{\gamma'\,gas}}^{c_{\mathrm{N}}^{(\gamma')}(x)} D_{\mathrm{N}}^{(\gamma')}\left(c_{\mathrm{N}}^{(\gamma')}\right) dc_{\mathrm{N}}^{(\gamma')}, \qquad (5.8)$$

where $c_{\mathrm{N}}^{\gamma'\,gas}$ denotes the N concentration in γ' at the gas$/\gamma'$ interface and x in the range $0 \leq x \leq \xi^{(\gamma')}$ represents a certain depth as measured from the surface ($x = 0$).

---

[25] Assuming the mobility in both sublattices to be different the total flux of nitrogen through the γ' layer is given by the sum of the fluxes in sublattices I and in sublattice II. According to Ref. [27] it holds that $M_{\mathrm{N}}^{(\gamma')} = M_{\mathrm{N}}^{\mathrm{II}} + M_{\mathrm{N}}^{\mathrm{III}}$.

[26] In quasi-steady state diffusion, the depth variation of the local concentration gradient $\partial c_{\mathrm{N}}^{(\gamma')}/\partial x$ is balanced by a concentration dependence of the intrinsic diffusion coefficient $D_{\mathrm{N}}^{(\gamma')}$ (here: due to the thermodynamic factor) such that the flux of nitrogen through the γ'-layer $J_{\mathrm{N}}^{(\gamma')}$ remains constant and independent of depth (cf. Eq. (5.4)). Then the local concentration gradient within the γ'-layer is directly proportional to the reciprocal of the diffusion coefficient. This quasi-steady state diffusion assumption in γ' could be validated by numerical calculations (see discussion in section 5.4) and is only an acceptable approximation of reality because of the very small homogeneity range of γ' together with the large nitrogen concentration difference of the γ' layer and the α-iron substrate.

The flux of nitrogen in γ', $J_N^{(\gamma')}$, can thus be obtained from Eq. (5.8) with the boundary condition $c_N^{(\gamma')} = c_N^{\gamma'/\alpha}$ at $x = \xi^{(\gamma')}$, where $c_N^{\gamma'/\alpha}$ is the nitrogen concentration at the γ'/α interface. Finally, dividing Eq. (5.8) with the upper limits of integration x and $c_N^{(\gamma')}(x)$ by Eq. (5.8) with the upper limits of integration $\xi^{(\gamma')}$ and $c^{\gamma'/\alpha}$, followed by substitution of $D_N^{(\gamma')}$ according to Eq. (5.6) with a constant $D_N^{(\gamma')*}$, yields an implicit expression for the steady-state nitrogen concentration profile

$$\int_{c_N^{\gamma'\,\text{gas}}}^{c_N^{(\gamma')}(x)} \varphi_N^{(\gamma')} dc_N^{(\gamma')} \times \left(\int_{c_N^{\gamma'\,\text{gas}}}^{c_N^{\gamma'/\alpha}} \varphi_N^{(\gamma')} dc_N^{(\gamma')} \right)^{-1} = \frac{x}{\xi^{(\gamma')}} . \tag{5.9}$$

The concentration-depth profile of nitrogen $c_N^{(\gamma')}(x)$ in γ' (with the depth x normalized with respect to the layer thickness $\xi^{(\gamma')}$) can be calculated from Eq. (5.9) if an expression for the temperature and concentration dependence of $\varphi_N^{(\gamma')}$ is available. Note that the assumed constancy of the nitrogen flux in γ' (at a given temperature) does not imply that the concentration-depth profile is linear: the shape of the concentration-depth profile is fully determined by the concentration dependence of the thermodynamic factor $\varphi_N^{(\gamma')}$.

The growth constant $k^{(\gamma')}$ in the parabolic growth law (see assumption (vi)) can now be derived assuming that all nitrogen atoms diffusing through the γ' layer are accumulated at the γ'/α interface to convert α into γ'. For quasi-steady state diffusion, the combination of Eq. (5.8) and a continuity equation for mass conservation at the moving interface between the γ' layer and the α-Fe substrate [54] yields

$$k^{(\gamma')} = \sqrt{\frac{2}{\left(c_N^{\gamma'/\alpha} - c_N^{\alpha/\gamma'}\right)} \int_{c_N^{\gamma'\,\text{gas}}}^{c_N^{\gamma'/\alpha}} D_N^{(\gamma')} dc_N^{(\gamma')}} \approx \sqrt{\frac{2 D_N^{(\gamma')*}}{c_N^{\gamma'/\alpha}} \int_{c_N^{\gamma'\,\text{gas}}}^{c_N^{\gamma'/\alpha}} \varphi_N^{(\gamma')} dc_N^{(\gamma')}} , \tag{5.10}$$

where $k^{(\gamma')}$ has the dimension [length/(time$^{1/2}$)], $D_N^{(\gamma')} = D_N^{(\gamma')*}\varphi_N^{(\gamma')}$ and $c_N^{\gamma'/\alpha} - c_N^{\alpha/\gamma'} \approx c_N^{\gamma'/\alpha}$.

The temperature dependence of $D_N^{(\gamma')*}$ was evaluated by Somers and Mittemeijer [54] as

$$\ln\left(D_N^{(\gamma')*}/m^2s^{-1}\right) = -21.48 - \left(9.14\times10^4\ Jmol^{-1}/RT\right) \quad \text{for}\ \ 777\ K\ (504\ °C)\ <\ T\ <\ 843\ K$$
(570 °C).

5.2.3 Evaluation of the thermodynamic factor of the diffusion coefficient of nitrogen in the γ'-phase

Several thermodynamic models of the γ'-phase in the binary Fe-N system have been proposed, e.g. the Langmuir-type (L) approach [86], the Hillert-Staffansson (HS) approach [21], the Wagner-Schottky (WS) approach [85, 86] and the Gorsky-Bragg-Williams (GBW) approach [86]. A comparison of these approaches shows that the WS approach and the GBW approach give the most accurate descriptions of the experimentally determined nitrogen-absorption isotherms of the γ'-phase, which directly reflect the thermodynamics of the γ'-Fe$_4$N$_{1-z}$ phase [86]. In fact, both approaches describe the experimental reality equally well, due to the very small degree of thermal disorder of the N atoms even at high temperatures [84, 86, 95, 97]. The N distributions over sites II and III according to the GBW approach (as required for the calculation of the thermodynamic factors) can only be determined numerically. For that reason, the analytical WS approach is adopted in the following (see Appendix A for a brief discussion of the other approaches).

According to the WS approach [85] for γ' it is assumed that ¼ of the octahedral interstices are preferentially occupied by nitrogen, whereas the remaining ¾ of the octahedral interstices are preferentially occupied by vacancies. By taking into account the thermodynamic exchange of nitrogen between the two types of octahedral sites pertaining to sublattices II and III, the chemical potential of nitrogen can be derived from the molar Gibbs energy per formula unit $Fe_4^I(N^{II}, Va^{II})_1(N^{III}, Va^{III})_3$ as [86]

$$\mu_N^{(\gamma')} = {}^0G_{N,\gamma'}^{WS} + RT \ln \left\{ \sqrt{1 + \left(\frac{u_N^{(\gamma')} - 1/4}{2K_{\gamma'}^{WS}} \right)^2} + \frac{u_N^{(\gamma')} - 1/4}{2K_{\gamma'}^{WS}} \right\}, \tag{5.11}$$

where $u_N^{(\gamma')}$ is given by Eq. (5.3), ${}^0G_N^{WS}$ is the Gibbs energy of one mole nitrogen in the reference state defined via the nitriding potential [61] pertaining to equilibrium of a NH_3/H_2 gas mixture with (hypothetical) γ'-Fe_4N (see Ref. [86]). $K_{\gamma'}^{WS}$ is a temperature-dependent constant, which is related to but not identical with the equilibrium constant for the exchange of nitrogen atoms between "ordered" sites II and "disordered" sites III. For small deviations from stoichiometry (i.e. Fe_4N) it was found that [86]

$$\ln 4K_{\gamma'}^{WS} = 2.98 - \frac{7.56 \times 10^3}{(T/K)}. \tag{5.12}$$

It is now possible to obtain the thermodynamic factor for nitrogen diffusion in γ' by combining Eq. (5.2), Eq. (5.7) and Eq. (5.11) as

$$\varphi_N^{(\gamma')} = \frac{u_N^{(\gamma')}}{RT} \frac{d\mu_N^{(\gamma')}}{du_N^{(\gamma')}} = \frac{4u_N^{(\gamma')}}{\sqrt{\left(1 + 16 \left(u_N^{(\gamma')} \right)^2 - 8u_N^{(\gamma')} + 64 \left(K_{\gamma'}^{WS} \right)^2 \right)}}. \tag{5.13}$$

The thermodynamic factor of nitrogen in γ'-Fe_4N_{1-z} is shown in Fig. 5.2 as a function of the concentration variable $4u_N^{(\gamma')} = 1 - z$ at 853 K (580 °C) for different thermodynamic models (WS, L, HS). The $\varphi_N^{(\gamma')}$ vs. $4u_N^{(\gamma')} = 1 - z$ curves in Fig. 5.2 reveal a strong concentration dependence of $\varphi_N^{(\gamma')}$ within the stability range of the γ' phase, in particular for nitrogen concentrations very close to the stoichiometric composition Fe_4N. For the Langmuir-type approach and the HS approach the thermodynamic factor diverges to infinity for $4u_N^{(\gamma')} \rightarrow 1$, whereas the WS approach exhibits a maximum of about $\varphi_N^{(\gamma')} \approx 180$ at $4u_N^{(\gamma')} = 1$ (note that the WS approach is also valid for nitrogen

concentrations exceeding the stoichiometric composition Fe$_4$N). For nitrogen concentrations below the stoichiometric composition, the Wagner-Schottky approach follows a Langmuir-type behaviour (cf. Appendix A). As shown in section 5.4, only concentrations of $0.966 < 4u_N^{(\gamma')} < 0.996$ (corresponding to a N content between 19.45 at.% and 19.93 at.%) are of relevance for the simulations of the concentration-depth profiles.
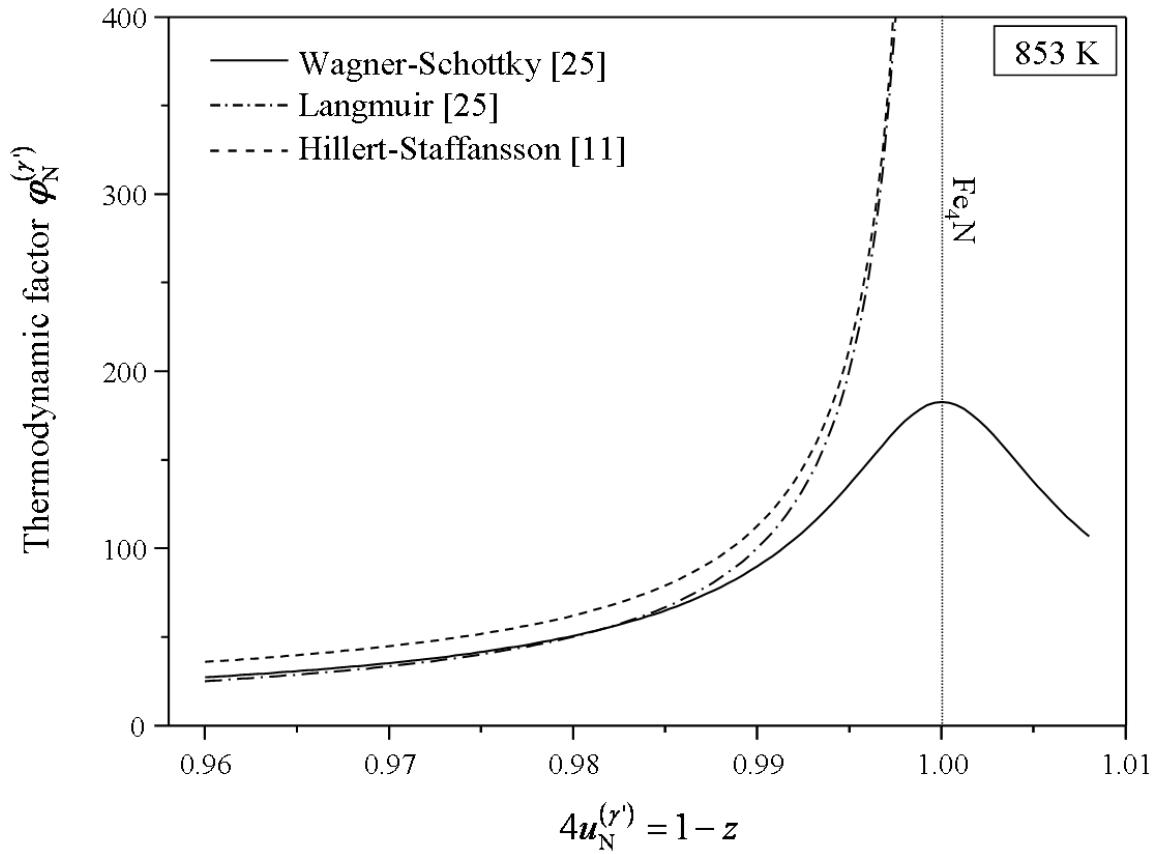
Fig. 5.2: The thermodynamic factor for nitrogen diffusion in γ'-Fe$_4$N$_{1-z}$ at 853 K (580 °C) calculated according to the Wagner-Schottky approach, the Langmuir-type approach and the Hillert-Staffansson approach, as function of the concentration variable $4u_N^{(\gamma')} = 1 - z$.

5.3   Experimentally determined nitrogen concentration-depth profiles

Somers and Mittemeijer [101] as well as Wohlschlögel et al. [44] quantitatively determined nitrogen concentration-depth profiles in γ'-Fe_4N_{1-z} layers grown on pure α-Fe substrates upon nitriding in NH_3/H_2 gas mixtures at 843 K (570 °C) [101] and 823 K (550 °C) [44], by application of dedicated X-ray diffraction analyses. Their results are shown in Figs. 5.3a-c. The nitrogen concentration-depth profiles in the investigated γ'-layers are all concave, i.e. the experimental concentration values within the layers are located above the straight line connecting the surface and interface concentrations. In particular considering the surface-adjacent region of the compound layer, the nitrogen-concentration gradient increases from the surface to the layer/substrate interface, while the nitrogen concentration decreases.

The process parameters applied for the nitriding experiments have been summarized in Table 5.1. Practically no porosity was found by optical microscopic analysis of the γ' layer cross-section (magnification 500x) for specimens A823 (Fig. 5.3a) [44] and A843 (Fig. 5.3b) [101], whereas pronounced grain-boundary porosity was observed for specimen B843 (Fig. 5.3c) [101].

Table 5.1: Process parameters applied for nitriding experiments at 823 K (550 °C) [44] and 843 K (570 °C) [101]. The nitriding potential r_N is defined as $r_N = p_{NH_3} / p_{H_2}^{3/2}$ and is directly related to the chemical potential of nitrogen in NH_3/H_2 gas mixtures [61].

Reference	Specimen	T [K]	t [h]	NH_3 [vol.%]	H_2 [vol.%]	r_N [atm$^{-1/2}$]
[44]	A823	823	5	43	57	1.00
[101]	A843	843	15	30	70	0.51
[101]	B843	843	30	40	60	0.86

5.4   Calculated nitrogen concentration-depth profiles

Calculation of the nitrogen concentration-depth profiles was divided into two steps: (i) calculation of the concentration-depth profiles as a function of the normalized depth $x/\xi^{(\gamma')}$ and (ii) calculation of the actual layer thicknesses $\xi^{(\gamma')}$.

Table 5.2: Calculated (cf. Eq. A6 in Ref. [54]) and experimental [44, 101] nitrogen concentrations in γ' at the surface and at the interface of the compound layer for different nitriding conditions.

Specimen	Calculated		Experimental[*]	
	$c_N^{\gamma'/gas}$ [at.%]	$c_N^{\gamma'/\alpha}$ [at.%]	$c_N^{\gamma'/gas}$ [at.%]	$c_N^{\gamma'/\alpha}$ [at.%]
A823	19.93	19.58	19.88	19.58
A843	19.83	19.45	19.82	19.49**
B843	19.90	19.45	19.88	19.47**

[*] The nitrogen concentrations were obtained from the strain-free lattice spacing d_0^{hkl} [44, 101].

[**] The nitrogen concentration in γ' could only be measured at some distance to the γ'/α interface due to the experimental method applied in Ref. [101]. The given concentration values are thus likely a little higher than the actual values at the γ'/α interface.

Table 5.3: Calculated (cf. the parabolic growth law given in section 5.2.2, assumption (vi) and Eq. (5.10)) as well as experimental [44, 101] γ'-layer thicknesses.

Specimen	Calculated layer thickness [µm]	Experimental layer thickness [µm]
A823	5.8	~ 6
A843	9.8	9.3 ± 0.4
B843	16.5	20.6 ± 1.0

The quasi steady-state nitrogen concentration-depth profile in γ' was calculated from Eq. (5.9) as a function of the normalized depth $x/\xi^{(\gamma')}$ for the case of (1) a concentration dependent thermodynamic factor $\varphi_N^{(\gamma')}$ according to the WS approach and (2) for the case of a concentration independent thermodynamic factor. In the latter case the thermodynamic factor disappears from Eq. (5.9) and a virtually linear concentration-depth profile is obtained[27], whereas in the first case distinctly non-linear concentration-depth profiles result[28], which are shown in Figs. 5.3a-c.

The calculated quasi steady-state nitrogen concentration-depth profiles were compared with profiles obtained by the numerical solution of Fick's second law for non-steady state diffusion using a Crank-Nicolson scheme and moving boundary conditions [56, 103] (results not shown here). For case (1), the profiles from the numerical solution and from Eq. (5.9) are in excellent agreement confirming the quasi-steady state

---

[27] The exact solution for case (2) would be a complementary error function [38], which, in view of the narrow concentration variation over the compound layer thickness and the large concentration difference between layer and substrate, leads to an approximately linear concentration-depth profile.

[28] The concentration-depth profiles obtained from adopting the Langmuir-type approach and the HS approach, for calculation of the thermodynamic factor, are in qualitative agreement with those obtained from adopting the WS approach and show in principle the same concave shape (results not shown here).

assumption to be a good approximation for nitrogen diffusion in γ'. Thus, the suggestion by Belmonte et al. [98] that quasi-steady state diffusion and thus a constant flux of nitrogen through the γ' phase cannot be applied to model the growth of a γ'-layer upon nitriding is not confirmed.

Finally, the thickness of the γ'-layer was calculated from the parabolic growth law $\xi^{(\gamma')} = k^{(\gamma')}\sqrt{t}$ and Eq. (5.10); for results see Table 5.3.

## 5.5   Comparison of experimental and calculated concentration-depth profiles

The experimental layer-thickness values reported for specimens A823 [44] and A843 [101] agree very well with the predicted ones (cf. Table 5.3). The results for specimen B843 [101] show that the experimentally determined layer thickness is larger than that predicted by the calculation. This difference can be ascribed to the pronounced porosity reported for the γ' layer of specimen B843, implying a strong influence of the pores/channels (=coalesced pores at grain boundaries) on the compound-layer evolution: the distinct porosity allows NH_3 transport from the nitriding gas atmosphere through the channels into the layer and thus the solid-state diffusion paths are shortened leading to a faster growth of the compound layer as compared to non-porous layers.

In most of the previous works dealing with the growth kinetics of iron-nitride surface layers, either the nitrogen concentration-depth profile in the γ' layer was not considered [59] or the intrinsic diffusion coefficient $D_N^{(\gamma')}$ was replaced by a concentration independent effective diffusion coefficient $D_{N,eff}^{(\gamma')}$ [38, 54, 73, 99], leading to a (virtually) linear nitrogen concentration-depth profile (see section 5.4). However, linear concentration depth profiles do not provide an accurate description of the experimental results (cf. Figs. 5.3a-c). Moreover, as shown in section 5.2.3, the assumption of a concentration independent intrinsic diffusion coefficient $D_N^{(\gamma')}$ is not consistent with the thermodynamic models derived for the γ'-phase.
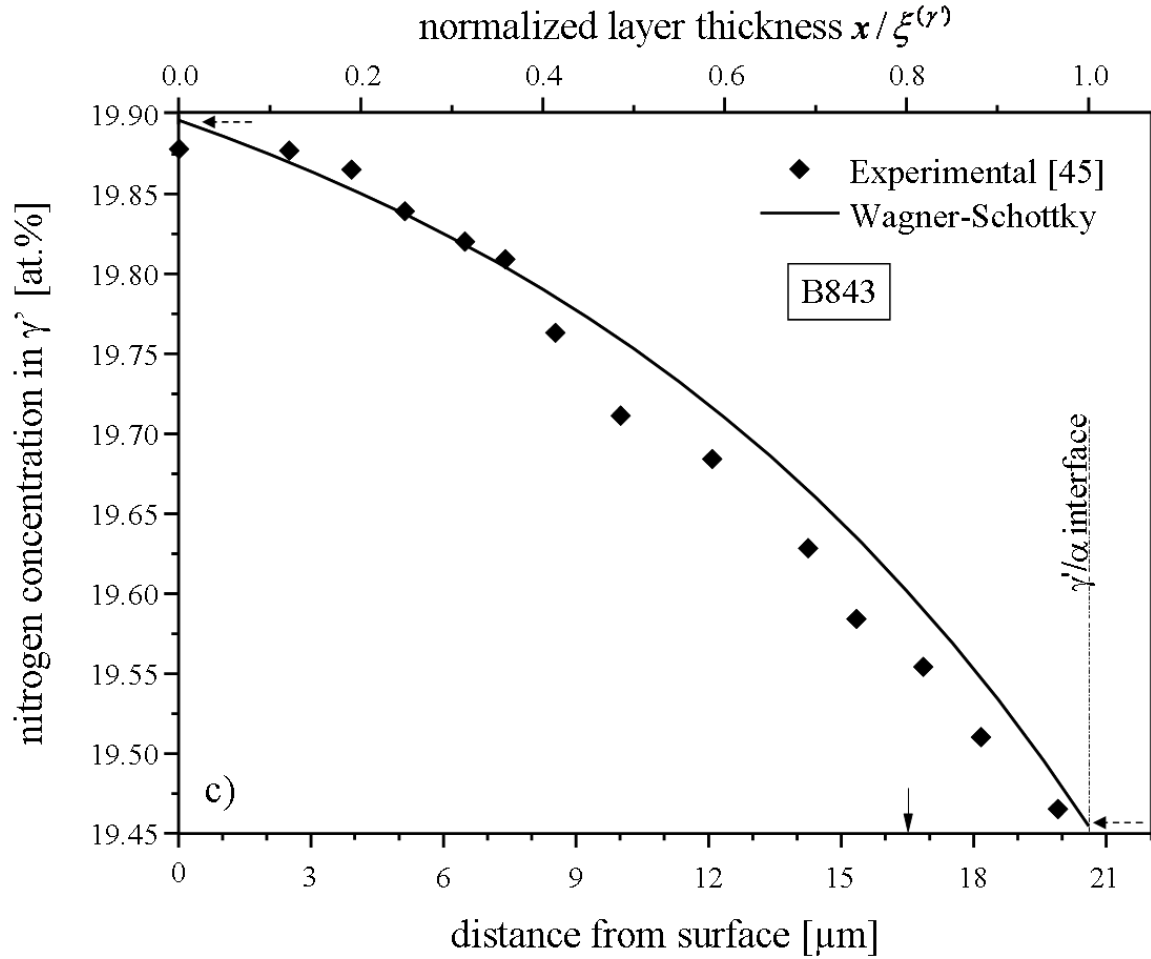
The nitrogen concentration-depth profiles calculated from the concentration dependent thermodynamic factor $\varphi_N^{(\gamma')}$, as given by the WS (or GBW) approach, are in reasonable agreement with the experimental data: the experimental X-ray diffraction

analyses confirm the theoretically predicted concave shape of the nitrogen concentration-depth profiles in γ'-Fe$_4$N$_{1-z}$. Such a concave shape of the nitrogen concentration-depth profiles in γ' was also obtained theoretically by Belmonte et al. [98] on the basis of a numerical model for nitrogen diffusion in ε / γ'-double layers using a Hillert-Staffanson approach to describe the concentration dependence of the thermodynamic factor $\varphi_N^{(\gamma')}$, without providing a comparison with experimental data.

Somers and Mittemeijer [101] and Wohlschlögel et al. [44] previously attributed the observed concaveness of the measured nitrogen concentration-depth profiles to pore formation in the surface-adjacent region of the γ' layer. The coalescence of the pores nucleated at grain boundaries upon nitriding leads to the development of grain-boundary channels in contact with the gas atmosphere, providing an additional uptake of nitrogen within the γ' layer by the lateral diffusion of nitrogen through the channel walls. Accordingly, the absolute value of the nitrogen-concentration gradient in the surface-adjacent region of the compound layer becomes smaller, yielding a (more) concave shape of the concentration-depth profile than would be the case in the absence of such porosity. The additional (lateral) uptake of nitrogen will certainly play a role in γ' layers exhibiting pronounced pore formation, as holds for specimen B843, which also shows an unexpectedly large layer thickness as consequence of the high porosity (see above). However, these effects are not expected for compound layers which are pore free or only contain isolated pores, as holds for specimens A823 and A843. For these specimens the observed concave shape of the nitrogen concentration-depth profiles can only be explained as a consequence of the specific, strong concentration dependence of the thermodynamic factor $\varphi_N^{(\gamma')}$ resulting from the thermodynamics of the γ'-phase (cf. section 5.2.3) as expressed by the concentration dependence of the Gibbs energy of γ'-Fe$_4$N$_{1-z}$.

a)
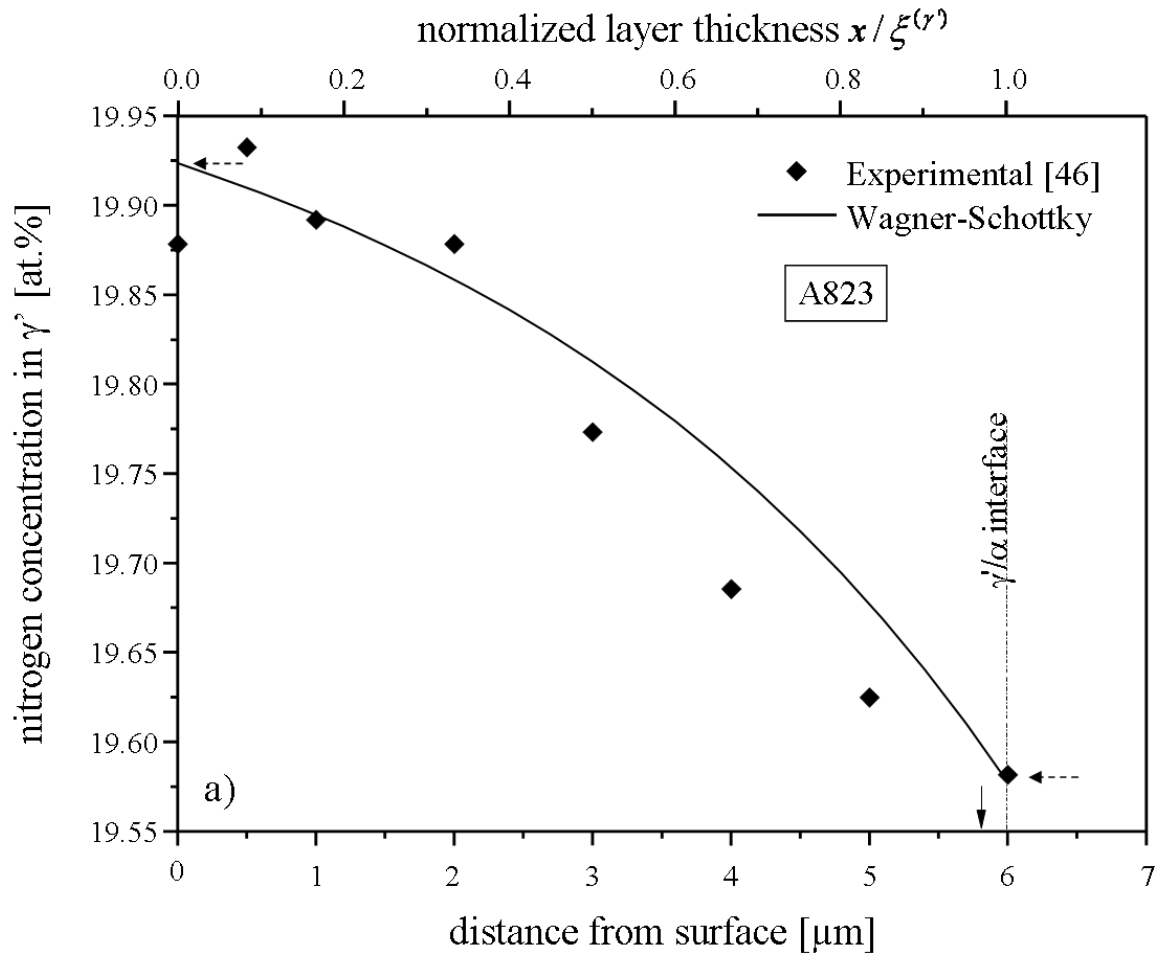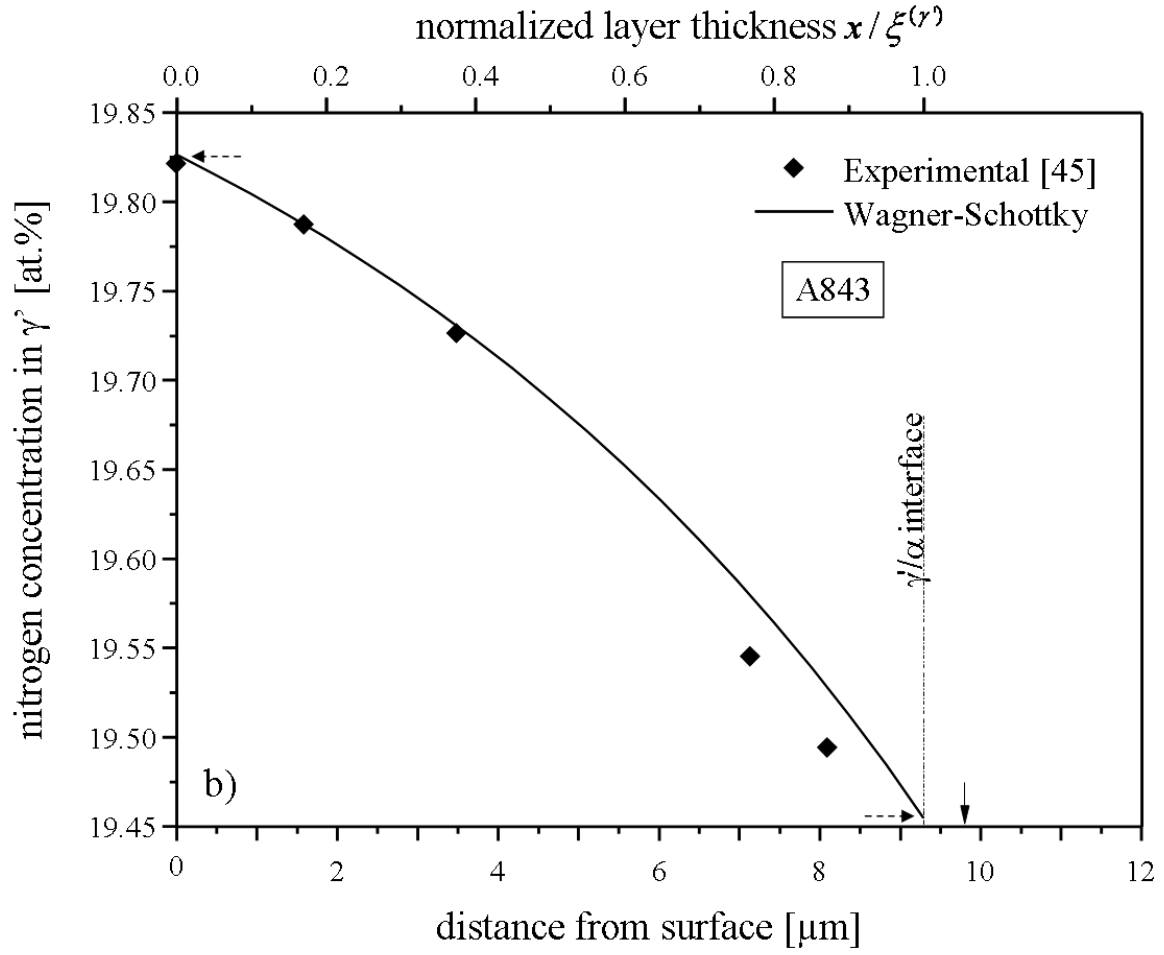
Fig. 5.3a-c: Calculated quasi-steady state nitrogen concentration-depth profiles for γ'-layers obtained by nitriding of pure α-iron substrates. The calculations were performed by applying a concentration dependent thermodynamic factor $\varphi_N^{(\gamma')}$ for nitrogen diffusion in the γ' layer according to the Wagner-Schottky approach (solid lines). The experimental data points have been indicated [44, 101]. (a) specimen A823, (b) specimen A843 and (c) specimen B843. The depth x has been normalized with respect to the measured thickness of the γ' layer $\xi^{(\gamma')}$. The solid arrow on the abscissa indicates the calculated layer thickness and the dashed horizontal arrows represent the nitrogen concentration calculated according to thermodynamic data [54] (cf. Table 5.2).

5.6 Conclusions

1. The experimentally observed concave shape of nitrogen concentration-depth profiles in the surface adjacent region of massive γ'-Fe_4N_{1-z} layers can be explained by the concentration dependence of the intrinsic diffusion coefficient of nitrogen in γ'. This concentration dependence is compatible with a concentration independent self-diffusion coefficient of nitrogen in γ' and a specific concentration dependence of the

thermodynamic factor as derived from different thermodynamic models for the Gibbs energy of the γ' phase taking into account the ordered arrangement of nitrogen atoms on the octahedral, interstitial lattice sites of the host lattice of iron atoms.

2. In porous γ' layers lateral diffusion of nitrogen from the nitriding gas atmosphere through channel walls at grain boundaries can contribute significantly to the compound layer thickness as well as to the concave shape of nitrogen concentration-depth profiles.

3. The present work indicates that the shape of concentration-depth profiles observed during diffusion-controlled growth of such phases can provide crucial information on the thermodynamics and/or the diffusion mechanism of the phase concerned.

Appendix A
Thermodynamic descriptions of the γ' phase

In the following the analytical expressions for the thermodynamic factor for nitrogen diffusion in γ', pertaining to several thermodynamic models, have been listed (for the Wagner-Schottky approach see Eq. (5.13)).

i) Langmuir-type approach

The Langmuir-type approach [86] assumes that only ¼ of the octahedral sites in γ' can be occupied by nitrogen. The thermodynamic factor $\varphi_N^{(\gamma')}$ can be derived as

$$\varphi_N^{(\gamma')} = \frac{u_N^{(\gamma')}}{RT} \frac{d\mu_N^{(\gamma')}}{du_N^{(\gamma')}} = \frac{1}{\left(1 - 4u_N^{(\gamma')}\right)} \tag{5.14}$$

The Langmuir-type approach is a limiting case of the Wagner-Schottky approach, i.e. for $K_{\gamma'}^{WS} \to 0$ (cf. section 5.2.3) only octahedral sites of the "ordered sublattice" II can be

occupied by nitrogen, whereas octahedral sites of the "disordered sublattice" III are no more available for nitrogen atoms.

ii) Hillert-Staffansson approach (compound-energy formalism)

Based on the Hillert-Staffansson approach [21, 59], the γ'-phase can be described as a subregular solution $Fe_4^I(N^{II}, Va^{II})_1$ with one substitutional sublattice composed of iron and one interstitial sublattice II, which can be occupied by nitrogen. For the thermodynamic factor of nitrogen it holds that

$$\varphi^{(\gamma')} = \frac{u_N^{(\gamma')}}{RT} \frac{d\mu_N^{(\gamma')}}{du_N^{(\gamma')}} = \frac{1}{\left(1 - 4u_N^{(\gamma')}\right)} - 8u_N^{(\gamma')} \frac{L_{Fe:N,Va}^{0,\gamma'} - 3L_{Fe:N,Va}^{1,\gamma'}\left(1 - 8u_N^{(\gamma')}\right)}{RT}. \tag{5.15}$$

The Hillert-Staffansson approach reduces to the Langmuir-type approach by assuming the interaction parameters $L_{Fe:N,Va}^{0,\gamma'}$ and $L_{Fe:N,Va}^{1,\gamma'}$ to be zero.

iii) Gorsky-Bragg-Williams approach

The Gorsky-Bragg-Williams approach [86] is a more general form of the Wagner-Schottky approach [86] considering pairwise interactions between neighboring nitrogen atoms on their specific crystallographic sites of type (1/2, 1/2, 1/2) and (1/2, 0, 0). As mentioned in section 5.2.3, an analytical formulation of $\varphi^{(\gamma')}$ is not possible.

Appendix B

Influence of the defect structure in hypostoichiometric γ' on the nitrogen concentration-depth profile

A theoretical analysis of diffusion in close-to stoichiometric interstitial compounds (including the γ' phase) taking into account constitutional and thermal defects (see section 5.1) in the crystal structure was recently presented by Hillert et al. [69]. Three scenarios for the flux of the interstitial element through the compound layer on the basis of Eq. (5.5) are presented in Ref. [69]. However, in contrast with the present paper and other works on diffusion in interstitial phases [54, 59, 98], the fraction of vacant sites y_{Va} available for diffusion was not a priori assumed to be constant and independent of the nitrogen concentration in the γ' layer (see footnote 24 and text below Eq. (5.7) in section 5.2.2). In the following the consequences of one of the three scenarios (one scenario is effectively the same as in section 5.2.2 and one scenario pertains to a hypothetical hyper-stoichiometric character of γ' and is irrelevant for the present paper) for the shape of the nitrogen concentration-depth profiles in γ' will be considered, which was not done in Ref. [69].

The formula used for the γ' phase is $Fe_4^I(N^{II}, Va^{II})_1(N^{III}, Va^{III})_3$ and the flux of nitrogen in γ' is assumed to be constant as for the case of quasi-steady state diffusion (cf. section 5.2.2). For hypo-stoichiometric γ' without thermal defects and nitrogen diffusion via vacancies exclusively on sublattice II, the flux of nitrogen can be derived as [69]

$$J_N^{(\gamma')} = -y_{Va}^{II,cst} \frac{M_{N,Va}^{II} RT}{V_m^{II}} \frac{1}{(1-y_N^{II})} \frac{dy_N^{II}}{dx} = -\frac{M_{N,Va}^{II} RT}{V_m^{II}} \frac{dy_N^{II}}{dx},$$
(5.16)

where $M_{N,Va}^{II}$ is the mobility of nitrogen in sublattice II, $y_{Va}^{II,cst} = 1 - 4u_N^{(\gamma')} = z$ is the fraction of constitutional vacancies on sublattice II, $y_N^{II} = 1 - y_{Va}^{II,cst}$ is the fraction of N atoms on sublattice II and V_m^{II} is the volume of one mole of sites on sublattice II. The concentration dependence of $D_N^{(\gamma')*} = y_{Va}^{II,cst} M_{N,Va}^{II} RT$ and the concentration dependence of

119

the thermodynamic factor $\varphi_N^{(\gamma')} = 1/(1 - y_N^{II}) = 1/y_{Va}^{II,cst}$ cancel out yielding a concentration independent intrinsic diffusion coefficient and thus a linear nitrogen concentration-depth profile in γ' is obtained from Eq. (5.16).

Chapter 6

Summary

6.1 Experimental

The thermodynamic and kinetics of phase transformations in the Fe-N-C system were investigated by nitriding and nitrocarburizing experiments. Therefore, rectangular α-iron samples of $20 \times 25 \times 1$ mm³ were cut from cold-rolled iron plates (Alfa Aesar, 99.98 wt. %), ground, polished (final stage 1 µm diamond suspension), cleaned ultrasonically in ethanol and recrystallized for 2 h at 973 K in a hydrogen gas flow of 200 ml·min^{-1}. Immediately before nitrocarburizing the specimens were polished (final stage 1 µm diamond suspension) and cleaned with ethanol. For gas nitriding/nitrocarburizing a vertical quartz-tube furnace with a diameter of 28 mm was used, where the sample was placed in the middle of the furnace by a quartz fiber. The process temperature of was controlled within $\pm$ 1 K. The nitriding/nitrocarburizing atmospheres were adjusted by separate mass-flow controllers for each gas component. The following gases were available: NH_3 as nitriding species, CO and CO_2 as carburizing species, N_2 as inert gas, evaporated H_2O and H_2 (all gases from Westfalen AG with a purity of 99.999 vol.% except CO with a purity of 99.997 vol.%). The overall linear gas-flow rate through the quartz-tube was chosen as 13.5 mm·s^{-1} (calculated for the gas volume at room temperature) in order to prevent significant ammonia dissociation and side reactions in the gas atmosphere, which would affect the composition of the gas mixture. Upon nitrocarburizing using evaporated H_2O the gas supply lines were heated to 393 K to avoid the formation of ammonium bicarbonate. After the heat treatment the samples were quenched in nitrogen-flushed water.

The microstructure of the nitrided/nitrocarburized samples was analyzed by optical microscopy, X-ray diffraction (XRD) and electron backscatter diffraction (EBSD). The composition of the compound layers (concentration-depth profiles) were measured by election probe microanalysis (EPMA) on cross-sections perpendicular to the surface. Hardness measurements were performed on using a Vickers micro-indentation system. For gravimetric analysis before and after the heat treatment a high-precision balance was used.

6.2   Results and Discussion

6.2.1   Microstructural and phase evolution of compound layers

Nitrocarburizing of α-iron showed a time-dependent and an atmosphere-dependent microstructural evolution of the compound layer. In both cases the evolution starts with the formation of carbon-rich cementite and develops through successive stages into the direction of the nitrogen-richer phases ε and γ'. The observed time-dependent microstructural evolution is a consequence of a higher transfer rate of carbon as compared to nitrogen from the gas atmosphere to the α-iron substrate and a lower solubility of carbon in ferrite than that of nitrogen. Thus, upon nitrocarburizing the substrate is much faster saturated with carbon than with nitrogen leading to the initial formation of cementite instead of a (carbo)nitride, which acts as a barrier for the diffusion of nitrogen into the substrate. After some time, the ε phase develops at the layer / substrate interface by exceeding the solubility of nitrogen in ferrite at the layer / substrate interface. The ε phase then growths at the expense of cementite. At intermediate treatment times the γ' phase is formed within the ε phase adjacent to the layer / substrate interface. The dependence of the phase evolution on the substrate saturation was clearly demonstrated by nitrocarburizing of non-saturated and nitrogen pre-saturated substrates using the same strongly carburizing atmosphere. In the first case a massive cementite layer was obtained and in the second case a θ / ε double layer had developed. Furthermore, the use of wedge-shaped non-saturated α-iron substrates using a strongly carburizing atmosphere resulted in a massive cementite layer at the thick end of the specimen (the substrate was not saturated with nitrogen) and the formation of a θ / ε double layer at the thin end of the specimen (the substrate was saturated with nitrogen upon nitrocarburizing).

The time-dependent evolution of the compound layer implies that local equilibrium conditions do not necessarily prevail at the gas/solid interface. The change of the microstructure within the compound layer is compatible with the ternary Fe-N-C phase diagram, i.e. evidently, local equilibrium conditions do prevail at the solid-solid phase boundaries. The evolution of the compound layers can be visualized by so-called diffusion paths shown at (the isothermal section) of the corresponding phase diagram.

6.2.2   Influence of the chemical potential of carbon on compound layer

Nitrocarburizing of pure α-iron substrates was performed at 823 K and 853 K under controlled conditions in $NH_3/H_2/CO/CO_2/H_2O$-containing gas mixtures, i.e. the chemical potentials of nitrogen μ_N and carbon μ_C can be adjusted by the composition of the gas atmosphere. At a given temperature and treatment time, the activities of nitrogen and carbon in the gas atmosphere strongly affect the microstructural evolution of the compound layer. Depending on the process parameters (time was kept constant) three different types of compound layers were obtained: single-phase γ' layer, ε / γ' double layers and $\varepsilon / \varepsilon + \gamma'$ double layers. The formation of $\varepsilon / \varepsilon + \gamma'$ double layer was only observed at 853 K and very high carbon activity a_C. At the interface between the gas atmosphere and the compound layers a local equilibrium may not occur, whereas within the compound layer local equilibrium between solid-solid phase interfaces prevails (the phases within the compound layers are compatible with the Fe-N-C phase diagram). The layer-growth kinetics strongly depend on the phase composition of the compound layer. Massive γ' layer showed the lowest layer growth rates. The ε / γ' double layers and in particular the in particular the $\varepsilon / \varepsilon + \gamma'$ double layers show the highest growth rates. The thickness and composition of ε / γ' double layers varies as a function of μ_C. With increasing μ_C the thickness of the ε sublayer increases, whereas the thickness of the γ' sublayer decreases until almost constant thicknesses are reached at very high μ_C. Moreover, a decreasing nitrogen content and an increasing carbon content in ε at the surface of the ε / γ' double layer is obtained by increasing μ_C, while the total amount of nitrogen and carbon remains almost constant, i.e. nitrogen is substituted by carbon.

6.2.3   Multicomponent interstitial diffusion in ε-$Fe_3(N,C)_{1+x}$

Up to now, the intrinsic diffusion coefficients of nitrogen and carbon in ε-$Fe_3(N,C)_{1+x}$ have not been determined experimentally. For that purpose several nitriding and nitrocarburizing experiments were performed at 823 K to investigate the growth of ε-$Fe_3(N,C)_{1+x} / \gamma'$-$Fe_4N_{1-z}$ -double layers on pure α-iron substrates. The time-dependent growth of the (sub)layers can be descried by a modified parabolic growth law. The

nitrogen and carbon concentration-depth profiles in the ε sublayer were found to be practically linear. The sublayer growth rates and the nitrogen and carbon concentration-depth profiles were used in combination with a model for the growth of a bilayer on a substrate to calculate the four intrinsic diffusion coefficients D_{NN}^{ε}, D_{CC}^{ε}, D_{NC}^{ε} and D_{CN}^{ε}, which were assumed to be independent of concentration. It is found that the values of $D_{kj}^{\varepsilon}\left(k,j=\text{N,C}\right)$ are all positive. The off-diagonal diffusion coefficients $D_{kj}^{\varepsilon}\left(k\neq j\right)$ have a strong influence on the diffusive fluxes of N and C in ε and can thus not be neglected for modeling the growth of ε / γ' double layers upon nitrocarburizing of pure α-iron. The ratios of the off-diagonal and diagonal diffusivities $D_{NC}^{\varepsilon}/D_{NN}^{\varepsilon}$ and $D_{CN}^{\varepsilon}/D_{CC}^{\varepsilon}$ imply significant thermodynamic interactions between both interstitial elements. The positive off-diagonal diffusion coefficients $D_{kj}^{\varepsilon}\left(k\neq j\right)$ contradict some of the available thermodynamic calculations given in the literature, where $D_{kj}^{\varepsilon}\left(k\neq j\right)<0$ was found. The discrepancies between the experimental and the theoretical values can be attributed to an incorrect thermodynamic assessment of the Fe-N-C system.

6.2.4 The shape of nitrogen concentration-depth profiles in γ'-Fe$_4$N$_{1-z}$ layers

The nitrogen concentration-depth profile in γ'-Fe$_4$N$_{1-z}$ layer grown on α-iron substrates were calculated and compared to experimental profiles presented in the literature. The strikingly concave nitrogen concentration-depth profiles in γ'-Fe$_4$N, as reported in the literature, can be explained by a concentration-independent self-diffusion coefficient of nitrogen in γ' in combination with the thermodynamics of the γ' phase, i.e. the concentration dependence of the Gibbs energy of the γ' phase taking into account the ordered arrangement of nitrogen atoms on the octahedral, interstitial lattice sites of the iron host lattice. Concentration depth profiles can thus contain valuable information about the thermodynamics of a phase considered. The presence of pores at the surface adjacent region of the γ' layer can contribute significantly to the compound-layer thickness as well as to the concave shape of nitrogen concentration-depth profile.

Chapter 7

Zusammenfassung in deutscher Sprache

7.1 Experimentelle Vorgehensweise

Die Thermodynamik und Kinetik von Phasenumwandlungen im System Fe-N-C wurden mittels Nitrier- und Nitrocarburierexperimenten untersucht. Dazu wurden rechteckige α-Eisenproben von 20 x 25 x 1 mm³ aus kaltgewalzten Eisenplatten (Alfa Aesar, 99,98 Gew.%) ausgeschnitten, geschliffen, poliert (Endstufe 1 µm Diamantsuspension), per Ultraschall in Ethanol gereinigt und anschließend für 2 Stunden bei 973 K unter Wasserstofffluss (200 ml.min^{-1}) rekristallisiert. Direkt vor der Wärmebehandlung wurden die Eisenproben nochmals mit 1 µm Diamantsuspension poliert und in Ethanol gereinigt. Das Gasnitrieren und Gasnitrocarburieren wurde in einem vertikal angeordneten Mehrzonenofen mit einem Innendurchmesser von 28 mm durchgeführt. Die Probe wurde durch einen Quarzfaden in der Ofenmitte platziert, wo die Prozesstemperatur mit einer Genauigkeit von ± 1 K eingestellt wurde. Die für das Nitrieren/Nitrocarburieren verwendete Gasatmosphäre wurde mittels separaten Masseflussreglern für jede Gaskomponente eingestellt. Die folgenden Gase standen dazu zur Verfügung: NH_3 als nitrierende Spezies, CO und CO_2 als carburierende Spezies, N_2 als Inertgas, H_2 und verdampftes H_2O (alle Gase mit einer Reinheit von 99,999 Vol.% bis auf CO mit 99,997 Vol.%). Um eine signifikante Zersetzung von Ammoniak sowie Nebenreaktionen in der Gasphase, welche zu Veränderungen in der Gaszusammensetzung führen würden, zu verhindern, wurde ein Gesamtgasdurchfluss von 13,5 mm.s^{-1} (berechnet nach dem Gasvolumen bei Raumtemperatur) ausgewählt. Beim Nitrocarburieren mit verdampften H_2O wurden zudem sämtliche Gaszuleitungen auf 393 K aufgeheizt, um die Bildung von Ammoniumbicarbonat zu verhindern. Nach der thermochemischen Behandlung wurde die Probe in stickstoffgespültem Wasser abgeschreckt.

Die Mikrostruktur der nitrierten/nitrocarburiereten Proben wurde mittels Licht-mikroskopie, Röntgenpulverdiffraktometrie und Elektronenrückstreubeugung untersucht. Die Zusammensetzung der beim Nitrieren/Nitrocarburieren gebildeten Verbindungs-schicht wurde mittels Elektronenstrahlmikrosonde an Querschliffen (senkrecht zur Oberfläche) analysiert. Härtemessungen wurden mittels eines Vickers-Mikrohärte-

messgerät durchgeführt. Gravimetrische Messungen erfolgten an einer Hochpräzisions-waage.

7.2 Ergebnisse und Diskussion

7.2.1 Mikrostrukturelle Entwicklung der Verbindungsschicht

Das Nitrocarburieren von α-Eisen resultierte in einer zeitabhängigen und einer gas-phasenabhängigen Entwicklung der Verbindungsschicht. In beiden Fällen bildete sich zuerst kohlenstoffreicher Zementit als Verbindungsschicht. Mit fortschreitender Behandlungsdauer wandelt sich die Verbindungsschicht schrittweise in die stickstoff-reicheren Phasen ε und γ' um. Die zeitliche Entwicklung der Verbindungsschicht ist dabei die direkte Folge einer erhöhten Aufnahme von Kohlenstoff aus der Gasatmosphäre in die Eisenprobe im Vergleich zu Stickstoff, sowie eine geringere maximale Löslichkeit des Kohlenstoffs im Vergleich zu Stickstoff im α-Eisen. Demzufolge wird das α-Eisensubstrat beim Nitrocarburieren viel schneller mit Kohlenstoff gesättigt als mit Stickstoff, was zur anfänglichen Bildung von Zementit anstelle eines (Carbo)Nitrides führt. Da die Zementitschicht als Diffusionsbarriere für Stickstoff wirkt, wird einige Zeit benötigt, bis das α-Eisensubstrat unterhalb der Zementitschicht mit Stickstoff gesättigt ist und in Folge dessen die ε Phase an der θ / ε Grenzfläche gebildet wird. Mit zunehmender Zeit wächst ε zugunsten von Zementit. Mit zunehmender Behandlungsdauer wird schließlich die γ' Phase in ε an der ε / α Grenzfläche gebildet. Die Abhängigkeit der Phasenentwicklung von der Substratsättigung beim Nitrocarburieren konnte zudem deutlich anhand von ungesättigten und bereits mit Stickstoff vorgesättigten α-Eisensubstraten unter Verwendung einer stark carburierenden Gasatmosphäre gezeigt werden. Im ersten Fall bildete sich eine reine Zementitschicht, während sich im zweiten Fall eine θ / ε Doppelschicht ausgebildet hat. Darüber hinaus resultierte bei einer keilförmigen, ungesättigten Probe nach dem Nitrocarburieren unter Verwendung einer stark carburierenden Gasatmosphäre eine Zementitschicht am dicken Ende (noch ungesättigtes Substrat) und eine θ / ε Doppelschicht am dünnen Ende (bereits mit Stickstoff gesättigtes Substrat) der Probe. Die zeitabhängige Entwicklung der

Verbindungsschicht impliziert, dass an der Gas/Festkörper-Grenzfläche kein lokales Gleichgewicht herrscht. Die Änderung der Mikrostruktur innerhalb der Verbindungs-schicht ist jedoch kompatibel mit dem Fe-N-C Phasendiagramm, was auf das Vorliegen von lokalen Gleichgewichtsbedingungen an den Fest/Fest-Phasengrenzen hindeutet. Die Entwicklung der Verbindungsschicht kann mit Hilfe von sogenannten Diffusionspfaden an isothermen Schnitten des Fe-N-C Phasendiagramms veranschaulicht werden.

7.2.2 Einfluss des chemischen Potentials von Kohlenstoff auf die Verbindungs-schicht

Reines α-Eisen wurde bei 823 K und 853 K unter kontrollierten Bedingungen in einer $NH_3/H_2/CO/CO_2/H_2O$-haltigen Gasatmosphäre nitrocarburiert, wobei die chemischen Potentiale von Kohlenstoff μ_C und Stickstoff μ_N über die Gaszusammensetzung variiert werden können. Bei gegebener Temperatur und Dauer konnte ein erheblicher Einfluss des chemischen Potentials von Kohlenstoff und Stickstoff in der Gasphase auf die Entwicklung der Verbindungsschicht festgestellt werden. In Abhängigkeit der Prozessparameter (bei einer konstanten Dauer von 4 h) traten insgesamt drei unterschiedliche Arten von Verbindungsschichten auf: eine reine γ' Schicht, eine ϵ / γ' Schicht und eine $\epsilon / \epsilon + \gamma'$ Schicht. Die Bildung einer $\epsilon / \epsilon + \gamma'$ Schicht wurde nur bei 853 K und sehr hohen Kohlenstoffaktivitäten beobachtet. An der Gas/Fest-Grenzfläche liegt möglicherweise kein lokales Gleichgewicht vor, wohingegen an den Fest/Fest-Grenzflächen in der Verbindungsschicht ein lokales Gleichgewicht herrscht (die Phasen in der Verbindungsschicht sind mit dem Fe-N-C Phasendiagramm kompatibel). Die Schichtwachstumskinetik hängt stark von der Phasenzusammensetzung in der Verbindungsschicht ab. Eine reine γ' Schicht wies dabei die geringste Wachstumsrate auf. Die ϵ / γ' Schicht, und insbesondere die $\epsilon / \epsilon + \gamma'$ Schicht, wiesen die höchsten Wachstumsraten auf. Die Dicke und Zusammensetzung der ϵ / γ' Schicht ändert sich als Funktion von μ_C. Mit steigendem μ_C nimmt die Dicke der ϵ Subschicht zu, wobei die Dicke der γ' Subschicht abnimmt, bis sich bei hohen μ_C ein jeweils (fast) konstanter Wert einstellt. Darüber hinaus nimmt der Anteil an Stickstoff in ϵ an der Oberfläche der ϵ / γ' Schicht mit zunehmenden μ_C ab, wohingegen der Anteil an Kohlenstoff entsprechend

zunimmt. Der Gesamtgehalt an Kohlenstoff und Stickstoff an der Oberfläche bleibt dabei jeweils näherungsweise konstant, was auf eine Substitution von Stickstoff durch Kohlenstoff hindeutet.

7.2.3 Mehrkomponentige interstitielle Diffusion in ε-Fe$_3$(N,C)$_{1+x}$

Bisher wurden die intrinsischen Diffusionskoeffizienten von Kohlenstoff und Stickstoff in ε-Fe$_3$(N,C)$_{1+x}$ nicht experimentell bestimmt. Aus diesem Grund wurden mehrere Nitrier- und Nitrocarburierexperimente bei 823 K durchgeführt, um das Wachstum von ε-Fe$_3$(N,C)$_{1+x}$ / γ'-Fe$_4$N$_{1-z}$ Doppelschichten auf α-Eisensubstraten zu untersuchen. Das zeitabhängige Wachstum der (Sub)schichten kann dabei durch ein modifiziertes parabolisches Wachstumsgesetz beschrieben werden. Die Kohlenstoff und Stickstoff-konzentrations-Tiefen-Profile in der ε Subschicht können als näherungsweise linear beschrieben werden. Die Wachstumsraten der Subschichten, sowie die Kohlenstoff- und Stickstoffkonzentrations-Tiefen-Profile, wurden zusammen mit einem Modell für das Doppelschichtwachstum dazu verwendet, um die intrinsischen Diffusionskoeffizienten D_{NN}^{ε}, D_{CC}^{ε}, D_{NC}^{ε} und D_{CN}^{ε}, welche als konzentrationsunabhängig angenommen wurden, zu berechnen. Die ermittelten Werte für $D_{kj}^{\varepsilon}\left(k, j = \text{N,C}\right)$ sind alle positiv. Zudem haben die Diffusionskreuzterme $D_{kj}^{\varepsilon}\left(k \neq j\right)$ einen starken Einfluss auf die Diffusionsflüsse von Kohlenstoff und Stickstoff in ε und können somit für die Modellierung des ε-Fe$_3$(N,C)$_{1+x}$ / γ'-Fe$_4$N$_{1-z}$ Doppelschichtwachstums beim Nitrocarburieren von α-Eisen nicht vernachlässigt werden. Das Verhältnis der Diffusionskoeffizienten $D_{NC}^{\varepsilon}/D_{NN}^{\varepsilon}$ und $D_{CN}^{\varepsilon}/D_{CC}^{\varepsilon}$ deuten auf signifikante thermodynamische Wechselwirkungen beider interstitieller Spezies hin. Die Diffusionskreuzterme $D_{kj}^{\varepsilon}\left(k \neq j\right)$ sind im Widerspruch zu einigen in der Literatur durchgeführten thermodynamischen Berechnungen, die negative Werte für $D_{kj}^{\varepsilon}\left(k \neq j\right)$ vorhersagen. Die Unstimmigkeiten zwischen den experimentell ermittelten Werten und den in der Literatur angegebenen Werten können auf inkorrekte thermodynamische Beurteilungen der Phasen im Fe-N-C System zurückgeführt werden.

7.2.4 Stickstoffkonzentrations-Tiefen-Profile in γ'-Fe$_4$N$_{1-z}$ Schichten

Stickstoffkonzentrations-Tiefen-Profile in auf α-Eisen erzeugten γ'-Fe$_4$N$_{1-z}$ Schichten wurden berechnet und mit experimentellen Profilen aus der Literatur verglichen. Die in der Literatur beschriebenen, auffällig konkaven Stickstoffkonzentrations-Tiefen-Profile in γ'-Fe$_4$N$_{1-z}$ können durch einen konzentrationsunabhängigen Selbstdiffusionskoeffizienten von Stickstoff in γ' im Zusammenspiel mit der Konzentrationsabhängigkeit der Gibbs Energie der γ' Phase (unter Berücksichtigung der Anordnung der Stickstoffatome in den Oktaederlücken des Eisengitters) erklärt werden. Konzentrations-Tiefen-Profile können somit nützliche Informationen über eine betrachtete Phase liefern. Weiterhin kann das Vorliegen von Poren in der Nähe der Oberfläche der γ' Schicht beträchtlich zur Gesamtschichtdicke, aber auch zur konkaven Form des Stickstoffkonzentrations-Tiefen-Profils beitragen.

8 References

[1]   T. Bell: Heat Treat. Met. 1975;2:39.

[2]   C. Dawes, D.F. Tranter: Heat Treat. Met. 1985;3:70.

[3]   T. Bell, D.H. Thomas: Metall. Mater. Trans. A 1979;10A:79.

[4]   E.J. Mittemeijer: J. Heat Treat. 1983;3:114.

[5]   P.M. Unterweiser. Source book on nitriding: ASM, Metals Park, OH, 1977.

[6]   E.J. Mittemeijer, J.T. Slycke: Heat Treat. Met. 1996;3:67.

[7]   E.J. Mittemeijer, M.A.J. Somers: Surf. Eng. 1997;13:483.

[8]   M.A.J. Somers: Heat Treat. Met. 2000;4:92.

[9]   R. Chatterjee-Fischer, R. Bodenhagen, F.-W. Eysell, R. Hoffmann, D. Liedke, H. Mallener, W. Rembges, A. Schreiner, G. Welker. Wärmebehandlung von Eisen und Stahl - Nitrieren und Nitrocarburieren. Renningen-Malmsheim: Expert Verlag, 1995.

[10]   P.B. Friehling, F.W. Poulsen, M.A.J. Somers: Z. Metallkunde 2001;92:589.

[11]   A.A. Kodentsov, G.F. Bastin, F.J.J. Van Loo: J. Alloys Compd. 2001;320:207.

[12]   J.S. Kirkaldy, D.J. Young. Diffusion in the Condensated State. London: The Institute of Metals, 1987.

[13]   N.H. Christensen: J. Am. Ceram. Soc 1977;60:293.

[14]   H. Du, M.A.J. Somers, J. Ågren: Metall. Mater. Trans. A 2000;31A:195.

[15]   J. Kunze. Nitrogen and Carbon in Iron and Steel: Akademie-Verlag Berlin, 1990.

[16]   E. Lehrer: Z. Elektrochem. 1930;36:383.

[17]   R. Hoffmann: Härterei-Tech. Mitt. 1996;51:5.

[18]   H.A. Wriedt, N.A. Gokcen, R.H. Nafziger: Bull. Alloy. Phase. Diagr. 1987;8:355.

[19]   M. Nikolussi, A. Leineweber, E.J. Mittemeijer: J. Mat. Sci. 2009;44:770.

[20]   H.J. Grabke: Archiv Eisenhütten. 1975;46:75.

References

[21] H. Du: J. Phase Equilib. 1993;14:682.

[22] M. Hillert, H. Du: Z. Metallkd. 1991;82:310.

[23] J. Slycke, L. Sproge, J. Ågren: Scand. J. Metall. 1988;17:122.

[24] M. Hillert. Phase Equilibria, Phase Diagrams, and Phase Transformations: Cambridge University Press, Cambridge, 2007.

[25] H.L. Lukas, S.G. Fries, B. Sundman. Computational Thermodynamics: Cambridge University Press, 2007.

[26] M. Hillert: J. Alloys Comp. 2001;320:161.

[27] J. Kunze: Härterei-Tech. Mitt. 1996;51:348.

[28] J. Philibert. Atom movements diffusion and mass transport in solids: Les Editions de Physique, 1991.

[29] M.E. Glicksman. Diffusion in Solids. New York: John Wiley & Sons, 2000.

[30] M.A.J. Somers, P.F. Colijn, W.G. Sloof, E.J. Mittemeijer: Z. Metallkd. 1990;81:33.

[31] M.A.J. Somers, E.J. Mittemeijer: Surf. Eng. 1987;3:123.

[32] M.A.J. Somers, E.J. Mittemeijer: 17th ASM Heat Treating Society Conference Proceedings Including the 1st International Induction Heat Treating Symposium 1997:321.

[33] P.F. Colijn, E.J. Mittemeijer, H.C.F. Rozendaal: Z. Metallkd. 1983;74:620.

[34] A. Wells: J. Mat. Sci. 1985;20:2439.

[35] H.C.F. Rozendaal, P.F. Colijn, E.J. Mittemeijer: Surf. Eng. 1985;1:30.

[36] L. Sproge, J. Slycke: J. Heat Treating 1992;9:105.

[37] H. Du: Thesis, Royal Institute of Technology 1994.

[38] H. Du, J. Ågren: Metall. Mater. Trans. A 1996;27A:1073.

[39] H. Du, M. Hillert: Z. Metallkunde 1991;82:310.

[40] J. Slycke: Berichtsband AWT-VWT-Tagung "Nitrieren und Nitrocarburieren" 1996:19.

[41] M. Nikolussi, A. Leineweber, E. Bischoff, E.J. Mittemeijer: Int. J. Mat. Res. 2007;98:1086.

[42] M. Nikolussi, A. Leineweber, E.J. Mittemeijer: Phil. Mag. 2010;90:1105.

[43] T. Gressmann, M. Nikolussi, A. Leineweber, E.J. Mittemeijer: Scripta Mater. 2006;55:723.

[44] M. Wohlschlögel, U. Welzel, E.J. Mittemeijer: J. Mater. Res. 2009;24:1342.

[45] F.J.J. Van Loo, M.R. Rijnders, K.J. Ronka, J.H. Gulpen, A.A. Kodentsov: Solid State Ionics 1997;95(1-2):95.

[46] F.J.J. Van Loo: Progr. Solid State Chem. 20 1990:47.

[47] J.M.G. Vilar, J.M. Rubí: Proc. Natl. Acad. Sci. USA 98 2001:11081.

[48] Y.H. Sohn, M.A. Dayananda: Acta Mater. 2000;48:1427.

[49] G. Ghosh: J. Electron. Mater. 1998;27:1154.

[50] J. Slycke, L. Sproge: Surf. Eng. 1989;5:125.

[51] T. Woehrle, A. Leineweber, E.J. Mittemeijer: HTM J. Heat Treatm. Mat. 2010;65:243.

[52] S.S. Hosmani, R.E. Schacherl, E.J. Mittemeijer: Acta Mater. 2006;54:2783.

[53] G. Petzow. Metallographic Etching. Ohio, USA: ASM International, 1999.

[54] M.A.J. Somers, E.J. Mittemeijer: Metall. Mater. Trans. A 1995;26A:57.

[55] T. Sone, Tsunasawa, E., Yamanaka, K.: Trans. Japan Inst. Met. 1981;22:237.

[56] J. Crank. The Mathematics of Diffusion: Oxford Science Publications, 1975.

[57] M. Weller: Mater. Sci. Forum 366-368 (2001) 95 2001.

[58] E.J. Mittemeijer, W.T.M. Straver, P.F. Colijn, P.J. van der Schaaf, J.A. van der Hoeven: Scr. Metall. 1980;14:1189.

[59] H. Du, J. Ågren: Z. Metallkd. 1995;86:522.

[60] T. Woehrle, A. Leineweber, E.J. Mittemeijer: Metall. Mater. Trans. A; accepted.

References

[61]   E.J. Mittemeijer, J.T. Slycke: Surf. Eng. 1996;12:152.

[62]   A. Leineweber, T. Gressmann, E.J. Mittemeijer: Surf. Coat. Technol.; accepted.

[63]   S. Pietzsch, S. Böhmer, H.-J. Spies: Proceedings of the Second International Conference on Carburizing and Nitriding with Atmospheres, 6-8 December 1995, Cleveland, Ohio 1995:295.

[64]   H. Mehrer. Diffusion in Solids: Fundamentals, Methods, Materials, Diffusion-Controlled Processes: Springer-Verlag Berlin Heidelberg, 2007.

[65]   R. Taylor, R. Krishna. Multicomponent Mass Transfer: Wiley, New York, 1993.

[66]   P. Shewmon. Diffusion in Solids. Warrendale, Pa. : Minerals, Metals & Materials Society 1989.

[67]   J.L. La Pouchau, F. Pichoir: Rech. Aerospatial 1983;3.

[68]   T. Woehrle, A. Leineweber, E.J. Mittemeijer: Metall. Mater. Trans. A; accepted.

[69]   M. Hillert, L. Höglund, J. Ågren: J. Appl. Phys. 2005;98.

[70]   K. Schwerdtfeger, P. Grieveson, E.T. Turkdogan: Trans. Metall. Soc. AIME 1969;245:2461.

[71]   E.L. Cussler. Diffusion: Mass Transfer in Fluid Systems 1997.

[72]   J.-O. Andersson, J. Ågren: J. Appl. Phys. 1992;72:1350.

[73]   L. Torchane, P. Bilger, J. Dulcy, M. Gantois: Metall. Mater. Trans. A 1996;27A:1823.

[74]   B. Prenosil: Kovove Mater. 1965;3:69.

[75]   M.A.J. Somers, B.J. Kooi, L. Maldzinski, E.J. Mittemeijer, A.A. van der Horst, A.M. van der Kraan, N.M. van der Pers: Acta Mater. 1997;45:2013.

[76]   B.J. Kooi, M.A.J. Somers, E.J. Mittemeijer: Metall. Mater. Trans. A 1996;27A:1063.

[77]   C.H. Knerr, T.C. Rose, J.H. Filkowski. ASM Handbook Heat Treating: ASM International, 1991.

[78]   H. Kato, T.S. Eyre, B. Ralph: Acta Metall. Mater. 1994;42:1703.

[79]   M. Hillert, M. Jarl: Metall. Trans. A 1975;6A:553.

[80]   K.H. Jack: Proceedings of the Royal Society of London A 1948;195:34.

[81]   H. Jacobs, D. Rechenbach, U. Zachwieja: J. Alloys Compd. 1995;227:10.

[82]   R. Brill: Z. Kristallogr. 1928;68:379.

[83]   G. Hägg: Nova Acta Reg. Soc. Sci. Upsaliensis 1929;7:6.

[84]   H.J. Grabke: Ber. Bunsenges. Physik. Chem. 1969;73:569.

[85]   C. Wagner, W. Schottky: Z. Phys. Chem 1930;B11:163.

[86]   B.J. Kooi, M.A.J. Somers, E.J. Mittemeijer: Metall. Mater. Trans. A 1996;27A:1055.

[87]   G. Hägg: Nature 1928;121:826.

[88]   E. Lehrer: Z. Tech. Phys. 1929;10:177.

[89]   E. Lehrer: Z. Elektrochem. 1930;36:460.

[90]   M.E. Brunauer, P.H. Jefferson, S.B. Emmett, J. Hendricks: J. Am. Chem. Soc. 1931;53:1778.

[91]   C. Guillard, H. Creveaux, C.R. Seances: Acad. Sci. Paris 1946;222:1170.

[92]   V.G. Paranjpe, M. Cohen, M.B. Bever, C.F. Floe: Trans. AIME 1950;188:261.

[93]   A. Burdese: Metall. Ital. 1955:357.

[94]   F.K. Naumann, G. Langenscheid: Archiv Eisenhütten. 1965;36:677.

[95]   H.A. Wriedt: Trans. Metall. AIME 1969;245:43.

[96]   O. Eisenhut, E. Kaupp: Z. Elektrochem. 1930;36:392.

[97]   C.T. Cheung, G. Simkovich: Reactivity of Solids 1988;5:177.

[98]   T. Belmonte, M. Goune, H. Michel: Materials Science and Engineering 2001;A302:246.

[99]   M. Keddam, M.E. Djeghlal, L. Barrallier: Appl. Surf. Sci. 2005;242:369.

[100]   C.T. Cheung, G. Simkovich: Reactivity of Solids 1989;7:115.

[101] M.A.J. Somers, E.J. Mittemeijer: Metall. Trans. A 1990;21A:189.

[102] B. Prenosil: Härterei-Tech. Mitt. 1973;28:157.

[103] S.V. Patankar, V. Suhas. Numerical Heat Transfer and Fluid Flow: Hemisphere, New York, 1980.

9 Curriculum Vitae

Persönliche Angaben

Name: Thomas Wöhrle

Geburtsdatum: 16.05.1981

Geburtsort: Heilbronn

Staatsangehörigkeit: deutsch

Promotion

2008 - 2012   Promotion am Max-Planck-Institut für Intelligente Systeme (ehemals Max-Planck-Institut für Metallforschung), Stuttgart, und Institut für Materialwissenschaft der Universität Stuttgart, Thema der Dissertation: "Thermodynamics and Kinetics of Phase Transformations in Fe-N-C alloys", Hauptberichter: Prof. Dr. Ir. E. J. Mittemeijer

Universitäre Bildung

2002 - 2007   Studium der Werkstoffwissenschaft an der Universität Stuttgart mit dem Abschluss Diplom-Ingenieur. Diplomarbeit am Institut für Materialwissenschaft der Universität Stuttgart mit dem Thema „Erzeugung reiner $\varepsilon\text{-Fe}_3(N,C)_{1+x}$-Schichten auf α-Eisen", Hauptberichter: Prof. Dr. Ir. E. J. Mittemeijer

Schulbildung und Wehrdienst

2001 - 2002   Stabssoldat bei den Heeresfliegern, Niederstetten

1999 - 2001   Mönchsee-Gymnasium Heilbronn, Abschluss: allgemeine Hochschulreife

1992 - 1999   Hohenstaufen-Gymnasium Bad Wimpfen

1988 - 1992   Grund- und Hauptschule Heilbronn-Biberach

10 List of Publications

1. T. Woehrle, A. Leineweber, E.J. Mittemeijer:
   Microstructural and phase evolution of compound layers growing on α-iron during gaseous nitrocarburizing. *Metallurgical and Materials Transactions A (2012);* accepted for publication. Chapter 2 of this thesis.

2. T. Woehrle, A. Leineweber, E.J. Mittemeijer:
   Influence of the chemical potential of carbon on the microstructural and compositional evolution of compound layers developing upon nitrocarburizing of α-Iron. *HTM - Journal of Heat Treatment and Materials 65 (2010) 243.* Chapter 3 of this thesis.

3. T. Woehrle, A. Leineweber, E.J. Mittemeijer:
   Multicomponent interstitial diffusion in and thermodynamic characteristics of the interstitial solid solution ε-Fe$_3$(N,C)$_{1+x}$; nitriding and nitrocarburizing of pure α-Iron. To be published. Chapter 4 of this thesis.

4. T. Woehrle, A. Leineweber, E.J. Mittemeijer:
   The shape of nitrogen concentration-depth profiles in γ'-Fe$_4$N$_{1-z}$ layers growing on α-Fe substrates; the thermodynamics of γ'-Fe$_4$N$_{1-z}$. *Metallurgical and Materials Transactions A (2011);* accepted for publication. Chapter 5 of this thesis.

5. T. Woehrle, H. Cinaroglu, A. Leineweber, E.J. Mittemeijer:
   Investigation of solid-state phase transformations and phase equilibria in the Fe-N and Fe-N-C system by means of nitriding/nitrocarburizing and secondary annealing experiments. To be published.

Danksagung